POLITECNICO DI TORINO

Master's degree in Environmental Engineering

ACLIMO Project: Deep Learning classification of aerial imagery for monitoring the effects of climate change on the mountain area of Maritime Alps

Supervisors

Prof. Andre Maria Lingua

Arch. Francesca Matrone

Student

Chiara Graziani

9th of Decembre 2024

Interreg France-Italia ALCOTRA

Cofinancé par l'Union Européenne
Cofinanziato dall'Unione Europea

ACLIMO

REGIONE PIEMONTE

Aree Protette Alpi Marittime

“A real loser is someone
Who’s so afraid of not winning,
they don’t even try”.
— Little Miss Sunshine

Contents

1. Abstract 1
2. Introduction 2
3. Materials and methods 4
3.1. Study area 4
3.2. Data 8
3.2.1. Orthophotos 8
3.2.2. DTM 11
3.2.3. Vegetation indices 11
4. Methodology 15
4.1. Deep Learning 16
4.1.1. U-Net architecture 18
4.1.2. MMSegmentation 20
4.2. Export Training Data for Deep Learning 21
4.2.1. Training data: Corine Land Cover 21
4.3. Train Deep Learning Model 24
5. Accuracy assessment 27
5.1. RGB ICE 2009-2011 imagery, CLC 2012 and U-Net 28
5.2. RGB+NIR ICE 2009-2011 imagery with NDVI and DTM, ROIs from CLC 2012 and U-Net 30
5.3. RGB+NIR ICE 2009-2011 imagery with DTM, wetlands class ROIs from CLC 2012 and U-Net 32
5.4. RGB+NIR ICE 2009-2011 imagery with DTM, ROIs from CLC 2012 and MMSegmentation 33
5.5. RGB+NIR ICE 2009-2011 imagery with ExG and DTM, ROIs from CLC 2012 and U-Net 34
5.6. RGB+NIR AGEA 2018 imagery with NDVI and DTM, CLC+Backbone 2018 and U-Net 35
6. Classification results 37
6.1. Change Detection analysis 39
7. Weather data 45
7.1. Temperature 46
7.2. Precipitation 51
8. Discussion 56
8.1. Change Detection results and climate analysis 56
8.2. Training of DL models 62
8.3. Critical analysis of the methodology and future perspective 63
9. Conclusion 65
Sources 66

List of figures

Figure 1 - Temperature change in the Alps and their sub-regions according to different emission scenarios 2
Figure 2 - APAM protected areas (marked in dark green) 5
Figure 3 - Large (red) and medium (blue) scale areas 5
Figure 4 - The area of interest at the medium scale 6
Figure 5 - Characteristic vegetation 8
Figure 6 - ICE 2009-2011 9
Figure 7 - AGEA 2018 10
Figure 8 - AGEA 2021 10
Figure 9 - Digital Terrain Model (DTM) 11
Figure 10 - Spectral signatures for land cover at different wavelengths 12
Figure 11 - NDVI from ICE 2009-2011 imagery 12
Figure 12 - ExG from ICE 2009-2011 imagery 13
Figure 13 - NDVI from AGEA 2018 imagery 14
Figure 14 - Workflow 15
Figure 15 - Artificial Intelligence subsets 16
Figure 16 - Neural network architecture 16
Figure 17 - Kernel filter 17
Figure 18 - Convolutional Neural Network architecture 18
Figure 19 - U-Net architecture 19
Figure 20 - Basic structure of MMSegmentation 20
Figure 21 - DeepLabv3 architecture 21
Figure 22 - Corine Land Cover 2012 vector dataset 22
Figure 23 - CLC+Backbone 2018 raster dataset 24
Figure 24 - Confusion Matrix elements in ArcGIS Pro 28
Figure 25 - ICE 2009-2011 classification result with U-Net algorithm, RGB only 29
Figure 26 - Squaring effects 30
Figure 27 - ICE 2010 classification with RGB+NIR+DTM+NDVI, U-Net 31
Figure 28 - ICE 2010 classification with RGB+NIR+DTM, U-Net 32
Figure 29 - ICE 2010 classification with RGB+NIR+DTM, MMSegmentation 33
Figure 30 - ICE 2010 classification with RGB+NIR+DTM+ExG, U-Net 34
Figure 31 - AGEA 2018 classification with RGB, NIR, DTM and NDVI 35
Figure 32 - Classification of ICE 2009-2011 37
Figure 33 - Classification of AGEA 2018 38
Figure 34 - Classification AGEA 2021 39
Figure 35 - Change Detection 2010-2018 40
Figure 36 - Change Detection 2018-2021 40
Figure 37 - Change Detection 2010-2021 41
Figure 38 - Brocan Lake in 2010 Figure 39 - Brocan Lake in 2021 42
Figure 40 - Percentage of class change with respect to the shift 42
Figure 41 - Variation of land cover classes in time 43
Figure 42 - Weather stations from ARPA Piemonte in our territory of interest 46
Figure 43 - Mean daily temperatures for 2002-2021 time period 48
Figure 44 - Mean annual anomaly for temperature, maximum and minimum temperature (1990-2021) 49

Figure 45 - Mean annual anomaly for seasonal temperature (1990-2021) 49
Figure 46 - Daily temperature series vs. periodic component from the Fourier transform 50
Figure 47 - Annual trend of residual temperature 51
Figure 48 - Mean monthly precipitation for the period 2000-2021 52
Figure 49 - Percentage frequency of daily precipitation (1993-2023) 53
Figure 50 - Annual precipitation anomalies for 1990-2021 compared to 2000-2021 time period 54
Figure 51 - Seasonal precipitation anomalies for 1990-2021 compared to 2000-2021 time period 54
Figure 52 - Precipitation intensity as SDII in Valdieri (1994-2023) 55
Figure 53 - Mean annual rainfall intensity from 2000 to 2021 55
Figure 54 - Temperature anomalies map (2010-2021) 56
Figure 55 - Precipitation anomalies map (2000-2021) 57
Figure 56 - Kernel density of land cover changes 58
Figure 57 - Box plot for each change category vs Temperature 58
Figure 58 - Box plot for each change category vs Precipitation 59
Figure 59 - Mean temperature anomaly with land cover changes (2010-2021) 60
Figure 60 - Mean precipitation anomaly with land cover changes (2010-2021) 61
Figure 61 - Standard deviation of temperature anomaly with land cover change (2010-2021) 61
Figure 62 - Standard deviation of precipitation anomaly with land cover change (2010-2021) 62

List of Tables

Table 1 - Aerial imagery detail 9
Table 2 - CLC 2012 classes at three levels of hierarchy 23
Table 3 - Confusion matrix for Test 1 29
Table 4 - Confusion matrix for Test 2 31
Table 5 - Confusion matrix for Test 3 32
Table 6 - Confusion matrix for Test 4 33
Table 7 - Confusion matrix for Test 5 34
Table 8 - Confusion matrix for Test 6 36
Table 9 - Resume of all DL model tests 36
Table 10 - Class area changes in 2018 and 2021 41
Table 11 - Ratio area for each land cover class 43
Table 12 - Weather stations for the area of interest (T: mean daily temperature [°C], Tmax: maximum daily temperature [°C], Tmin: minimum daily temperature [°C], P: precipitation [mm]) 45
Table 13 - Mean annual and monthly temperature for 2000-2021 time period 47
Table 14 - Annual and seasonal trends of temperature in the time period 1990-2021 [°C/decade] ... 50
Table 15 - Maximum, minimum and future trend of temperature for six weather stations 51
Table 16 - Precipitation and rainy days 52
Table 17 - Statistics of T [°C] and P [mm] anomalies for each land cover change class 60
Table 18 - Pros and Cons of the methodology 64

1. Abstract

Earth observation is a major tool for studying the effects of climate change on mountain areas, which are very sensitive to these effects. The thesis focuses on analysing changes on Valle Gesso, in Piedmont, Italy, with the classification of aerial orthophotos (RGB+NIR) in three different periods: 2010, 2018, 2021. The classification has been performed with Deep Learning models on ArcGIS Pro, using different parameters to better discriminate land cover classes, like the Normalized Difference Vegetation Index (NDVI), Excess Green Index (ExG) and the Digital Terrain Model (DTM). The classes were extrapolated from the CORINE Land Cover (CLC) datasets at the third level of detail. After some trials with different parameters, spectral bands and algorithms, the best classifier resulted in the U-Net model using the CLC+Backbone 2018 classes and adding NIR band, NDVI and DTM. This model was then applied to classify all other orthophotos; the resulted maps were then compared to generate a change detection raster, to observe which land covers have changed in a 10 years' time frame. This result was supported with climate data from 17 weather stations, to link land cover changes with climate change. From the weather analysis, we observed an increase in temperature from 1990 to 2021 (+0.4 °C/decade) and this rise is expected to continue in the next 100 years. As for precipitations, we could not detect a trend, just a tendency to drier periods.

The change detection shows a decrease of the coniferous forest cover, an increase in low-growing vegetation compared to tall trees, and, most notably, a broader expansion of herbaceous vegetation over areas previously dominated by high vegetation. Furthermore, lakes have experienced a lowering in their water level from 2010 to 2021, as a response to more frequent drier years. In general, all land cover classes suffered the climate change effects in the form of rise of temperature and drought events, and this trend is expected to increase in the future. Authorities must intervene with mitigation and adaptation techniques to protect the ecosystem and the socio-economic aspects in this mountain area.

2. Introduction

Although seen by many as an unattainable place far from our everyday life, the mountain is a source of many indispensable resources from an ecological and social-economic point of view: just think of all the water resources that arise from the glaciers, the wood of the forests, the electricity produced from hydropower, the winter tourism. At the same time, the mountain is also one of the most sensitive ecosystems to climate change, sentinel of the dramatic changes that are taking place on our Earth due to global warming.

Over the last 150 years, the air temperature in the troposphere has increased by about 1 °C, an increase that doubles in high altitude regions such as the Alps. Not only the temperature has increased, but changes in precipitation have also been observed in their temporal and spatial distribution, with an increase during the winter period, opposed to a strong reduction in the summer period [1].

Based on global and regional climate models, this same trend of the past will presumably be repeated in the future: according to an article published on Springer Nature [2], a temperature increase of between 2.2 and 3.1 °C is expected for 2055, compared to the average for the period 1961-1990, and a further warming of 2.8 and 5.2 °C in 2085, depending on the emission scenarios. A reduction in annual precipitation in a range of 1 to 10% is also expected for 2050 [3].

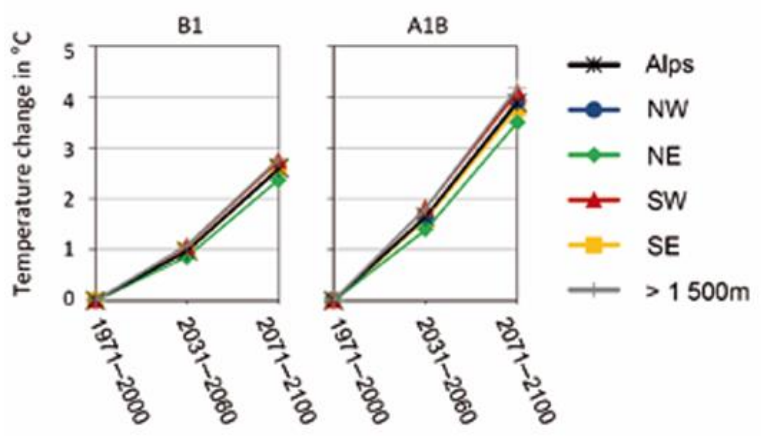

Note: Regional statistics: G = Greater Alpine Region, A = Alps, NW = north-western Alps, NE = north-eastern Alps, SW = south-western Alps, SE = south-eastern Alps, H = higher than 1 500 m.

Source: EURAC, 2008, based on data from CLM climate scenarios (Lautenschalger *et al.*, 2008).

Figure 1 - Temperature change in the Alps and their sub-regions according to different emission scenarios [4]

The transformation of the Alpine ecosystem will lead to a series of impacts with environmental and socio-economic damage on natural systems and controlled systems, such as: melting of mountain glaciers and permafrost, increase in the frequency of extreme weather events, water and agricultural crises, alteration of habitats and reduction of biodiversity, loss of primary forests and migrations [5].

Monitoring climate change in the alpine environment is of great importance to provide support to the management of the territory for the study of risk and vulnerability conditions and the prediction of any dynamic evolutions. To pursue this goal, one possible tool is the image classification.

In this thesis we will analyse the effects of climate change in Valle Gesso, a valley in the Maritime Alps, located in the province of Cuneo, in south Piemonte, Italy. In particular, the focus is to study the changes on the vegetation on two lakes in the valley, Brocan and Vej del Bouc. To enlighten these changes, the method consisted in performing a pixel-based classification of RGB+NIR aerial imagery from four different time periods: 2010, 2015, 2018, 2021. The classification has been carried out with a Deep Learning model on ArcGIS Pro 3.3. software, using as training samples the Corine Land Cover (CLC) 2012 and the CLC+Backbone 2018 datasets with their thematic classes at the third level of detail. After some trials, the Deep Learning model was built starting from the 2018 orthophoto with CLC2018 + Backbone raster product, then the classification was performed on all other orthophotos. In support of the classification, other products were taken into consideration: the digital terrain model (DTM) and vegetation indices. After the classification, a multitemporal analysis was made to highlight the changes in the land cover, using the Change Detection tool in ArcGIS Pro that compute the categorical change of classes.

Finally, the results obtained with the classification process are integrated with weather data from 18 stations inside or nearby the area of interest, to link the changes observed in the image classification with temperature and precipitation data with geostatistical methodologies.

Many limitations were found in the whole analysis: first, the computational effort for the deep learning classification; the coarse segmentation of CLC classes; the absence of near infrared band or errors in its spectral signal; the lack of imagery and climate information over longer time period. Despite these obstacles, we could obtain significant results of land cover changes in agreement with the conducted climate analysis in the territory.

3. Materials and methods

My thesis is part of the ACLIMO project, an ALCOTRA collaboration plan.

Interreg ALCOTRA is an EU program whose goal is to strengthen the cohesion between Italian and French cross-border regions. It covers the alpine territory between these two countries. The main goal is to overcome obstacles and challenges with this strong cooperation [6].

ACLIMO is an ALCOTRA project carried out by Aree Protette Alpi Marittime (APAM) and Politecnico di Torino, with the support of geomatics, geology and hydraulics expertise. The work was structured with a three levels multi-scale approach:

- large scale, with remote sensing techniques (satellite data) for the identification of trends and variations in the study area relating to vegetation, snow cover and land use. Sentinel imagery data and Copernicus services over 5-6 years epochs are used for the monitoring, with a resolution of 10 meters or more.
- Medium scale: an analysis will be carried out on the historical data and on aerial photogrammetry acquisitions for the creation of 3D models of the territory. An automatic or semi-automatic classification will be attempted using appropriately trained artificial intelligence techniques.
- Detail scale: two lakes will be analysed, on which to carry out bathymetric surveys, drone surveys in the visible, thermal and multispectral areas. Also in this case, the objective is to classify the area around these two lakes with artificial intelligence techniques, to identify some elements like vegetation and algae. Other chemical analyses could be carried out to characterize the two water bodies. The level of detail is in the order of ≤ dm.

This thesis will focus on the medium scale approach, analysing and classifying the aerial photogrammetry acquisitions of three years: 2010, 2018, 2021. The pixel-based classification is performed using a Deep Learning model trained with the Corine Land Cover dataset, with a focus on vegetation and water basins.

3.1. Study area

We are inside Parco Naturale Alpi Marittime, which falls under the protection of the Aree Protette Alpi Marittime (APAM) body. APAM supervises two natural parks (Alpi Marittime Natural Park and Marguareis Natural Park) and eight natural reserves distributed over a wide territory, from Alps to Alta Langa, crossing the plain, as safeguards for some of the most important sites of naturalistic, archaeological and paleontological interest in the province of Cuneo. The overall protected territory extends over 38,290 hectares and involves 16 Piedmonts municipalities, and the altitude ranges from 645 to 3297 m a.s.l., with Monte Argentera as the highest peak in the territory [7].

The main activities in this area are tourism, especially for mountain climbing and for natural reserves, and energy production, with the presence of the biggest hydropower plant in Italy, Luigi Einaudi plant in Entracque, which has three reservoirs in Piastra, Rovina and Chiotas lakes [8].

Figure 2 - APAM protected areas (marked in dark green) [5]

The following figure shows the three areas of interest for ACLIMO Project:

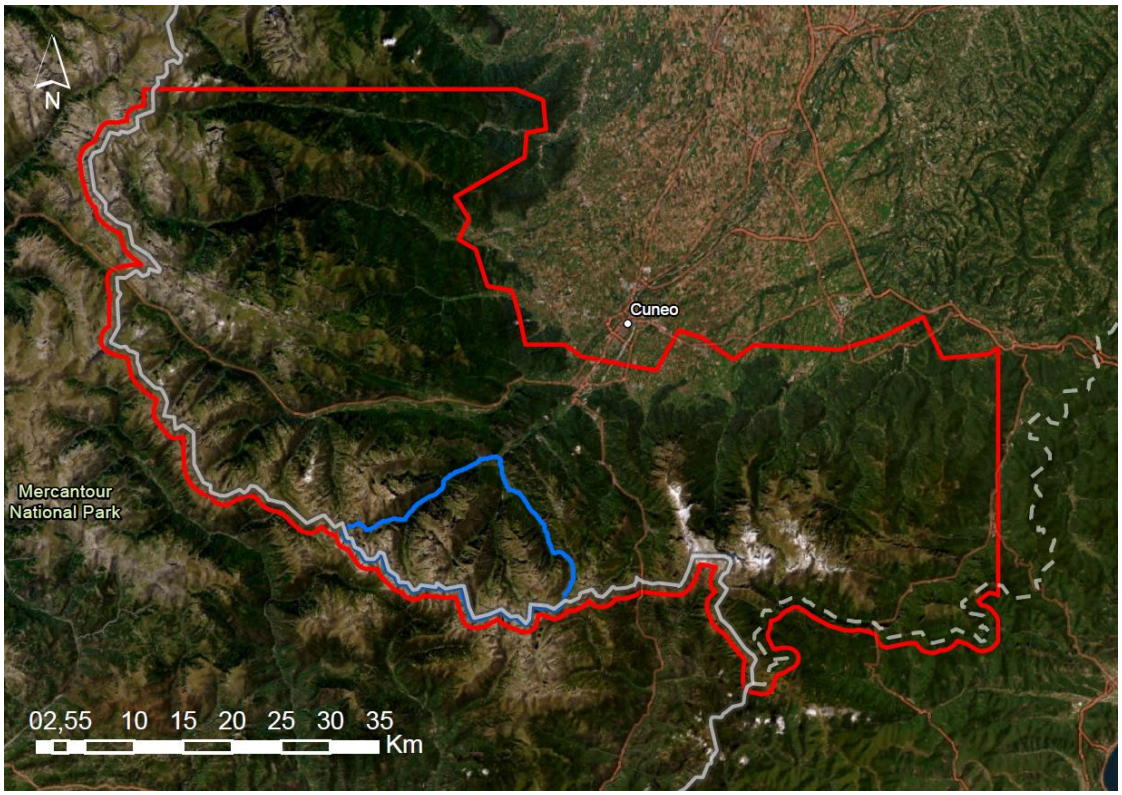

Figure 3 - Large (red) and medium (blue) scale areas

Our area of study, at the medium scale, consists in the entire territory of Valle Gesso, the heart of Parco Naturale Alpi Marittime. It has a triangular shape, delimited to the East with Valle Vermenagna, to the South with Valle della Tinea (France) and to the North-West with Valle Stura di Demonte. The vertex of our area of interest ends close to Valdieri, with a surface of 195 km^2.

The territory has a complex conformation, being on the curvature of the South-Western Alps. It is characterized by high peaks and sharp crests, steep depressions and large stony ground, wide surfaces with no vegetation, few woods, perennial snowfields and some glaciers. In fact, 200.000 years ago Valle Gesso was covered by two big glaciers; nowadays, there are few glaciers who survived in this area: Gelas, Maledía, Ciafraion, Lourousa, Clapier, Peirabroc.

The presence of glaciers and of watercourses involves the alternation of narrow valleys fluvial-originated and of wider U-shaped valleys of glacial origin. These are characterized by the presence of large glacial cirques, within which many small and medium sized lakes form; we can count 8 lakes with glacial origin and 3 artificial lakes inside the Park [5].

The two lakes for the analysis of this thesis are Brocan lake and Vej del Bouc lake; the first one is characterized by a strong presence of anthropic activities, while the second one by eutrophication. The following image shows the shapefile of the lakes in our area of interest; the shapefile comes from Tavola P2.0 “Beni Paesaggistici” (Quadro d’unione 1:250000), a project by Regione Piemonte reporting the protected landscape assets present in the regional territory [9].

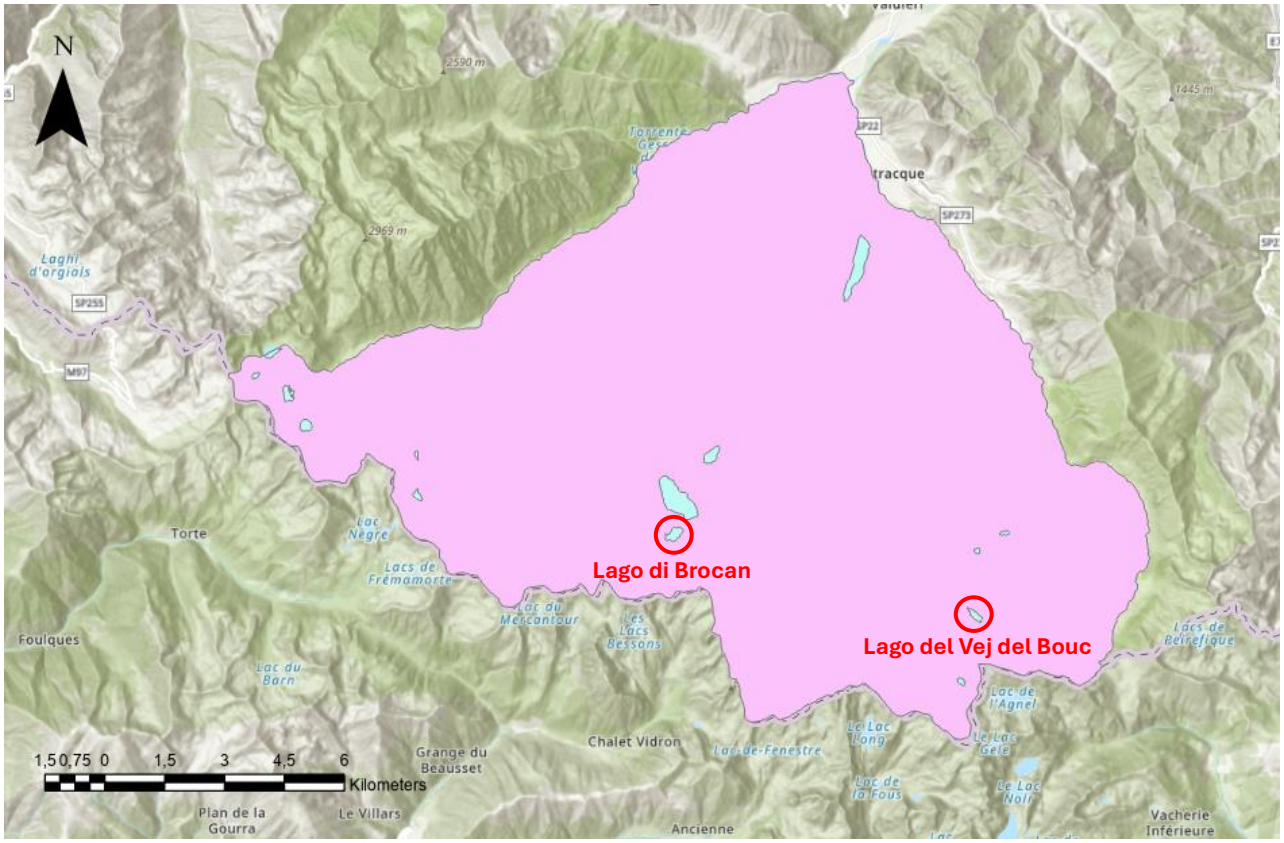

Figure 4 - The area of interest at the medium scale

Some of these lakes undergo a process of "burial", which causes the formation of wetland. The term "wetland" refers to a variety of environments characterized by the co-presence of water and vegetation. According to the definition of the Ramsar Convention: "Wetlands are areas of moist meadows, swamps, bogs or flooded areas, whether natural or artificial, permanent or temporary, with still or moving water, whether fresh, brackish or salty, including seawater areas whose depth, at low tide conditions, does not exceed six metres". They represent one of the most important ecosystems: they act as natural filters for fluids; as reserves of fresh water during dry periods and as enlargement areas during flood events; they also represent vital habitats for the conservation of biodiversity [10]. Wetlands should have been part of our classification and identification analysis, but unfortunately it was not possible to detect them with our approach.

Vegetation is characterized by the prevalence of broad-leaved forest, in particular beech, and a smaller area is occupied by coniferous forest, which consists in silver fir, norway spruce, swiss pine. The difference in forest cover are:

- the oceanic, temperate and humid climate of Alpi Marittime, which favours the growth of the beech and of broaded-leaved trees, in contrast with coniferous trees that prefer instead a more continental climate, except for the silver fir;
- the harsh and uneven geomorphology of this territory, where tree species with adaptable growth habit, such as broad-leaved trees in general, can colonize more easily.
- man, who involuntarily favoured beech forests over coniferous forests for timber.

The beech forest extends for 1000-1800 m in altitude, appearing as a dense group of even trees with a bushy habit, which produces a strong shade of the slopes.

Preferring a more continental climate, coniferous trees managed to settle in the innermost areas of the valleys or in the shelter of the large mountain massifs, where more favourable conditions are created. The larch, a forest essence that loves sunlight, colonizes the edges of the gullies and the slopes covered with stones and debris accumulations, managing to reach up to 2500 meters above sea level. The stone pine reaches up to 2800 meters above sea level on ridges and cliffs, taking on a twisted and suffering appearance [11].

Figure 4 displays the typology of vegetation in our area with the CLC nomenclature at the 3rd level; this shapefile is provided by BDTRE (Banca Dati Territoriale di Riferimento degli Enti) in the Geoportale Piemonte [12].

Figure 4 also displays pastures and uncultivated zones in yellow. The harsh and rocky morphology with snowfields and debris does not allow for the presence of extensive high-altitude meadows, mostly reduced to strips of discontinuous prairie and grassy ledges. The best grasslands from a forage point of view are the fat meadows, starting from 800 meters above sea level; the best is found in the Val Grande around Palanfrè and in the Esterate area, where however, following abandonment due to depopulation, we are now witnessing the advance of the forest. There are also thin prairies in this area, formed by the thinning of the sward and the progressive appearance of frugal species, and

nardets, produced by the excessive trampling of livestock, which eliminates the more delicate species to make room for Nardus stricta, grass that tolerates compact and poorly aerated soil well [13].

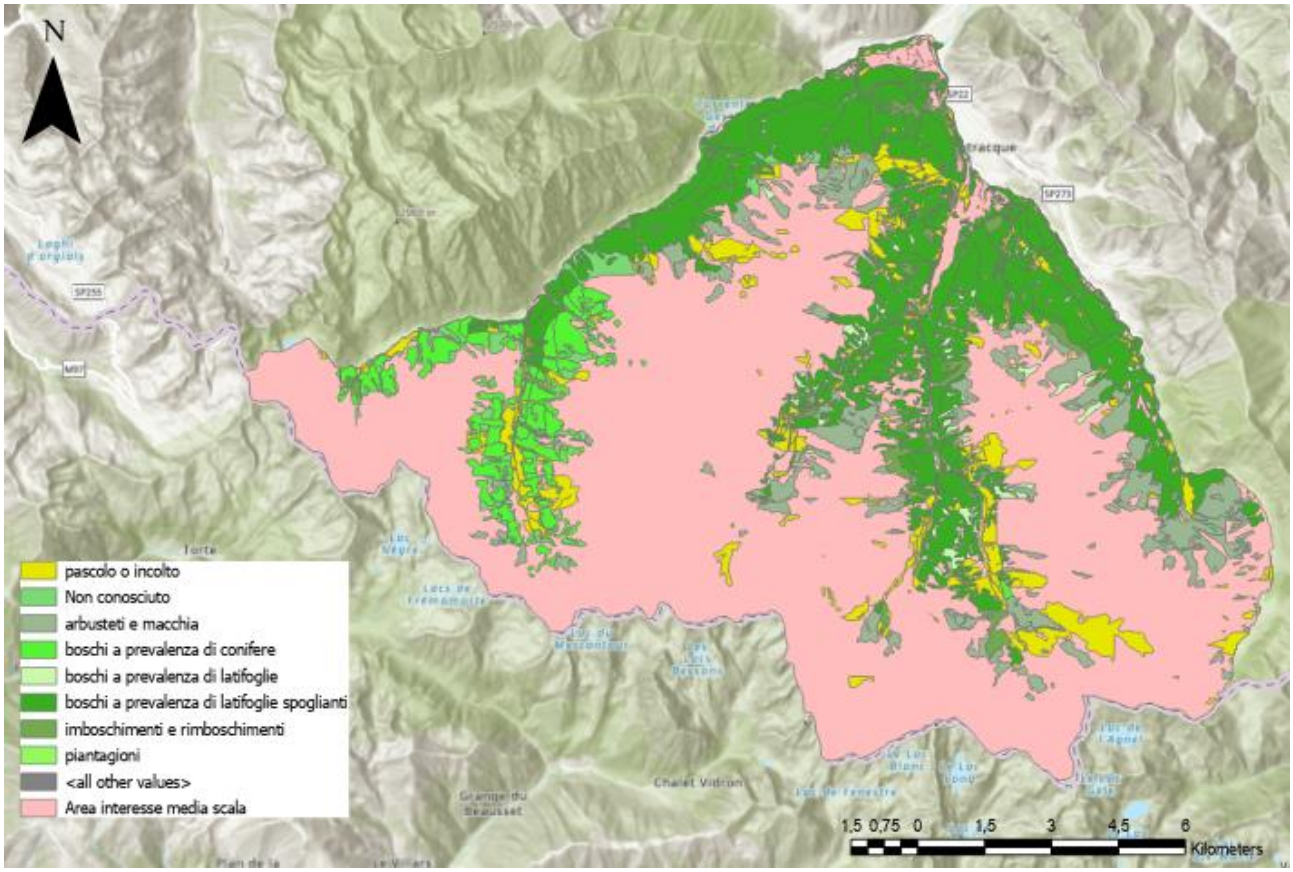

Figure 5 - Characteristic vegetation

3.2. Data

The classification was performed on RGB+NIR orthophotos for three different time period: 2010, 2018, 2021. In addition to the imagery products, the Digital Terrain Model and vegetation indices were used to improve the recognition of different classes in the area.

3.2.1. Orthophotos

Three orthophotos were analysed to classify the area of interest. Orthophotos of 2018 and 2021 are RGB+NIR imagery produced with an airplane flight made by Consorzio TeA during the summer period all over Piedmont region on behalf of AGEA (Agenzia per le Erogazioni in Agricoltura); they have a ground resolution of 30 cm each.

Orthophoto from year 2010 has RGB and NIR bands and it comes from the frames of the ICE aerial shot made during 2009-2011 over the entire Piedmont region. It has a resolution of 50 cm. From the same mission of 2009-2011 we were able to download also the Digital Terrain Model (DTM) and the Digital Surface Model (DSM), both with a resolution of 5 m.

All orthophotos were provided by Regione Piemonte. We don't have any information about the exact month and hour the images were taken by plane.

YEAR	SPECTRAL	RESOLUTION (cm)	COMPANY
2010	RGB+NIR	50	ICE
2018	RGB+NIR	30	AGEA
2021	RGB+NIR	30	AGEA

Table 1 - Aerial imagery detail

There should have been other three imagery for the analysis, but unfortunately we were not able to elaborate them to obtain the orthophotos: 1991, 2000 and 2015 imagery data. For 2000 we had 3793 frames from the aerial shot of 2000 made by Regione Piemonte, to study a flooding event occurred in South Piedmont. The company that performed the flight was ROSSI BRESCIA. These frames were not correctly oriented, so as the 14 frames from CRG-ROSSI flight in 1991, and we could not have the orienting parameters of the cameras. AGEA 2015, instead, was corrupted with some NoData pixel and it was not possible to add other channels for the classification.

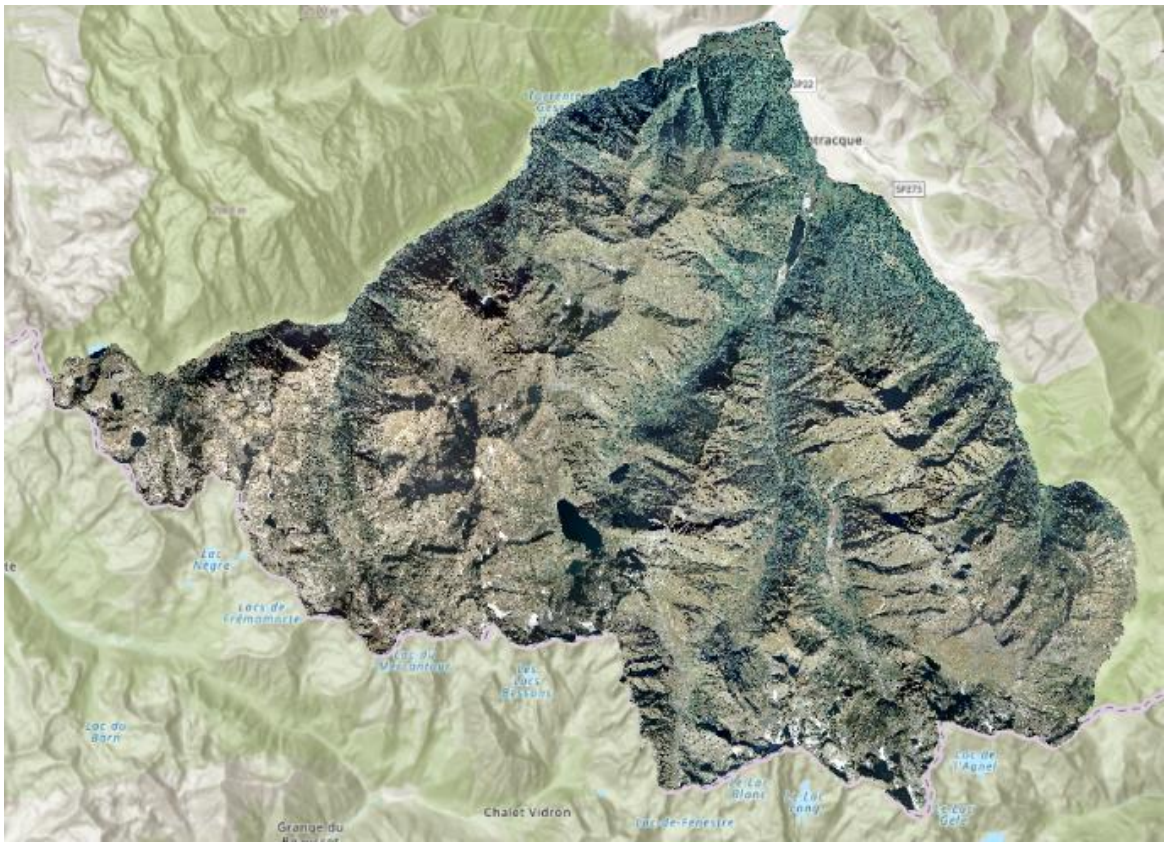

Figure 6 - ICE 2009-2011

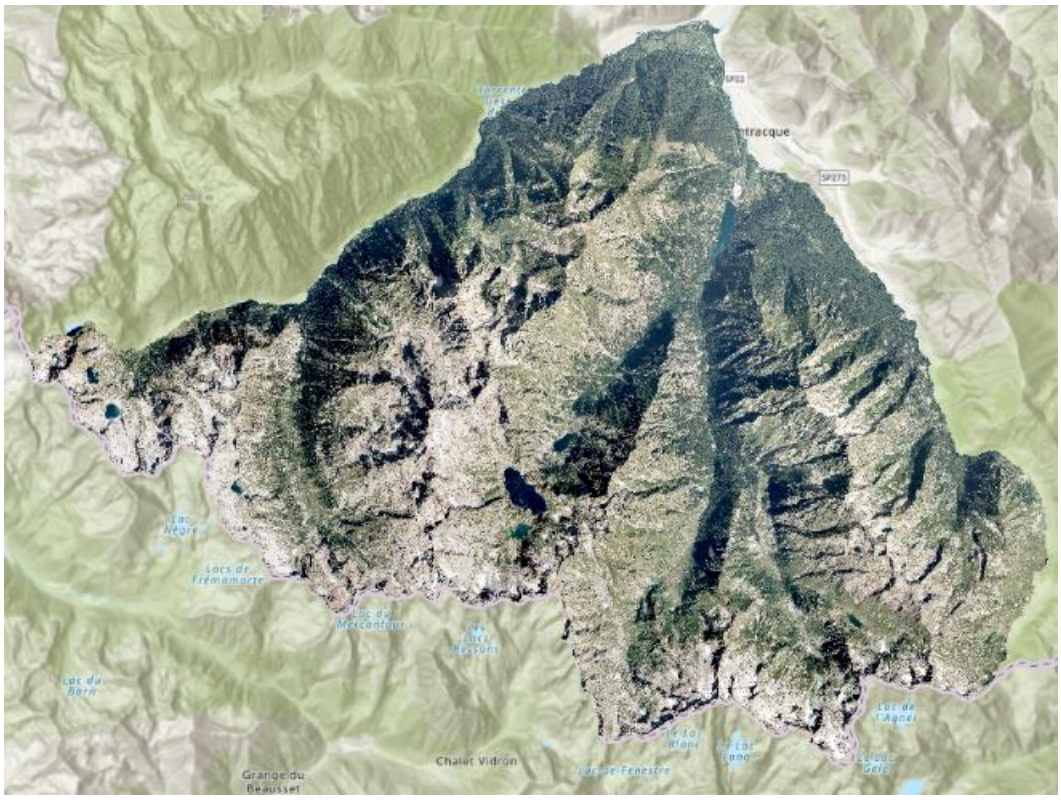

Figure 7 - AGEA 2018

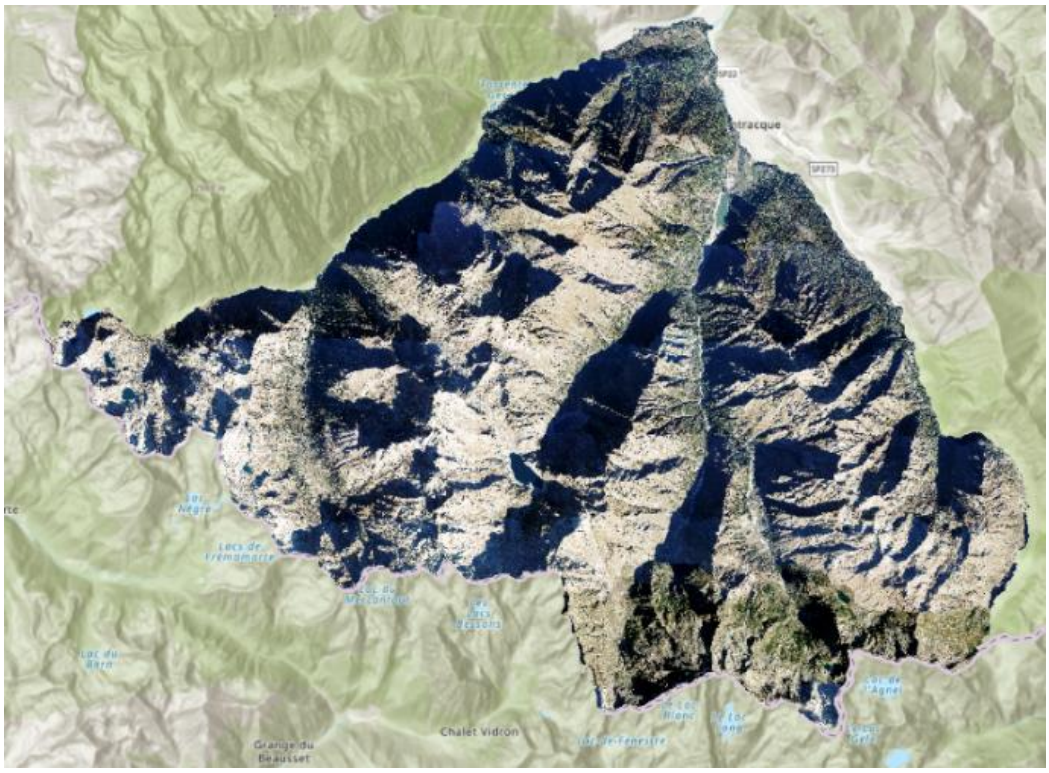

Figure 8 - AGEA 2021

3.2.2. DTM

The Digital Terrain Model (DTM) is a raster product that represents the distribution of the elevation values in an area, only considering the bare ground surface without any object above it, like plants and buildings.

For our area of interest, the DTM was available on the Geoportale Piemonte and it was acquired by the ICE 2009-2011 photogrammetric flight with a LIDAR survey. The resolution is of 5 meters, the elevation precision is equal to ±0.30 m (±0.60 m in woodlands and urban areas).

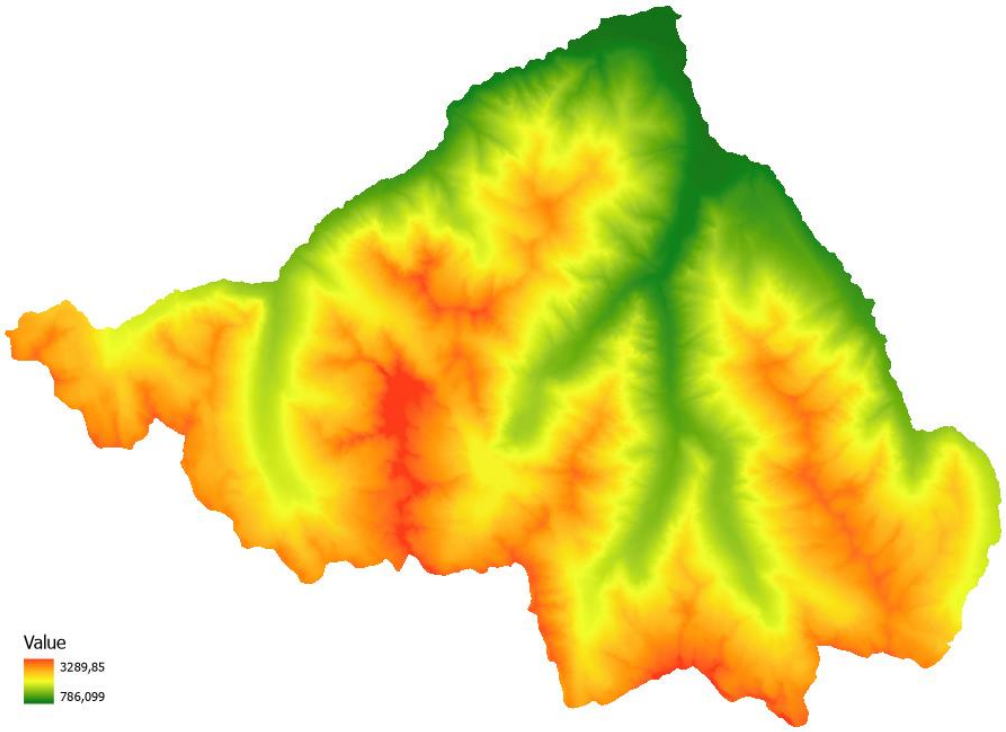

Figure 9 - Digital Terrain Model (DTM)

3.2.3. Vegetation indices

Vegetation indices are combinations of surface reflectance at two or more wavelengths designed to enhance the contribution of vegetation properties and allow reliable spatial and temporal inter-comparisons of terrestrial photosynthetic activity and canopy structural variations. They are really useful to distinguish different land covers among each other, in particular what is vegetation and what is not.

The most exploited image band for the calculation of vegetation indices is the infrared band, in particular the concept of reflectance is of major importance: in fact, the vegetation reflects very well the infrared band, at the contrary water absorbs it.

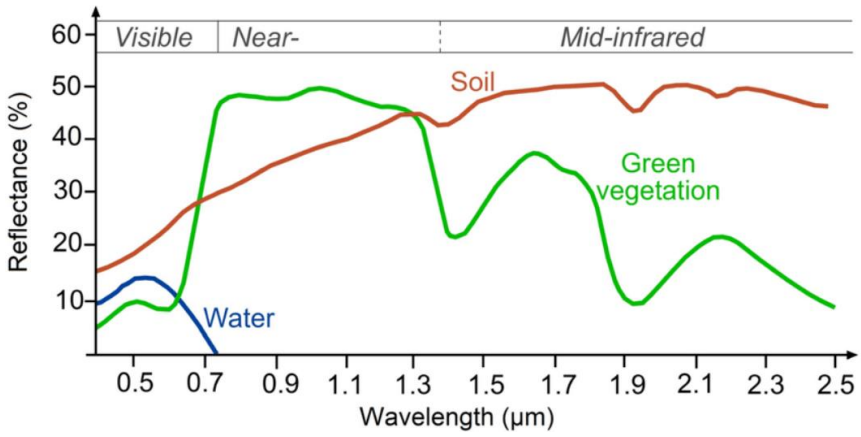

Figure 10 - Spectral signatures for land cover at different wavelengths [14]

We considered NDVI (Normalized Difference Vegetation Index) as adding features for the classification. NDVI is a widely used index for the density and the health of the vegetation in a given area. It is calculated from spectrometric data at two bands, the red and the near infrared. The formula is the following:

$$NDVI = \frac{NIR - RED}{NIR + RED}$$

Where NIR and RED stand for the spectral reflectance in the red and near-infrared regions. The result varies between -1 and +1, where negative values represent water surfaces, 0 bare ground and values close to 1 healthy and dense vegetation.

For the 2009-2011 imagery, the result for NDVI is the following:

Figure 11 - NDVI from ICE 2009-2011 imagery

As we can notice, the output is incorrect, in fact the water has value 1 for the NDVI. This could be due to a spectral error in the infrared band of the 2010 orthophoto: in fact, for water surfaces we observe high values of reflectance, which contrasts the spectral signature of figure n.

Given the incorrect output of the NDVI for ICE 2009-2011 imagery, we also calculated the Excess Green Index (ExG), an RGB-based spectral index: it contrasts the green portion of the spectrum against red and blue to distinguish vegetation from soil.

$$ExG = 2 * G - R - B$$

G, R, B represent, respectively, the digital number (DN) value of green, red and blue bands [15].

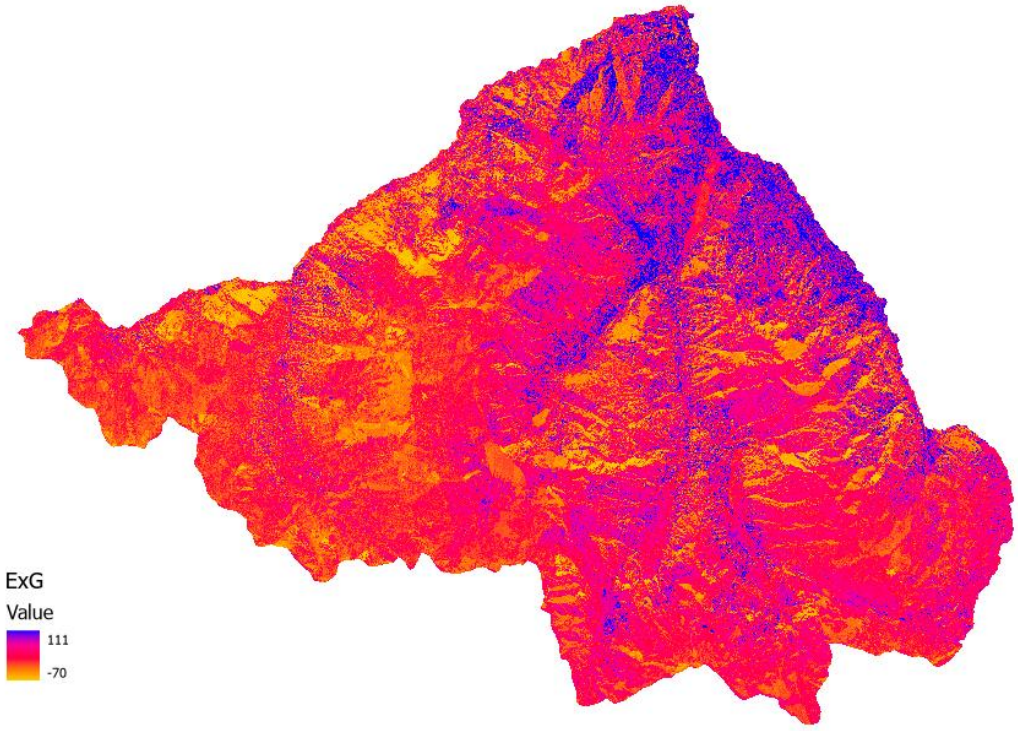

Figure 12 - ExG from ICE 2009-2011 imagery

High values of ExG stand for the presence of green vegetation; close to zero, absence of vegetation, bare soil, rocks, streets and buildings; negative values, absence of vegetation or presence of other land cover surfaces, like water or shadows.

For the 2018 imagery, instead, we have the following NDVI:

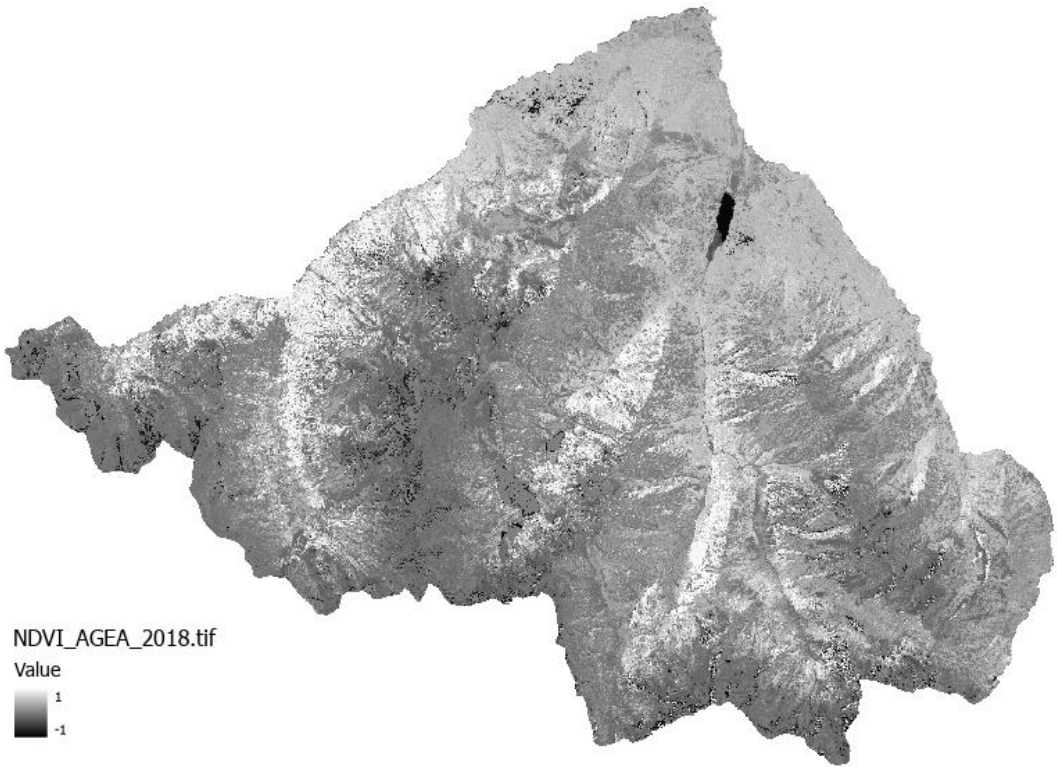

Figure 13 - NDVI from AGEA 2018 imagery

Differently from ICE 2010 imagery, the 2018 NDVI is correct and does not have spectral errors in the near infrared band.

4. Methodology

The pixel-based classification was performed in ArcGIS Pro 3.3., applying the Deep Learning package for this software. These ArcGIS Pro tools consume the models that have been trained to detect specific features in third-party deep learning frameworks—such as TensorFlow, CNTK, and PyTorch—and output features or class maps.

The pixel-based classification with a DL model in ArcGIS Pro consists in three main operations, which make part of the Deep Learning toolset, inside the Image Analyst Tools: Export Training Data for Deep Learning, Train Deep Learning Model, Classify Pixels Using Deep Learning.

With the aim of determining which is the best method for the classification of this area, different approaches were developed, with distinct input parameters, training samples and deep learning architectures, starting from the 2010 and 2018 imagery for the training. Once the best model was obtained based on accuracy assessments, the best performing classifier was used to classify all other imagery data, to finally have a Land Cover Change analysis of our area of interest.

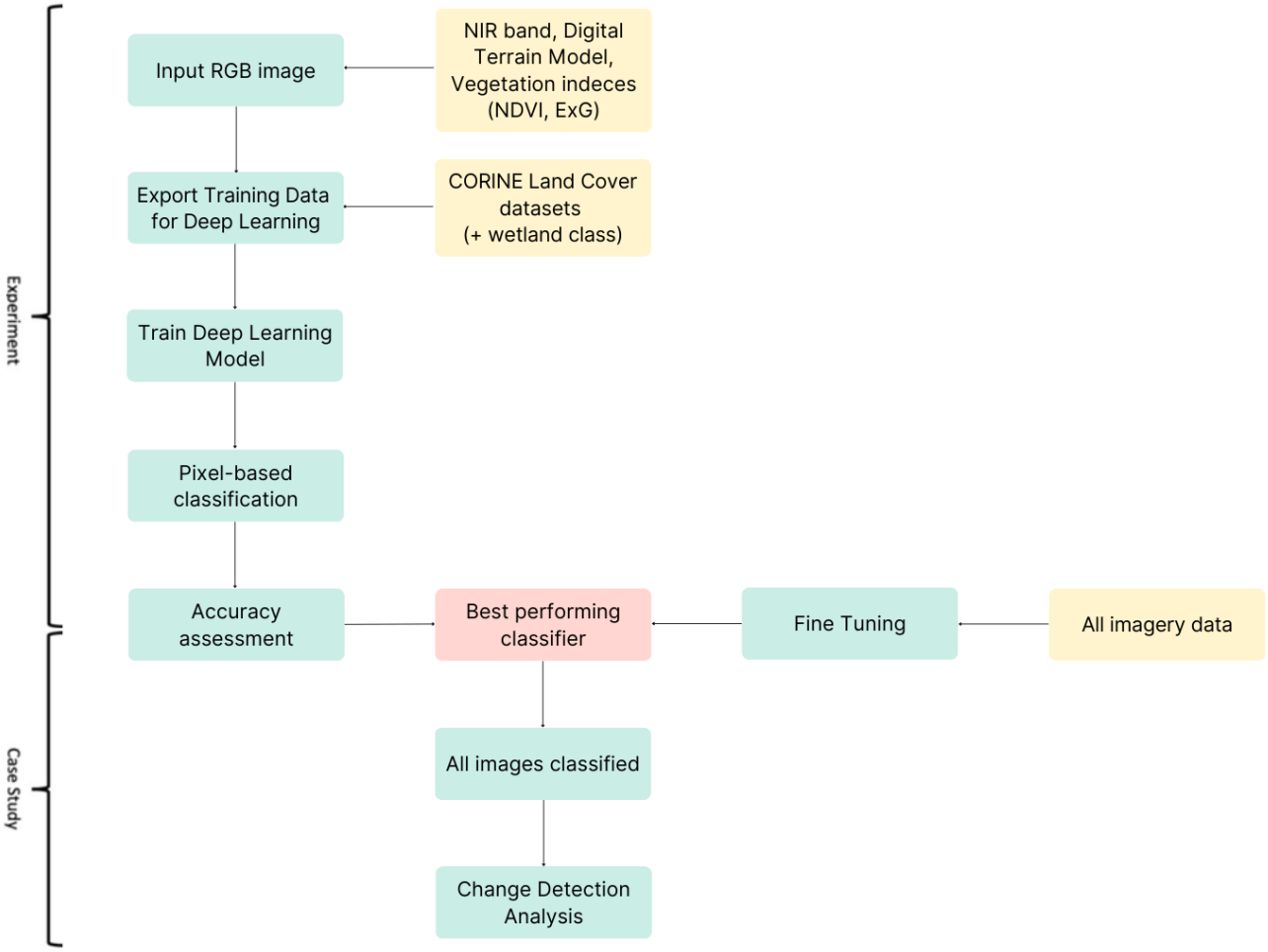

Figure 14 - Workflow

4.1. Deep Learning

Deep Learning is a subset of machine learning that uses several layers of algorithms in the form of artificial neural networks. This neural network simulates the functioning of the human brain, so that the system can learn from a big amount of data. Differently from machine learning, deep learning models can extract themselves the features directly from data, without the support of human manual extraction [16].

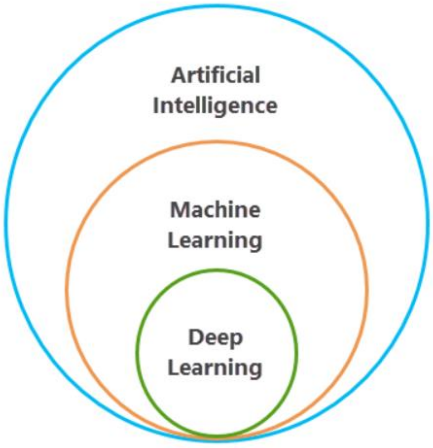

Figure 15 - Artificial Intelligence subsets [16]

The neural network is constituted by interconnected nodes (neurons) in a stratified structure that links inputs with outputs. Neurons between input levels and output levels are called hidden layers. The term "deep" refers to the use of multiple layers in the network; each layer defines specific features and patterns of data, optimizing at each level the processing of the information [17].

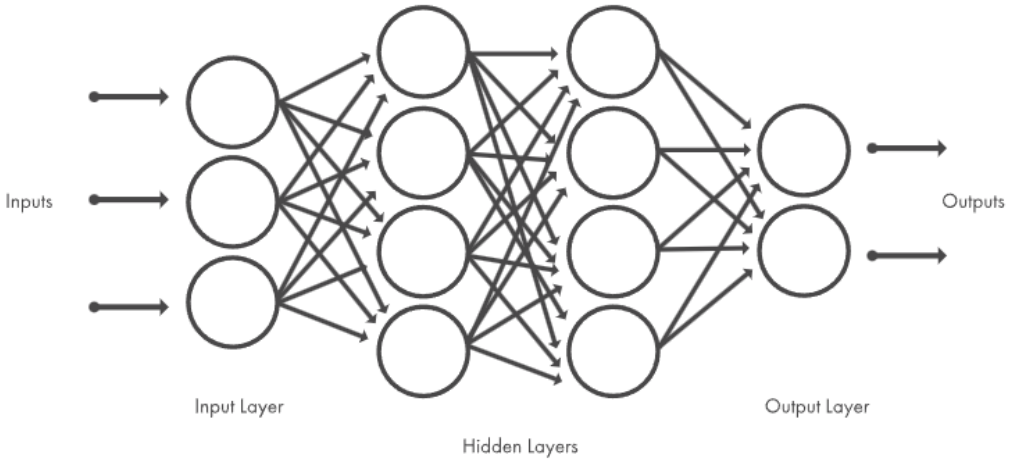

Figure 16 - Neural network architecture [17]

There are many computer vision tasks that can be accomplished with deep learning neural networks. One such task of interest to us is the image classification. For treating this kind of task, a common

type of deep learning neural network is used: the Convolutional Neural Network (CNN). CNNs are in fact widely used in Image Recognition, Detection and Classification.

CNN uses a specific architecture: it has an input layer, an output layer, and hidden layers. The hidden layers usually consist of convolutional layers, Rectified Linear Unit (ReLU) layers, pooling layers, and fully connected layers [18].

A convolutional neural network starts by taking an input image, which is then transformed into a feature map through a series of convolutional and pooling layers. The convolutional layer applies a set of kernel filters to the input image. The kernel filter consists in a little matrix (3x3 or 5x5) that scans every portion of the image, pixel by pixel, and each pixel is multiplied by the value inside the kernel matrix element; this operation is called convolution. The final result is a new image with the pixel values transformed and that highlights a specific aspect of the input image (colour, shape, etc.).

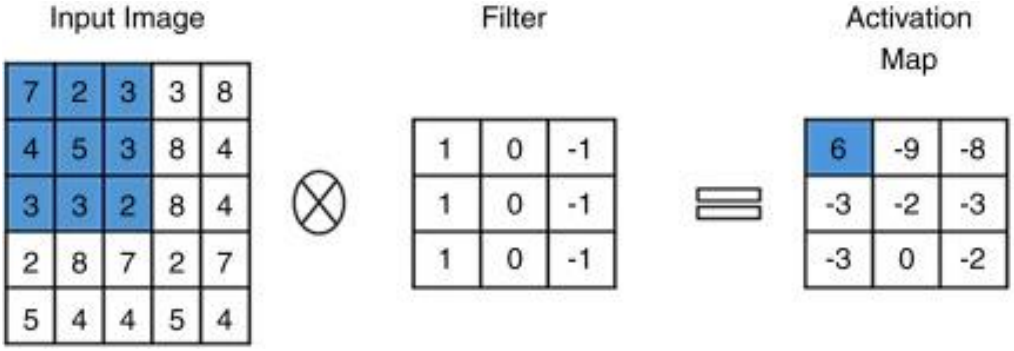

Figure 17 - Kernel filter [19]

The pooling layer then downsamples the feature map from the convolution to reduce its size, while retaining the most important information, in order to also reduce the computational complexity. The feature map produced by the convolutional layer is then passed through multiple additional convolutional and pooling layers, each layer learning increasingly complex features of the input image. Activation functions, like ReLU, are applied to the outputs of convolutional and pooling layers element by element to introduce non-linearity into the network, so that it can understand complicated association and make non-linear decisions. Finally, the fully connected layer connects the neurons in the previous layer to all the neurons in the next layer: it is responsible for combining the features learned by the convolutional and pooling layers, allowing the network to learn global representations and make high-level prediction. The final output of the network is in fact a predicted class label or probability score for each class, depending on the task [20] [21].

For our classification process we will use Res-Net 18, a CNN with 18 convolutional layers.

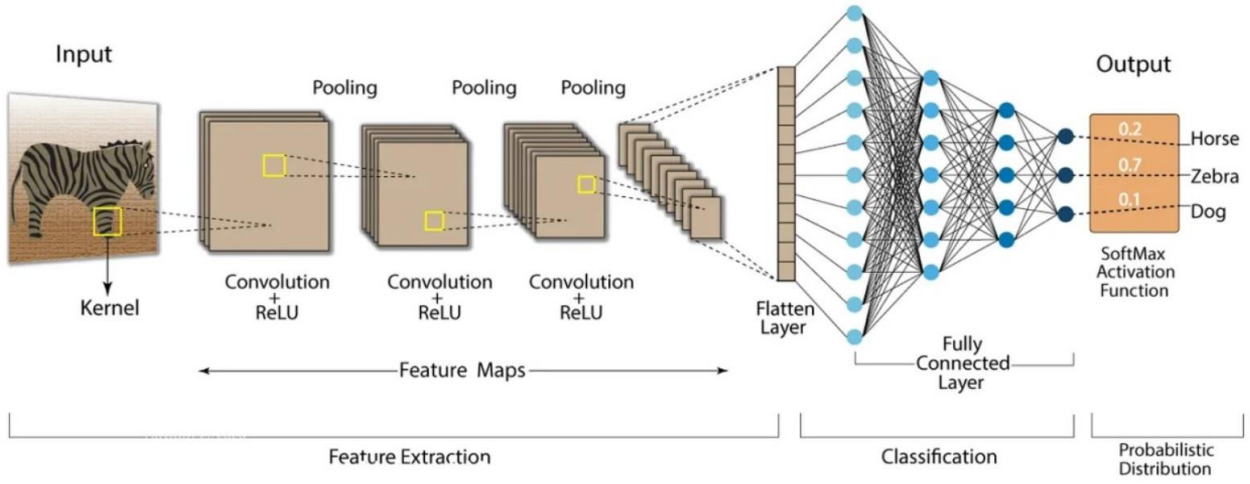

Figure 18 - Convolutional Neural Network architecture [20]

So, as previously said, in a deep learning CNN there is no need for manual feature extraction, so the features are not pre-trained, but they are directly extracted from images while the model is training. This aspect makes Deep Learning models very accurate for image classification.

4.1.1. U-Net architecture

The model type exploited for training the deep learning model is U-Net, one of the most well-recognized image segmentation algorithms. Semantic segmentation, or pixel-based classification, classifies each pixel of an image as belonging to a particular class.

U-Net is a fully convolutional neural network (FCN): it is like a CNN, but with a deconvolution layer (decoder) that allows the construction of a dense segmentation map the pixel-level forecasts by upsampling the feature maps. In this way, the spatial resolution of the final result of the classification process is the same of the input image.

The "U" stands for the shape of the architecture of this model. It consists in an encoder network followed by a decoder network. The encoder is usually a pre-trained classification network where you apply convolution blocks followed by a maxpool downsampling to encode the input image into feature representations at multiple different levels, plus ReLU activation functions. After this contracting path, there is the decoder, or expanding path, which includes the upsampling and the concatenation followed by regular convolution operations. The upsampling consists in enhancing the spatial dimensions of feature maps onto pixel space at higher resolution.

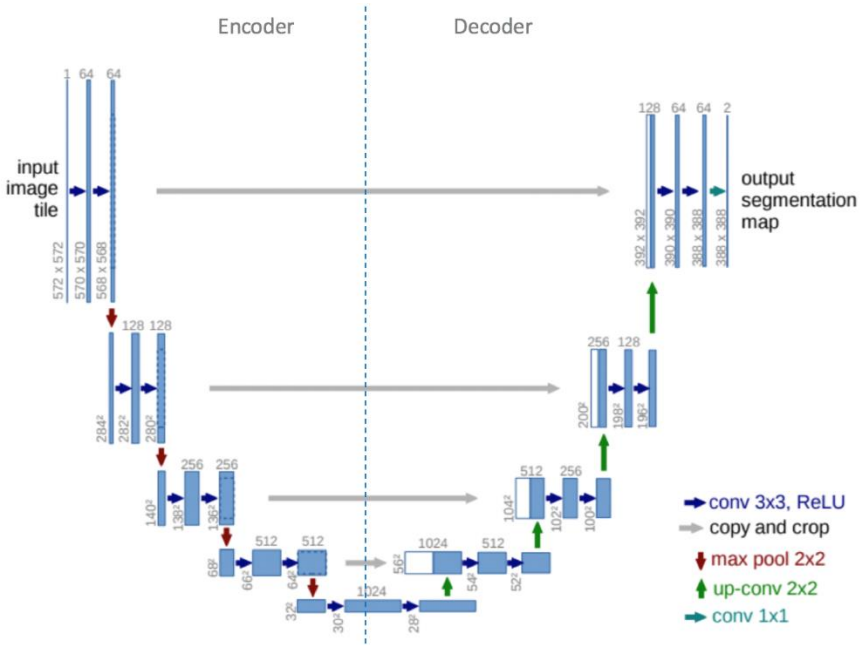

Figure 19 - U-Net architecture [22]

In the concatenation, the feature maps from the encoding path are concatenated with the upsampled feature maps from the decoding path during the upsampling procedure. This step enables the network to aggregate multi-scale information for a correct segmentation. The idea is to restore the condensed feature map to the original size of the input image, that's why we expand the feature dimensions [22]. Encoder and decoder are linked together at the same levels through skip connections: in this way, the model can preserve the resolution during the expansion phase.

The figure n represents the schema of the U-Net architecture and its functioning: the input image of size 572x572x1 is converted into a binary segmented output map of size 388x388x2 During the contracting path, the input image is progressively reduced in height and width but increased in the number of channels. This increase in channels allows the network to capture high-level features as it progresses down the path. At the bottleneck, a final convolution operation is performed to generate a 30×30×1024 shaped feature map. The expansive path then takes the feature map from the bottleneck and converts it back into an image of the same size as the original input.

This is done using upsampling layers, which increase the spatial resolution of the feature map while reducing the number of channels. Finally, each pixel in the output image represents a label that corresponds to a particular object or class in the input image. In this case, the output map is a binary segmentation map where each pixel represents a foreground or background region [23].

4.1.2. MMSegmentation

MMSegmentation is a very popular open-source library for the semantic segmentation developed by OpenMMLab, for the project MMDetection. It supports many architectures for the deep learning model training.

The architecture mainly consists in an initial backbone, which extracts the characteristics of the input image that will be used throughout the model. The image is then transformed in a feature map. This process continues in the Neck and then the feature map is transformed into a segmentation mask in the Decode Head. The last part of the model is the Auxialiary Head: the characteristics of the image are all elaborated to finally produce an output map that indicates the class for each pixel.

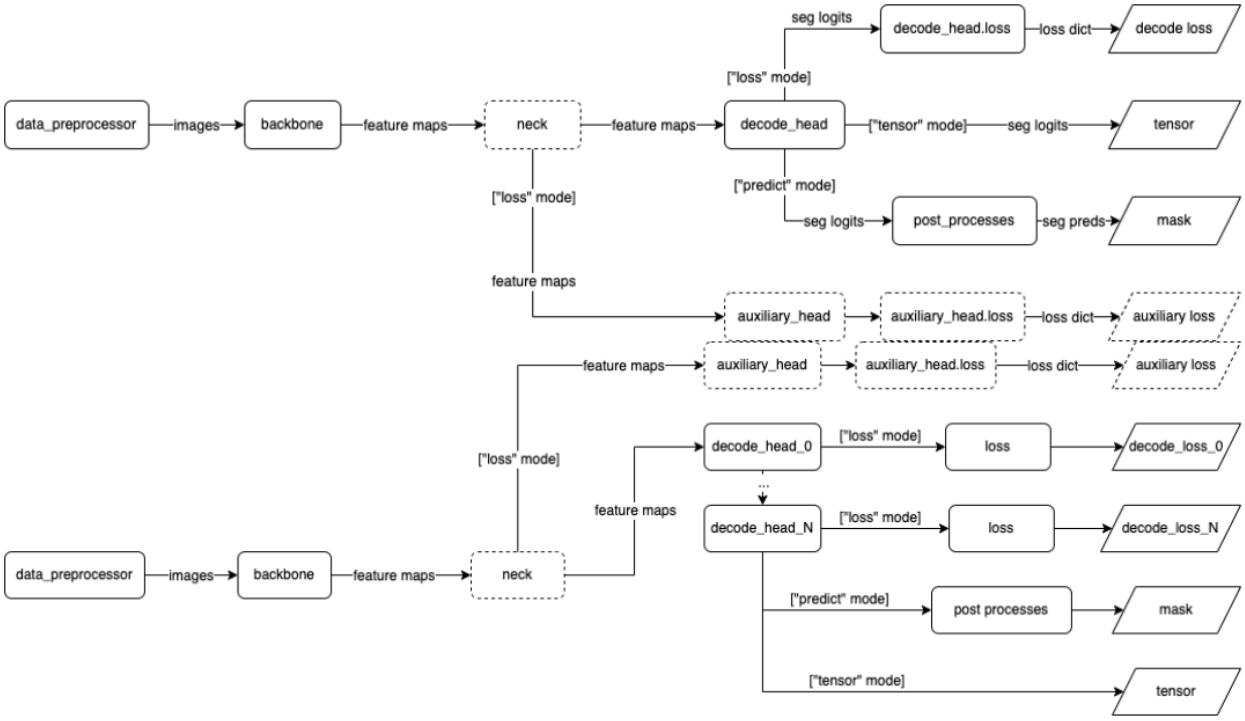

Figure 20 - Basic structure of MMSegmentation [24]

The backbone model used in ArcGIS Pro is DeepLabv3. It is a deep neural network architecture for semantic segmentation. Differently from the U-Net architecture, which uses an encoder and a decoder, DeepLabv3 applies the Atrous (Dilated) Convolution to obtain a finer resolution feature maps and it uses a bilinear upsampling to obtain the desired resolution [25].

After a convolution phase for feature extraction and downsampling of the input image, there is the Atrous convolution. A “dilated” kernel is applied on the feature map: zeros are inserted into the convolution kernel to increase the size of the filter without increasing the number of learnable parameters. With this approach, the model can retain high level and detailed information without reducing the resolution of the image; we get more dense feature maps.

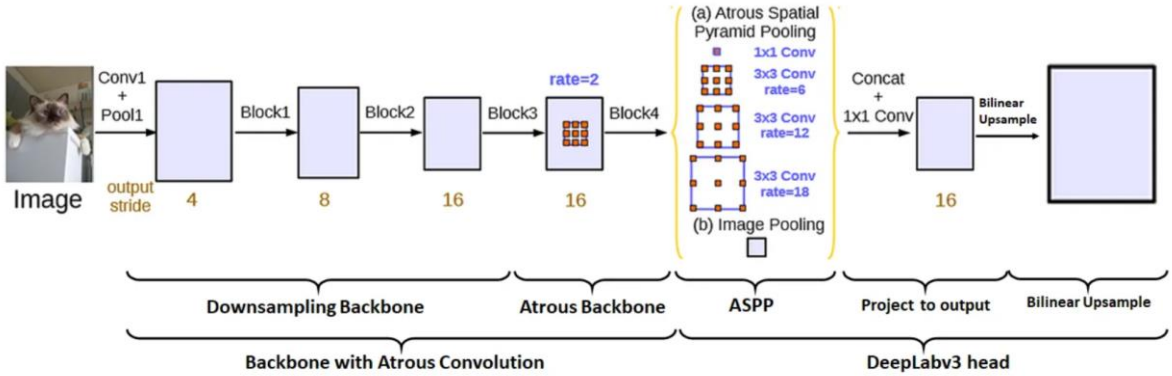

Figure 21 - DeepLabv3 architecture [25]

The next step is the Atrous Spatial Pyramid Pooling (ASPP): it applies more Atrous convolutions with different dilatation rate, so it resamples features at multiple scales and then pools them together. The output of ASPP is upsampled to the resolution of the input image, and then a finale convolution applies to get the segmentation of the image.

4.2. Export Training Data for Deep Learning

The Export Training Data for Deep Learning tool converts the source imagery and training samples to deep learning training data. The output is a folder of image chips of 256 pixel rows by 256 pixel columns and a folder of metadata files [16].

The Metadata Format chose for the export was the Classified Tiles, which is primarily used for pixel classification: the output is one classified image chip per input image chip with the statistics of all classes.

The inputs for this tool were the aerial image to be classified and the training samples from the CORINE Land Cover datasets.

4.2.1. Training data: Corine Land Cover

CORINE Land Cover is a pan-European land cover and land use inventory, created by the European Commission as a database of the Copernicus Land Monitoring Service (CLMS), in order to have a comprehensive, detailed, and harmonized dataset on the land cover (LC) and land use (LU) of the European continent. The aim of the initiative is to dynamically verify the state of the environment in the community area, to provide support for the development of common policies, monitor their effects and propose any corrective measures.

The Corine (Coordination of Information on the Environment) program was launched in 1990, with the first dataset, and it has been updated in 2000, 2006, 2012, 2018. The CLC products are based on the photointerpretation of satellite images carried out by the national teams of the participating States (32 European Union Member States + UK and six cooperating States, total area of 6 Mkm^2),

following a standard methodology and nomenclature with the following characteristics: 44 land cover classes at the third level of the hierarchy, a Minimum Mapping Unit (MMU) of 25 hectares for areal phenomena and a Minimum Mapping Width (MMW) of 100 m for linear phenomena. These products are distributed in the standard European Coordinate Reference System defined by the European Terrestrial Reference System 1989 (ETRS89) datum and Lambert Azimuthal Equal Area (LAEA) projection (EPSG:3035) [26].

Two CLC products were used as reference data to train the Deep Learning model: CLC 2012 and CLC+Backbone 2018.

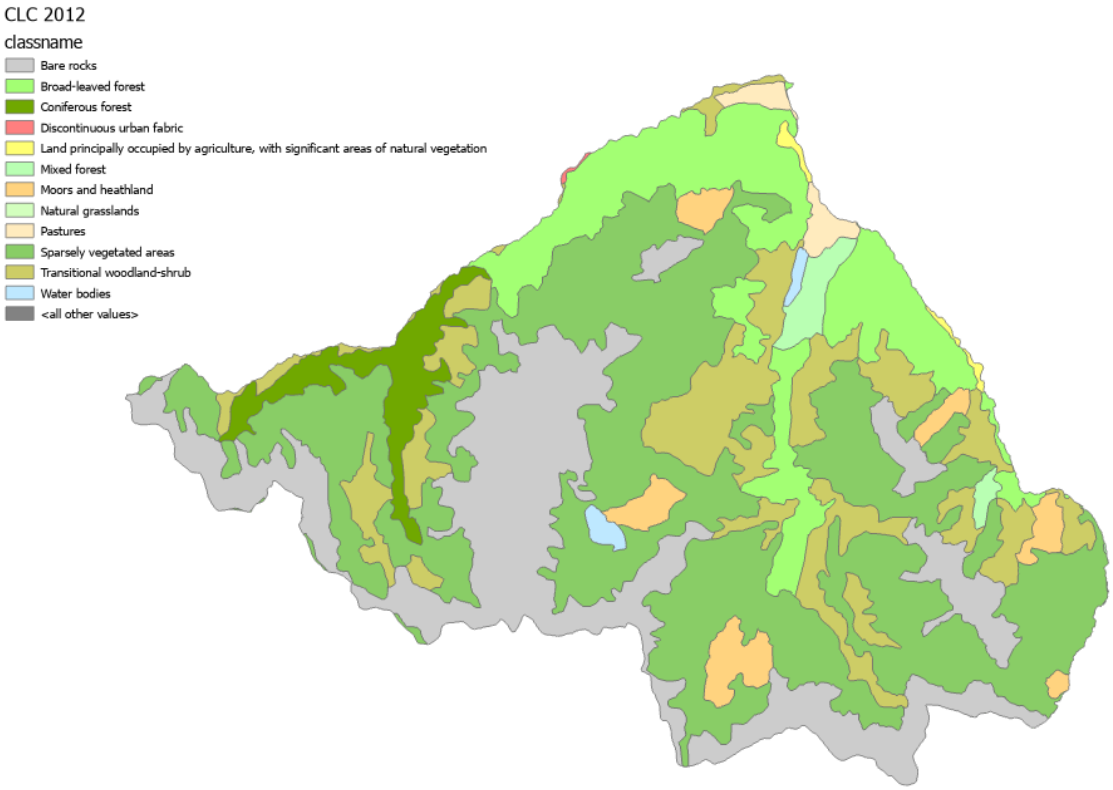

Figure 22 - Corine Land Cover 2012 vector dataset

CORINE Land Cover 2012 provides a dataset with a MMU of 25 ha and a MMW of 100 m for linear phenomena and it is available as vector and as 100 m raster data. This means that objects having less than 25 ha area and 100 m width cannot be present in the database; they are generalized in a neighbouring feature with >25 ha and >100 m width, respectively.

For our area, 12 classes at the third level of hierarchy were detected: discontinuous urban fabric; pastures; broad-leaved forest; coniferous forest; mixed forest; moors and heathland; land principally occupied by agriculture, with significant areas of natural vegetation; natural grassland; sparsely vegetated areas; transitional woodland-shrub; water bodies.

CLC CODE	LABEL 1	LABEL 2	LABEL 3
112	Artificial surfaces	Urban fabric	Discontinuous urban fabric
231	Agricultural areas	Pastures	Pastures
243		Heterogeneous agricultural areas	Land principally occupied by agriculture, with significant areas of natural vegetation
311	Forest and semi natural areas	Forests	Broad-leaved forest
312			Coniferous forest
313			Mixed forest
321		Scrub and/or herbaceous vegetation associations	Natural grassland
322			Moors and heathland
324			Transitional woodland-shrub
332		Open spaces with little or no vegetation	Bare rock
333			Sparsely vegetated areas
512	Water bodies	Inland waters	Water bodies

Table 2 - CLC 2012 classes at three levels of hierarchy

The values of the MMU and MMW parameters and the mixture of land cover and land use classes give some limitations in the use of CLC2012 dataset: the layers are too coarse and human interpretation and combination with other geographical information is needed. In the Accuracy Assessment chapter, we are going to examine this aspect in depth.

Among the improvements carried out by the CLMS, there is the development of a second generation CLC+ products, as the new European baseline for LC/LU monitoring for the future.

CLC+Backbone 2018 provides a pixel-based, multi-temporal Sentinel 2 time series based, wall-to-wall raster product with 10 m spatial resolution and 11 basic land cover classes. Given to a higher spatial resolution, this product provides a more detailed information on land cover than CLC 2012; it has in fact an overall thematic accuracy of 90%, against 85% of CLC2012. It also comprises a vector product, which delineates landscape objects with an MMU of 0.5 ha and assigns 18 classes to each object polygon according to the land cover composition of the raster product; it enriches the raster product in attributes [27].

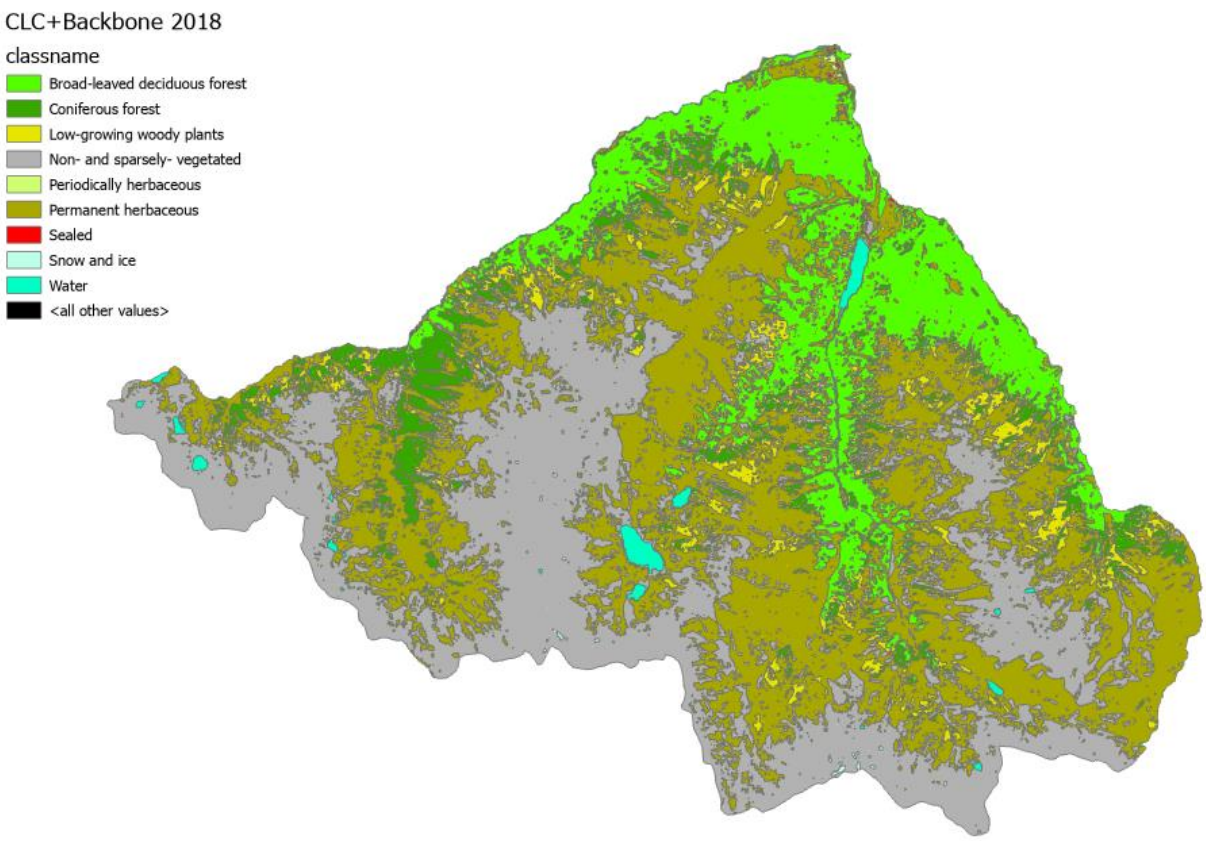

Figure 23 - CLC+Backbone 2018 raster dataset

The classes detected from the raster of our area are nine: sealed (urban fabric); woody – needle leaved trees; woody – broaded decideous trees; low-growing woody plants (bushes, shrubs); permanent herbaceous; periodically herbaceous; non- and sparsely- vegetated; water; snow and ice. The two missing classes are woody – broaded evergreen trees and lichens & mosses.

4.3. Train Deep Learning Model

The Train Deep Learning Model tool trains a DL model using the output from the Export Training Data for Deep Learning tool [16].

- Max epochs: the maximum number of epochs for which the model will be trained. It indicates the number of times that the dataset is passed forward and backward through the neural network.
- Data preparation:
    - Batch Size: the number of trainings to be processed for training at one time. We put it equal to 10.

- Advanced:

- Backbone Model: it specifies the preconfigured neural network that is used as the architecture for training the new model. We chose the ResNet-18: it is a residual network trained on the Imagenet Dataset that contains more than million images and is 18 layers deep.
- Monitor Metric: it specifies the metric that will be monitored while checkpointing and early stopping. We chose "Accuracy": it is the ratio between the number of correct predictions to the total number of predictions. When this value no longer changes significantly, the model will stop.

According to the type of architecture we choose for building the DL model, we have some parameters to set. For the U-Net algorithm:

- Model Arguments:
  - class_balancing: specifies whether the cross-entropy loss inverse will be balanced to the frequency of pixels per class. The cross-entropy loss is a function that measures the dissimilarity in the class distribution: for this reason, the class balancing applies a weight inversely proportional to the frequency of the classes, so that the most distributed ones are not favorited [28].
  - focal_loss: specifies whether focal loss will be used. The focal loss is a function that modifies the cross-entropy loss by introducing a weighting factor; in this way, it reduces the contribution of classes which are better classified [29].
  - mixup: it is a data augmentation technique that mixes up the features of an image and their corrisponding labels, linearly. In this way, overfitting is reduced and the model is more robust against noises and data variations [30].

For the MMSegmentation algorithm:

- Model Arguments:
  - model: the backbone model used to train the model. The default for MMSegmentation is deeplabv3.
  - model_weight: specifies whether pretrained model weights will be used, those coming from MMSegmentation, so that these weights are not chosen randomly. In this way, the training is speed up.

We made several tests for building the best model for the pixel-based classification, with a total of six trials:

1. RGB ICE 2009-2010 imagery, using the polygon of CLC 2012 as training samples, U-Net architecture;
2. RGB+NIR+DTM+NDVI, using ROIs as training samples based on the CLC 2012 classification on the ICE 2009-2010, U-Net architecture;
3. RGB+NIR+DTM, using ROIs as training samples based on the CLC 2012 classification on the ICE 2009-2010 and considering the ARPA Piemonte shapefile of wetlands, U-Net architecture;

4. RGB+NIR+DTM, using ROIs as training samples based on the CLC 2012 classification on the ICE 2009-2010, MMSegmentation architecture;
5. RGB + ExG + DTM, using ROIs as training samples based on the CLC 2012 classification on the ICE 2009-2010, U-Net architecture;
6. RGB + NIR + NDVI, using the polygon of CLC+Backbone 2018 on the AGEA 2018 imagery, U-Net architecture;

5. Accuracy assessment

To measure how good a classifier is, we performed the Accuracy Assessment which is one of the most common methods. It gives back the quality of the information obtained with the classified map, by comparing the classification output with a reference map, in our case the CORINE Land Cover dataset. This comparison consists in the Classification Error Matrix, also called Confusion Matrix [31].

The accuracy assessment of the classification process has been performed on ArcGIS Pro, using three main tools in the Image Analyst Toolsets: Create Accuracy Assessment Points and Compute Confusion Matrix.

With the Create Accuracy Assessment Points tool we import the classification points from the classification map. We generated 300 points for each test, chosen randomly. These points are then compared with the aerial image and with the CLC polygons to check if the classification assigned the right class. Finally, the classified points and the updated points (ground truth points) are used for the computation of the confusion matrix, with the tool Compute Confusion Matrix [32].

This last tool generates a matrix that shows the ground truth points versus the classified points and some other measurements are displayed:

- Omission error: represent pixels that belong to the actual class but fail to be classified into the actual class (ex. 4 pixels which should be classified as c_2 but classified as c_1).
- Commission error: represents the pixels that belong to another class but are classified to a class (ex. 3 pixels of c_1 and 3 pixels of c_2 included in c_3).
- Producer's accuracy: it's the total number of pixels classified correctly for a class, divided by the total number of pixels in that class, as determined from the ground truthing data. In the example:

$$Pa1 = \frac{49}{54} \qquad Pa2 = \frac{40}{47} \qquad Pa3 = \frac{59}{65}$$

  It refers to the probability that a certain feature of an area on the ground is classified as such.
- User's accuracy: it's obtained by dividing the accurately classified pixels by the total numbers of pixels classified in this category. In the example:

$$Ua1 = \frac{49}{57} \qquad Ua2 = \frac{40}{44} \qquad Ua3 = \frac{59}{65}$$

  It refers to the probability that a pixel labelled as a certain class in the map is really this class.
- Kappa Coefficient: it is a multivariate technique that calculates the level of agreement between two qualitative evaluations of the same statistical measures. It gives the accuracy of the entire classification, and it is calculated as follows:

$$K = \frac{N * \sum_{i=1}^{r} x_{ii} - \sum_{i=1}^{r} (x_{i+} * x_{+j})}{N^2 - \sum_{i=1}^{r} (x_{i+} * x_{+j})}$$

  Where:

N is the total number of observations in the matrix
r is the number of rows in the matrix
x_{ii} is the number of observations in row i and column i
x_{i+} is the total number of observations in row i
x_{+j} is the total number of observations in column i
[33]

	c_1	c_2	c_3	Total	U_Accuracy	Kappa
c_1	49	4	4	57	0.8594	0
c_2	2	40	2	44	0.9091	0
c_3	3	3	59	65	0.9077	0
Total	54	47	65	166	0	0
P_Accuracy	0.9074	0.8511	0.9077	0	0.8916	0
Kappa	0	0	0	0	0	0.8357

Figure 24 - Confusion Matrix elements in ArcGIS Pro [32]

The cell where U_Accuracy and P_Accuracy meet represent the Overall Accuracy (OA). It is obtained by dividing the total numbers of correctly classified pixels by the total number of reference pixels.

$$OA = \frac{\sum_{i=1}^{r} x_{ii}}{N}$$

It represents the total classification accuracy.

We didn't use the Update Accuracy Assessment Points tool in ArcGIS Pro as the classification points because the software gave me problems and warnings and the result of the confusion matrix was too low.

5.1. RGB ICE 2009-2011 imagery, CLC 2012 and U-Net

In this trial, the pixel-based classification was performed using only the RGB bands of the 2009-2011 imagery and giving the CLC 2012 polygons as training samples. The architecture for the DL model is U-Net.

The result is the following:

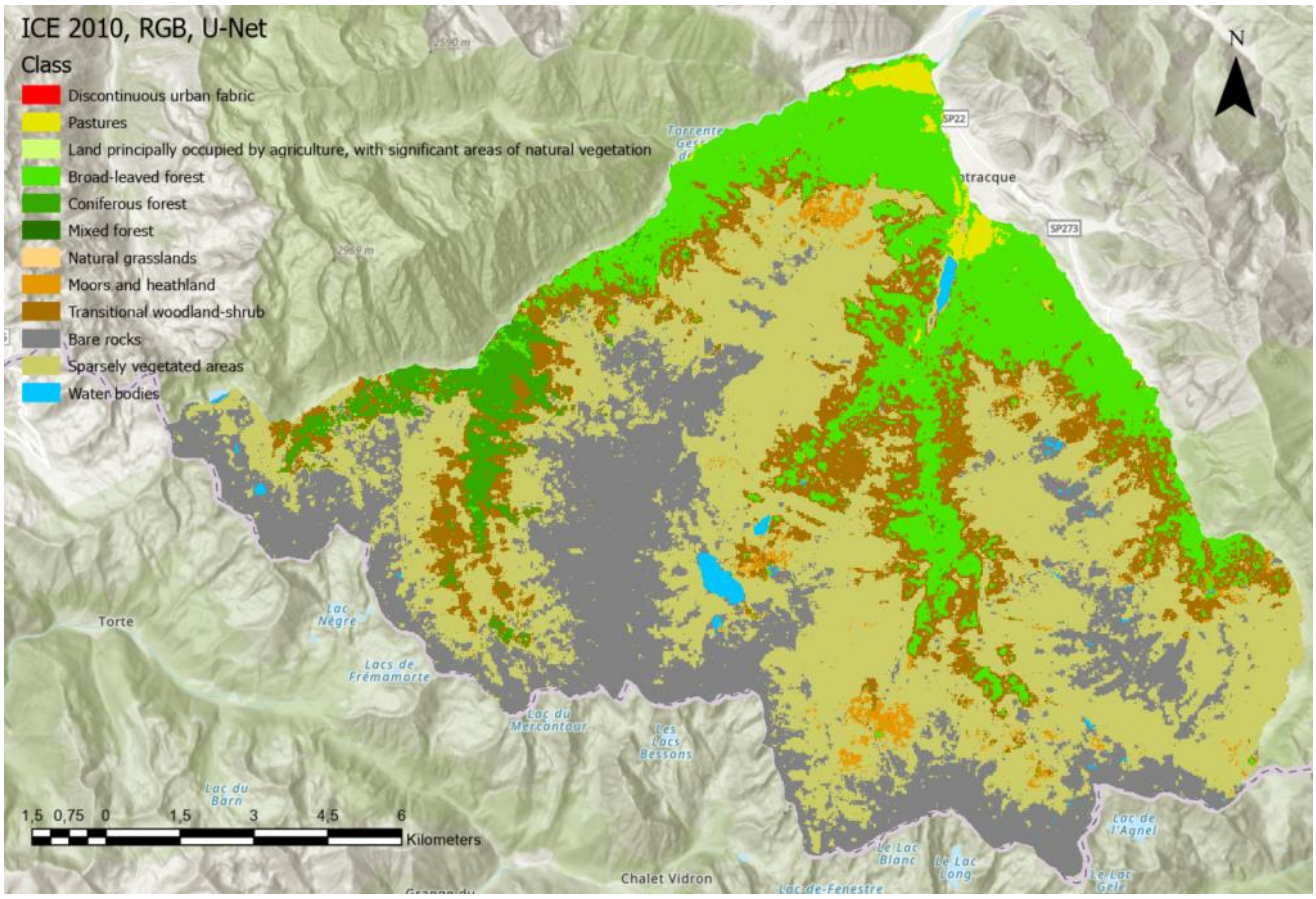

Figure 25 - ICE 2009-2011 classification result with U-Net algorithm, RGB only

The classification is very accurate and fits well the CLC2012 segmentation with a higher detail. Still, the coarse segmentation of CLC dataset makes difficult to classify land at the resolution of our imagery, in fact the OA reaches 65 %.

CLASS VALUE	C_0	C_112	C_231	C_243	C_311	C_312	C_313	C_322	C_324	C_332	C_333	C_512	Total	U accuracy	kappa
C_0	0	0	0	0	0	0	0	0	0	0	0	0	0	0	0
C_112	0	0	0	0	0	0	0	0	0	0	0	0	0	0	0
C_231	0	0	8	1	1	0	0	0	0	0	0	0	10	0,8	0
C_243	0	1	1	2	5	0	0	1	0	0	0	0	10	0,2	0
C_311	0	0	1	0	39	1	0	1	4	1	0	0	47	0,829787	0
C_312	0	0	0	0	0	5	0	0	2	3	0	0	10	0,5	0
C_313	0	0	0	0	0	0	7	0	0	3	0	0	10	0,7	0
C_322	0	0	0	0	1	0	0	8	0	1	0	0	10	0,8	0
C_324	0	0	0	0	11	1	0	3	19	5	0	0	39	0,487179	0
C_332	3	0	0	0	0	0	0	0	0	66	2	0	71	0,929577	0
C_333	0	0	0	0	0	0	0	2	12	51	62	0	127	0,488189	0
C_512	0	0	0	0	0	0	0	0	0	0	0	10	10	1	0
Total	3	1	10	3	57	7	7	15	37	130	64	10	344	0	0
P_Accuracy	0	0	0,8	0,666667	0,684211	0,714286	1	0,533333	0,513514	0,507692	0,96875	1	0	0,656977	0
Kappa	0	0	0	0	0	0	0	0	0	0	0	0	0	0	0,578641

Table 3 - Confusion matrix for Test 1

If we zoom in the raster, we can notice the presence of a squaring effect. The U-Net architecture creates tiles of a certain dimension during the inference phase, but the problem should not be in the model architecture, since this effect is not repeated in the next tests. The cause of the squaring could be due to a lack in spectral bands, linked also to the difference in resolution between the training samples (100 m) and the image (50 cm). The addition of other channels, even with different resolution

(DTM, for example), helps the model to better distinguish classes and provides more topographic and spatial information of the area to the model.

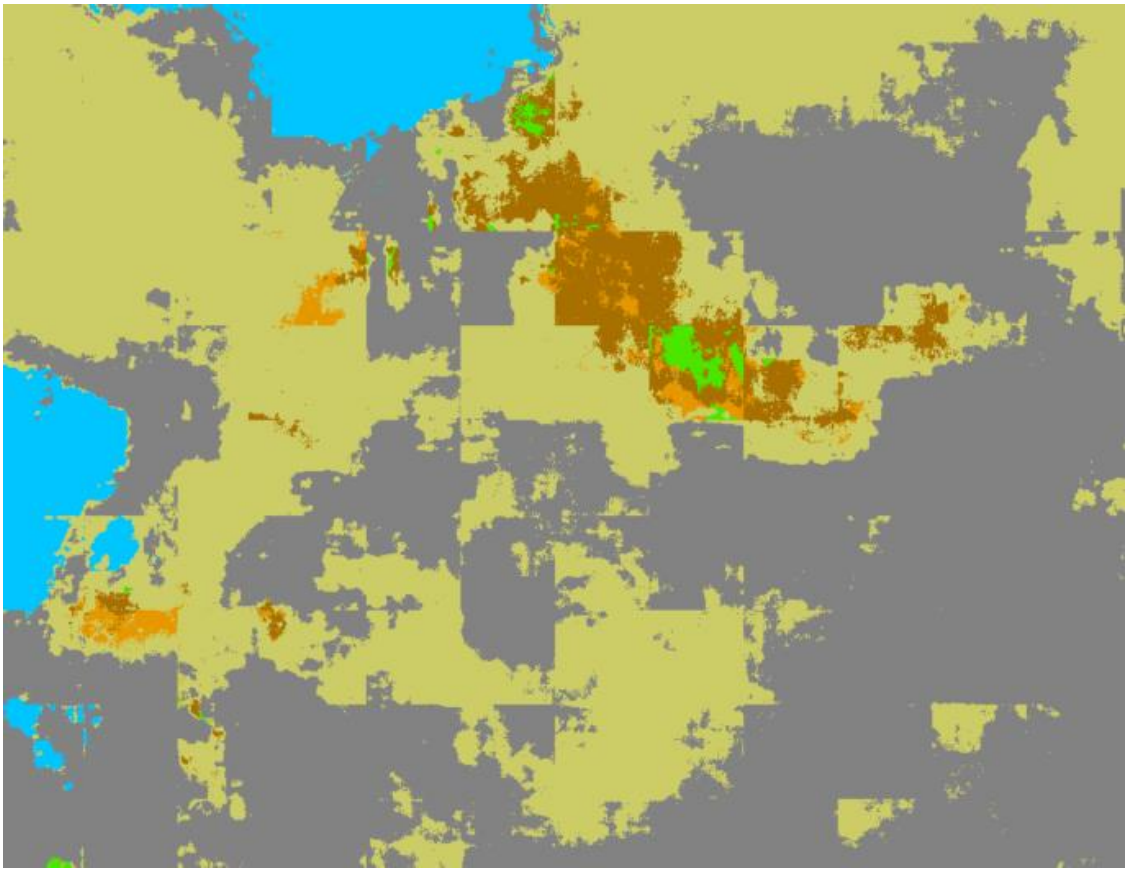

Figure 26 - Squaring effects

5.2. RGB+NIR ICE 2009-2011 imagery with NDVI and DTM, ROIs from CLC 2012 and U-Net

In this case, we do not only use the RGB bands, but also the NIR band, the NDVI calculated for the 2009-2011 imagery and the DTM: all these data were merged with the Composite Band tool in ArcGIS Pro. The DL model is the U-Net with the same parameter of the previous trial. Differently from the antecedent case, we created ROIs as training samples, based on the CLC datasets, and we did not import directly the vector layer of CLC.

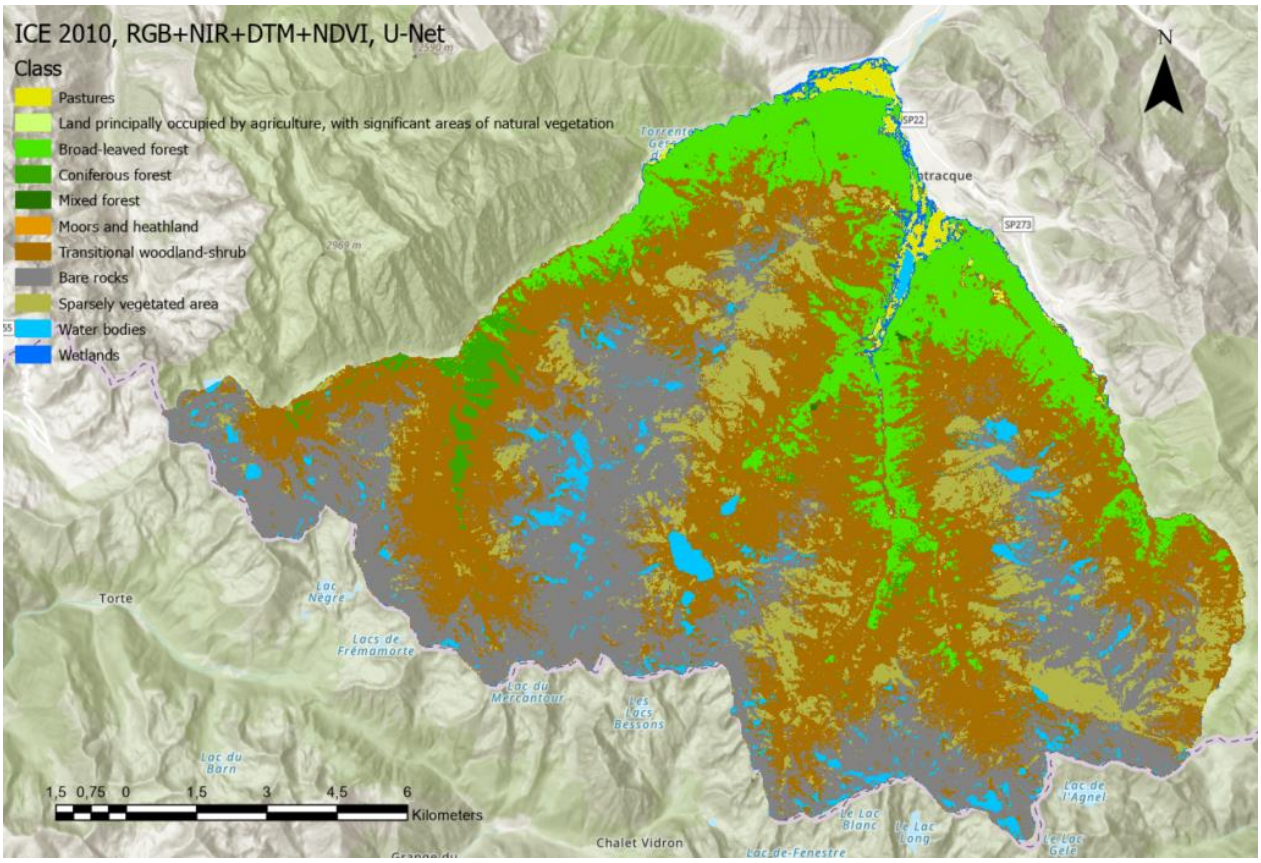

Figure 27 - ICE 2010 classification with RGB+NIR+DTM+NDVI, U-Net

The main problem of this classification is that many shadow areas, especially the rocky ones, are classified as Water. At first, we thought the reason of this error was the addition of NDVI, since it is not correct for ICE 2010 imagery, as we have seen in Chapter 4.2.3. However, this same error is repeated in all successive tests made on ICE 2010, even without the NDVI. We suppose it could be caused by a spectral problem in the NIR band. Moreover, also Transitional woodland class is overestimated, replacing surfaces which in reality belong to the Sparsely vegetated area.

These two errors are repeated for the consecutive tests on ICE 2009-2011.

The OA decreases compared to the first test, from 66% to 55%.

CLASS_VALUE	C_0	C_231	C_243	C_311	C_312	C_313	C_322	C_324	C_332	C_333	C_512	wetland	Total	U accuracy	kappa
C_0	0	0	0	0	0	0	0	0	0	0	0	0	0	0	0
C_231	2	7	0	0	0	0	0	0	0	1	0	0	10	0,7	0
C_243	0	6	0	2	0	0	0	1	1	0	0	0	10	0	0
C_311	0	0	0	39	1	0	0	1	0	0	0	0	41	0,95122	0
C_312	0	0	0	1	8	0	0	1	0	0	0	0	10	0,8	0
C_313	0	0	0	6	0	3	0	1	0	0	0	0	10	0,3	0
C_322	0	0	0	0	0	0	8	0	2	0	0	0	10	0,8	0
C_324	3	0	0	5	3	0	14	10	52	17	0	1	125	0,24	0
C_332	2	0	0	0	0	0	2	1	66	9	0	0	80	0,825	0
C_333	0	0	0	0	0	0	1	0	4	28	0	0	33	0,848485	0
C_512	1	0	0	0	0	0	0	1	6	0	2	0	10	0,2	0
wetland	0	1	0	6	0	0	0	1	0	0	0	2	10	0,2	0
Total	8	14	0	59	12	3	25	37	131	55	2	3	349	0	0
P_Accuracy	0	0,5	0	0,661017	0,666667	1	0,32	0,810811	0,503817	0,509091	1	0,666667	0	**0,553009**	0
Kappa	0	0	0	0	0	0	0	0	0	0	0	0	0	0	**0,465565**

Table 4 - Confusion matrix for Test 2

5.3. RGB+NIR ICE 2009-2011 imagery with DTM, wetlands class ROIs from CLC 2012 and U-Net

The RGB imagery was combined with the NIR band and the DTM. This trial is very similar to the second one, expect for the NDVI absence, and among the training samples we considered another class: wetlands. This class is well characterised in the classification, delineating all water courses in the territory, especially at the border of the area where Gesso della Valletta stream (West) and Gesso di Entracque stream after Diga La Piastra flow and are marked in blue.

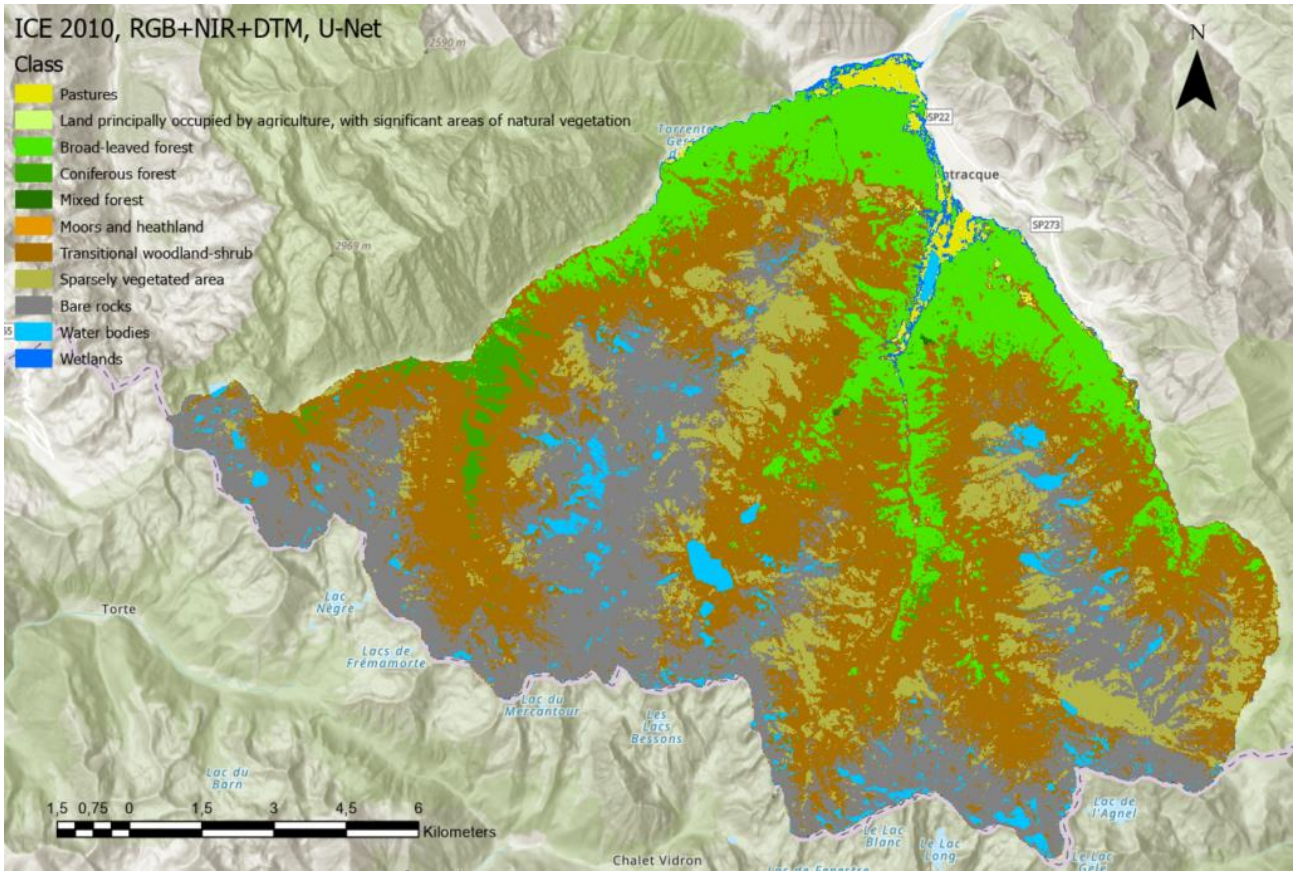

Figure 28 - ICE 2010 classification with RGB+NIR+DTM, U-Net

Also in this case, water is overclassified in the shadow areas. The OA is around 54.8%.

CLASS_VALUE	C_0	C_231	C_243	C_311	C_312	C_313	C_322	C_324	C_332	C_333	C_512	wetland	Total	U accuracy	kappa
C_0	0	0	0	0	0	0	0	0	0	0	0	0	0	0	0
C_231	1	8	0	0	0	0	0	0	1	0	0	0	10	0,8	0
C_243	2	6	0	2	0	0	0	0	0	0	0	0	10	0	0
C_311	0	0	0	29	0	1	2	1	1	0	0	0	34	0,852941	0
C_312	0	0	0	3	6	1	0	0	0	0	0	0	10	0,6	0
C_313	0	0	0	5	0	3	0	2	0	0	0	0	10	0,3	0
C_322	0	0	0	0	0	0	10	0	0	0	0	0	10	1	0
C_324	1	0	0	4	1	0	8	24	44	20	0	2	104	0,230769	0
C_332	0	0	0	0	0	0	1	0	61	3	1	0	66	0,924242	0
C_333	0	0	0	0	0	0	0	0	6	21	0	0	27	0,777778	0
C_512	1	0	0	1	0	0	0	0	7	0	0	0	9	0,1	0
wetland	0	1	0	5	0	0	0	2	0	0	1	2	11	0,2	0
Total	5	15	0	49	7	5	21	29	120	44	2	4	**301**	0	0
P_Accuracy	0	0,533333	0	0,591837	0,857143	0,6	0,47619	0,827586	0,508333	0,477273	0,5	0,5	0	**0,548173**	0
Kappa	0	0	0	0	0	0	0	0	0	0	0	0	0	0	**0,463282**

Table 5 - Confusion matrix for Test 3

5.4. RGB+NIR ICE 2009-2011 imagery with DTM, ROIs from CLC 2012 and MMSegmentation

This trial is equal to the third one, but in this case we adopted another CNN architecture, the MMSegmentation. The goal was to use another DL algorithm for the classification.

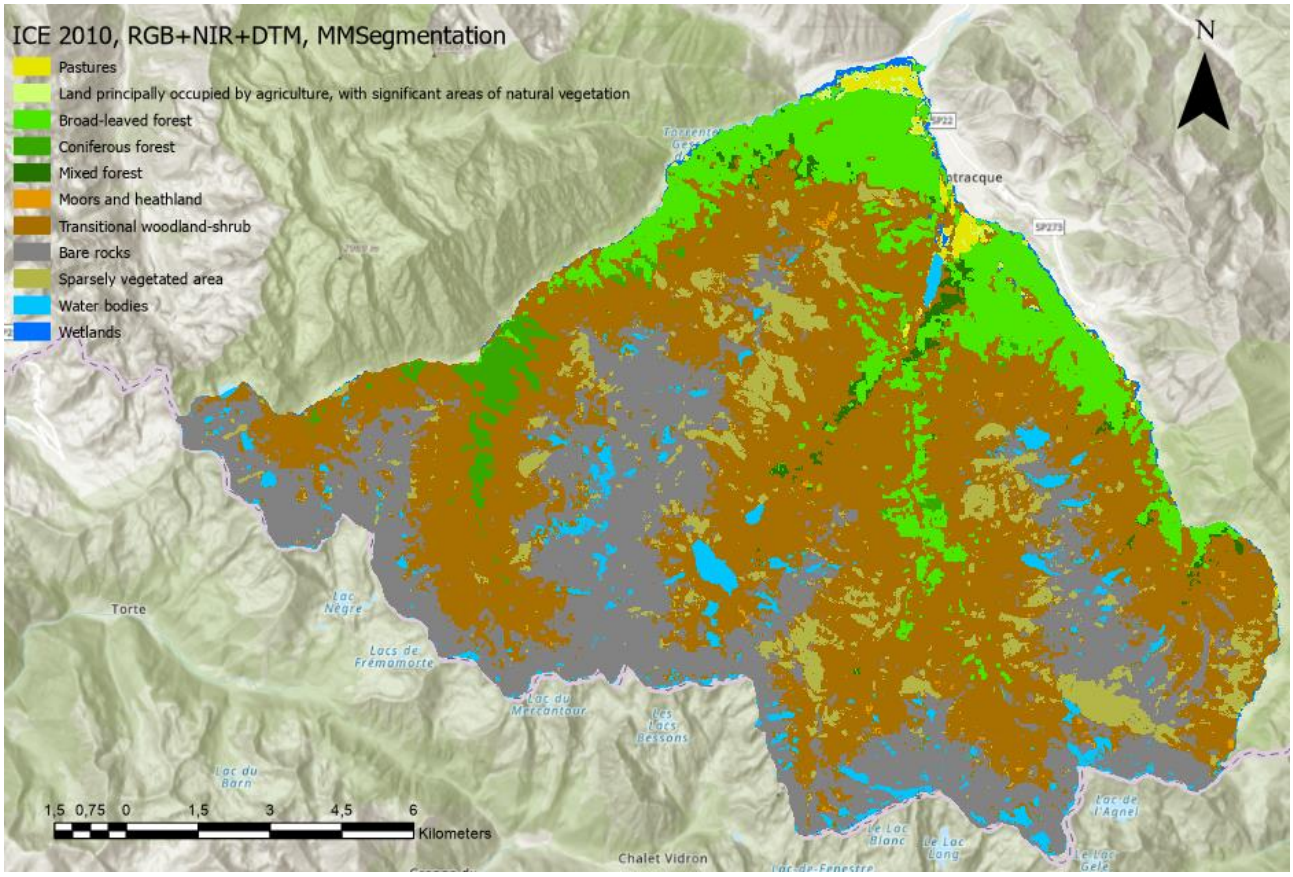

Figure 29 - ICE 2010 classification with RGB+NIR+DTM, MMSegmentation

As already reported, the Bare Rocks class, especially the shadowed areas, are often misclassified as Water bodies, so as Sparsely vegetated surfaces are confused with Transitional woodland zones. Wetland areas are less represented than the previous test.

The OA decreases to 53.4%.

CLASS_VALUE	C_0	C_231	C_243	C_311	C_312	C_313	C_322	C_324	C_332	C_333	C_512	wetland	Total	U accuracy	kappa
C_0	0	0	0	0	0	0	0	0	0	0	0	0	0	0	0
C_231	0	8	1	0	0	0	0	0	0	1	0	0	10	0,8	0
C_243	1	2	2	2	0	0	0	3	0	0	0	0	10	0,2	0
C_311	0	0	0	32	0	1	0	0	0	0	0	0	33	0,969697	0
C_312	0	0	0	1	9	0	0	0	0	0	0	0	10	0,9	0
C_313	0	0	0	5	0	3	1	0	1	0	0	0	10	0,3	0
C_322	0	0	0	0	0	0	8	0	2	0	0	0	10	0,8	0
C_324	0	0	0	13	10	0	13	32	49	29	0	0	146	0,219178	0
C_332	3	0	0	0	0	0	1	0	69	4	0	0	77	0,896104	0
C_333	0	0	0	0	0	0	0	0	4	18	0	0	22	0,818182	0
C_512	1	0	0	1	0	0	0	0	8	0	0	0	10	0	0
wetland	1	0	0	4	0	0	0	0	0	0	0	5	10	0,5	0
Total	6	10	3	58	19	4	23	35	133	52	0	5	**348**	0	0
P_Accuracy	0	0,8	0,666667	0,551724	0,473684	0,75	0,347826	0,914286	0,518797	0,346154	0	1	0	**0,534483**	0
Kappa	0	0	0	0	0	0	0	0	0	0	0	0	0	0	**0,447592**

Table 6 - Confusion matrix for Test 4

5.5. RGB+NIR ICE 2009-2011 imagery with ExG and DTM, ROIs from CLC 2012 and U-Net

Given the inaccuracy of the NDVI for the 2009-2011 imagery, in this trial we exploited another vegetation index, the ExG, combined with the NIR band and the DTM. We did not consider the wetland class.

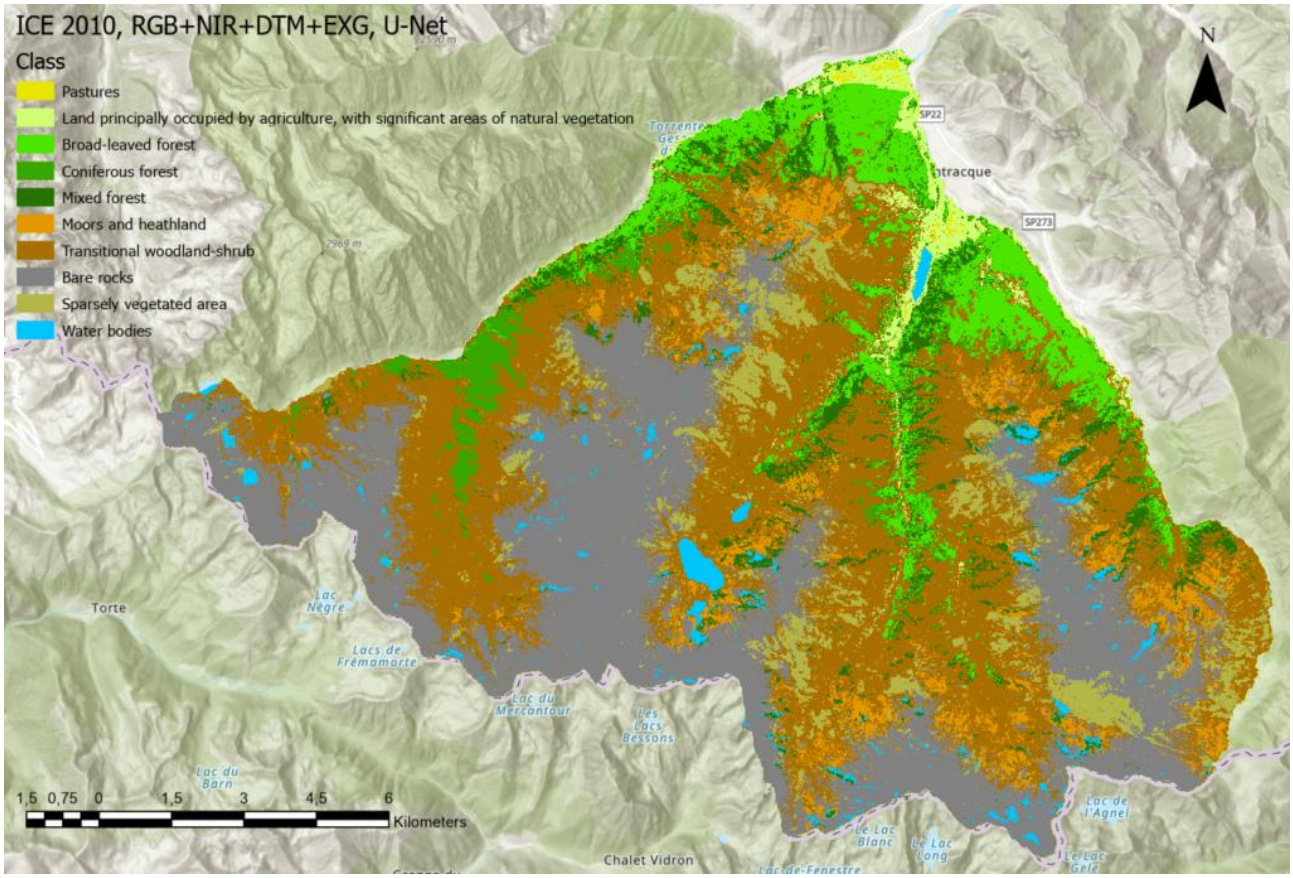

Figure 30 - ICE 2010 classification with RGB+NIR+DTM+ExG, U-Net

The problem with Water overclassification in shadow areas has decrease a lot with respect to previous tests. The error in Transitional woodland-Sparsely vegetated classes remains.

For this reason, the OA remains at 55%.

CLASS_VALUE	C_0	C_231	C_243	C_311	C_312	C_313	C_322	C_324	C_332	C_333	C_512	Total	U accuracy	kappa
C_0	0	0	0	0	0	0	0	0	0	0	0	0	0	0
C_231	2	7	0	0	0	0	0	0	1	0	0	10	0	0
C_243	0	5	0	1	0	0	0	1	2	1	0	10	0	0
C_311	0	0	0	24	0	0	0	1	0	0	0	25	0	0
C_312	0	0	0	4	6	0	0	0	0	0	0	10	0	0
C_313	0	0	0	12	1	0	2	2	2	0	0	19	0	0
C_322	0	0	0	0	0	0	14	1	0	0	0	15	0	0
C_324	0	0	0	11	1	0	11	29	39	22	0	113	0	0
C_332	3	0	0	0	0	0	2	0	78	4	0	87	0	0
C_333	0	0	0	0	0	0	0	0	4	18	0	22	0	0
C_512	0	0	0	0	0	0	0	0	9	0	1	10	0	0
Total	5	12	0	52	8	0	29	34	135	45	1	321	0	0
P_Accuracy	0	0,583333	0	0,461538	0,75	0	0,482759	0,852941	0,577778	0,4	0	0	0,551402	0
Kappa	0	0	0	0	0	0	0	0	0	0	0	0	0	0,453093

Table 7 - Confusion matrix for Test 5

5.6. RGB+NIR AGEA 2018 imagery with NDVI and DTM, CLC+Backbone 2018 and U-Net

The last test was performed on the AGEA 2018 imagery, including the NIR band, DTM and NDVI. The CLC+Backbone 2018 classes were used to the classification process, applying the U-Net algorithm. The final classification result is the following:

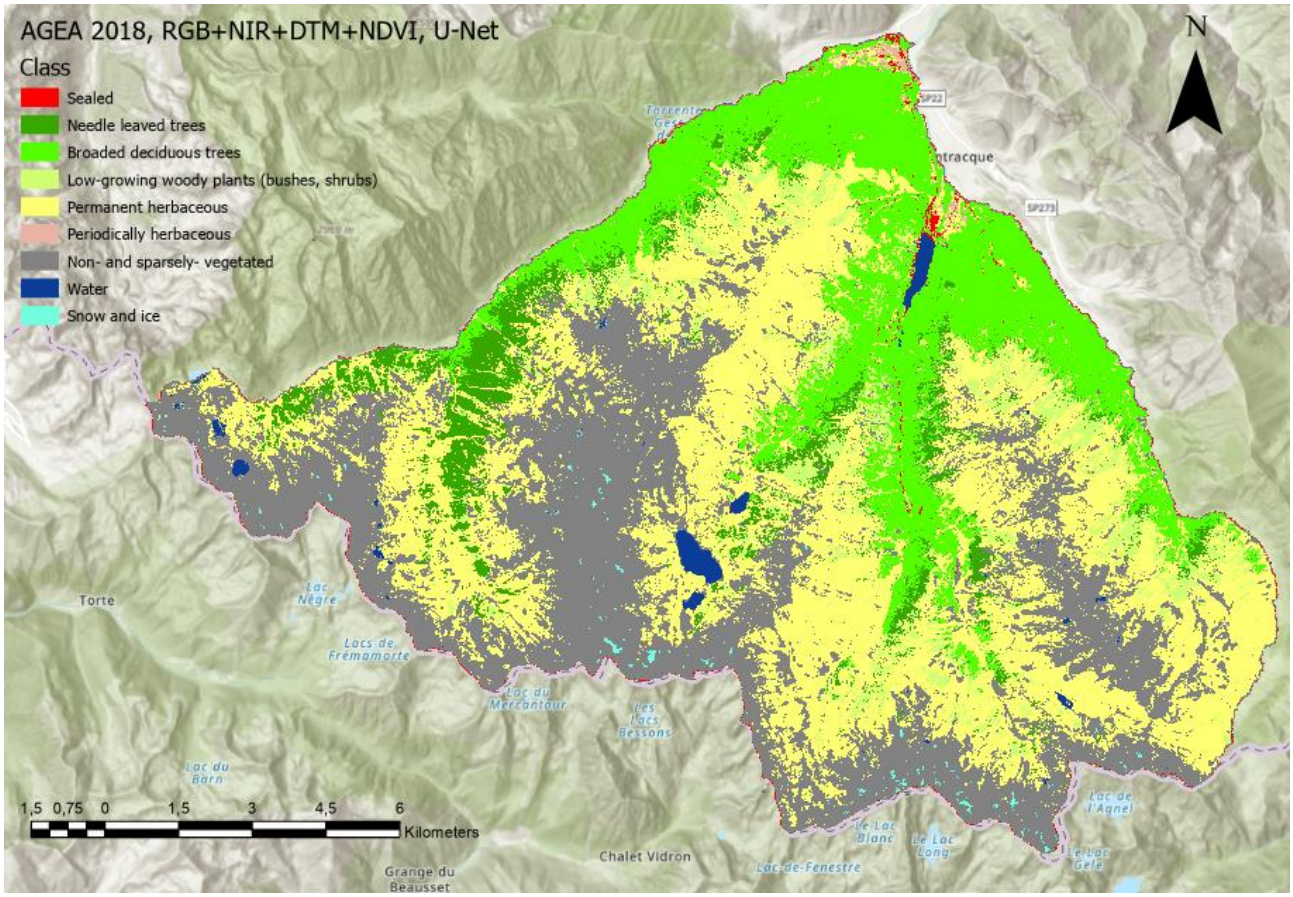

Figure 31 - AGEA 2018 classification with RGB, NIR, DTM and NDVI

Among all tests performed, this shows the best result in terms of Overall Accuracy, with 82%. In fact, from a first look at the classified image, we notice an accurate land cover classification. Of course, there are some errors, especially for two classes: Permanent herbaceous and Non- and sparsely-vegetated, which are confused each other in many cases; furthermore, many areas of Non- and sparsely-vegetated are wrongly classified as Sealed surfaces, especially along water courses like Gesso stream, so as Permanent herbaceous are considered as Periodically herbaceous. For this last aspect, it is difficult to understand the difference between these two classes for our area of interest.

Despite these mistakes, the classification shows high values of accuracy.

CLASS VALUE	C_1	C_2	C_3	C_4	C_5	C_6	C_7	C_8	C_9	Total	U accuracy	kappa
C_1	3	0	1	0	3	0	3	0	0	10	0,3	0
C_2	0	10	2	3	0	0	3	0	0	18	0,555556	0
C_3	0	1	50	0	2	0	0	0	0	53	0,943396	0
C_4	0	0	0	16	0	0	3	0	0	19	0,842105	0
C_5	0	1	0	2	82	0	24	0	1	110	0,745455	0
C_6	0	0	0	0	5	5	0	0	0	10	0,5	0
C_7	0	0	1	0	2	0	89	0	2	94	0,946809	0
C_8	0	0	0	0	0	0	0	10	0	10	1	0
C_9	0	0	0	0	0	0	0	0	10	10	1	0
Total	3	12	54	21	94	5	122	10	13	334	0	0
P_Accuracy	1	0,833333	0,925926	0,761905	0,87234	1	0,729508	1	0,769231	0	0,823353	0
Kappa	0	0	0	0	0	0	0	0	0	0	0	0,770757

Table 8 - Confusion matrix for Test 6

The best classification DL model results in the U-Net model used for AGEA 2018 imagery with CLC 2018 + Backbone class dataset.

TEST	IMAGERY	BANDS	SAMPLES	MODEL	MODEL ARGUMENTS	BATCH SIZE	MAX EPOCH	ACCURACY (OA)
1	ICE 2010	RGB	CLC 2012	U-Net	class_balancing: False focal_loss: False	8	10	0,656
2	ICE 2011	RGB+NIR DTM NDVI	CLC 2012	U-Net	class_balancing: False focal_loss: False	8	10	0,553
3	ICE 2012	RGB+NIR DTM	CLC 2012 + wetland shapefile from Regione Piemonte	U-Net	class_balancing: False focal_loss: False	8	10	0,548
4	ICE 2013	RGB+NIR DTM	CLC 2012 + wetland shapefile from Regione Piemonte	MMSegmentation	model: deeplabv3plus model_weight: False	8	10	0,534
5	ICE 2014	RGB+NIR DTM ExG	CLC 2012	U-Net	class_balancing: True focal_loss: True	8	10	0,511
6	AGEA 2018	RGB+NIR DTM NDVI	CLC 2018 + Backbone	U-Net	class_balancing: True focal_loss: True	8	10	0,823

Table 9 - Resume of all DL model tests

The main problem with CLC 2012 consists in the areas of heterogeneous land cover and small landscape features: they, in fact, typically cause a relatively high uncertainty, due to mixed spectral temporal signals. Similarly, in landscapes with a generally strong mixture of different land cover types at the pixel level it remains sometimes difficult to capture the dominant type for all pixels correctly. In fact, the main difficulties were in some classes like Transitional woodland-shrubs, Land principally occupied by agriculture and Mixed forest, which contain many land cover surfaces, plus the low resolution of CLC2012 (100 m) does not help in characterize in detail the area of our interest [26].

CLC+Backbone 2018 has instead a higher resolution (10 m) and its classes does not create confusion about the land cover.

6. Classification results

Once the best classifier has been identified, the classification was performed to all other orthophotos with the Classify Pixels Using Deep Learning tool. A fine-tuning process was needed before the classification: in Deep Learning, the fine-tuning consists in training a pre-trained model on new datasets. We need to repeat the Export Training Samples for the new image and then the Train Deep Learning Model tool, adding the pre-trained model, in our case the one trained on AGEA 2018 imagery with CLC+Backbone 2018 classes. Unfortunately, for ICE 2009-2011 and AGEA 2015, not having the NIR band, we had to build another model with the same parameters of the one trained on AGEA 2018 with CLC+Backbone 2018, but only for imagery with 4 channels (RGB, DTM); this is because it is not possible to apply a model on imagery with different characteristics.

The result for each orthophoto is the following:

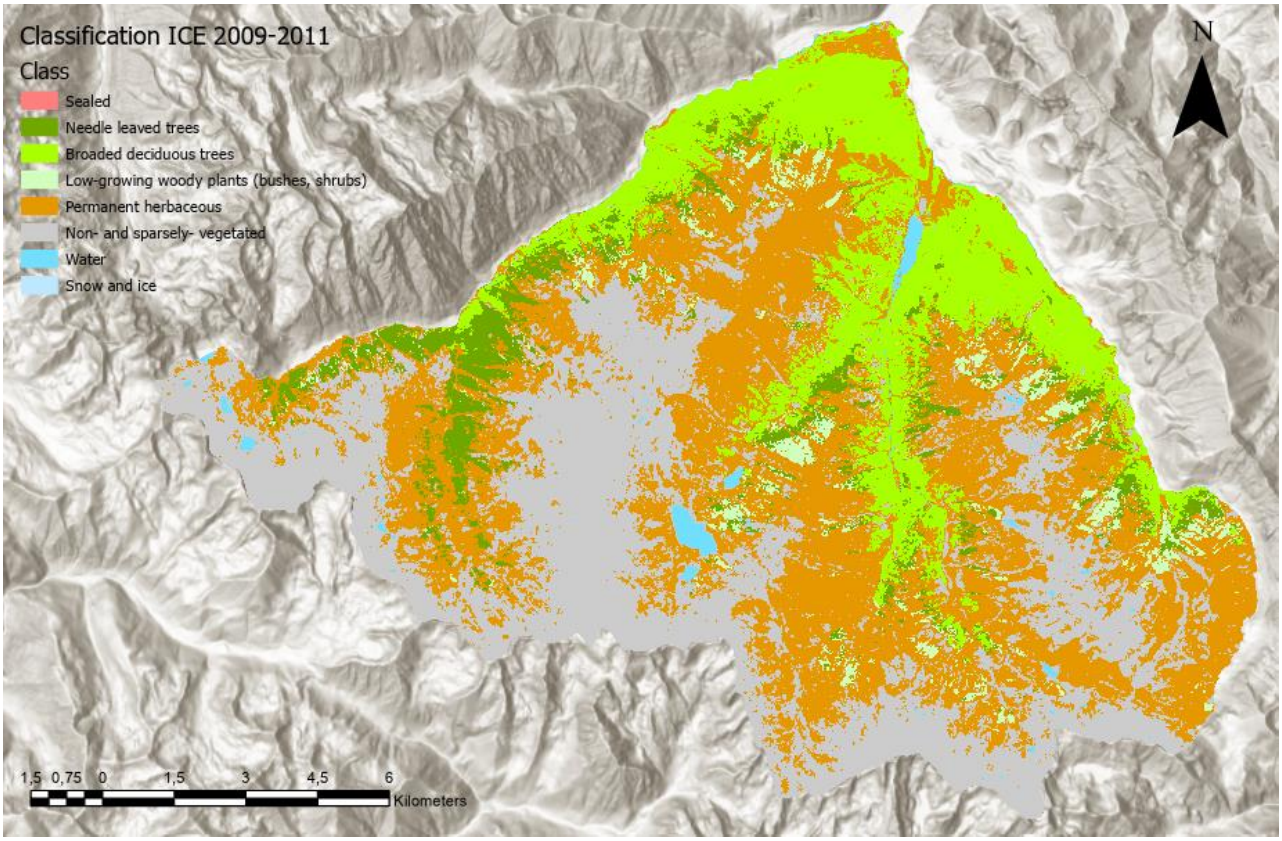

Figure 32 - Classification of ICE 2009-2011

The classification of ICE 2009-2011 shows a good accuracy, higher than the 2018 classification: the OA reaches the 87.76%. Sealed surfaces are better recognized and not classified as rocky surfaces like in previous cases. There are still some shadowed areas classified as water and snow is not well discriminated, often categorized as Non- and sparsely- vegetated. The Periodically herbaceous class was not identified by the model in this imagery.

As already discussed, 2018 classification better discriminates water and snow, but many rocky surfaces are classified as Sealed.

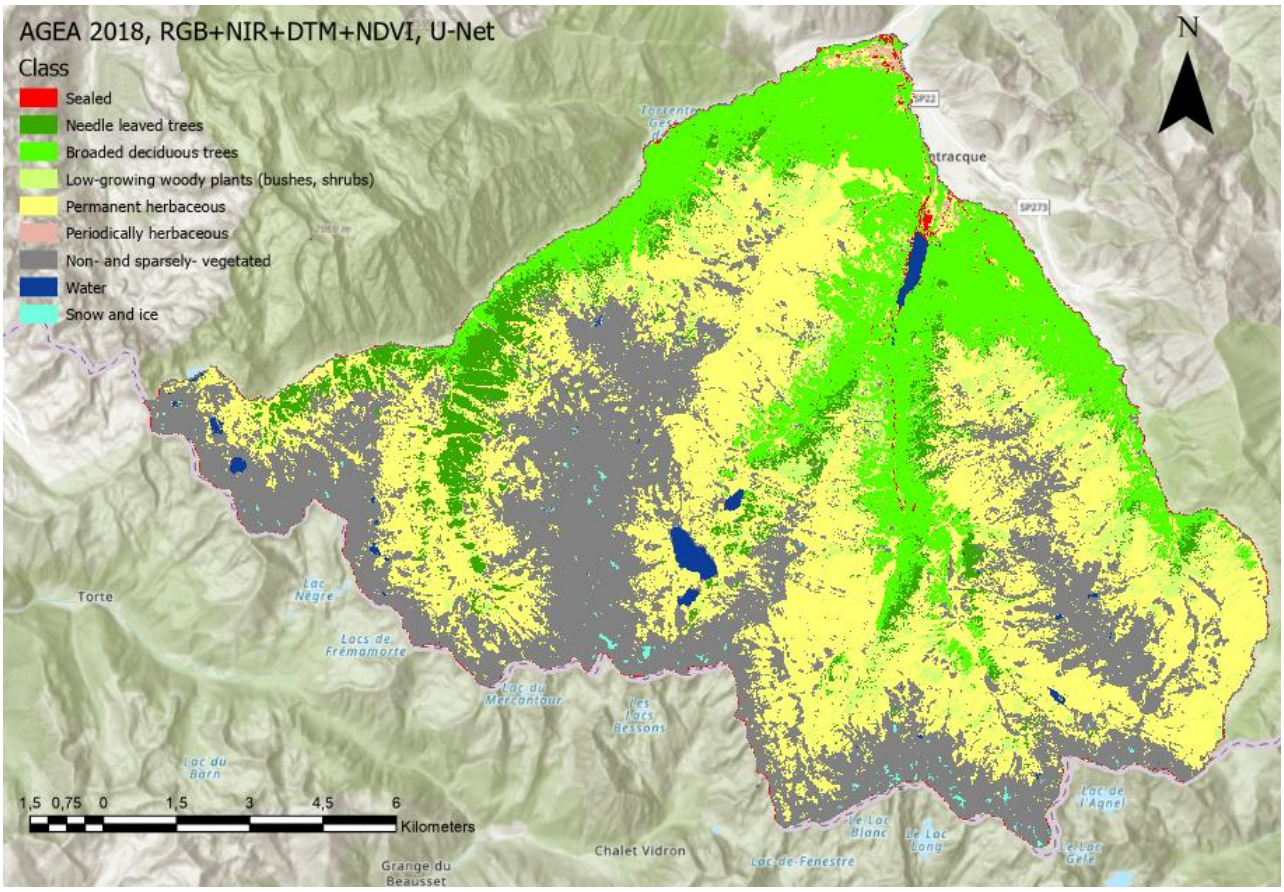

Figure 33 - Classification of AGEA 2018

At the contrary, the 2021 classification is less accurate (77%), in particular the salt-and-pepper effect is present in the classified raster, with isolated pixel erroneously classified as a different class compared to surrounding classes: Non- and sparsely- vegetated is often misclassified as Sealed or Permanent herbaceous surfaces; Snow and Ice is barely represented in the classification and often confused with rocky surfaces; visually, during the manual updating of accuracy points, we noticed that many herbaceous areas were classified as forest.

AGEA 2021 imagery is also darker and shader than other imagery data; as observed, Shadow makes difficult the classification of land cover.

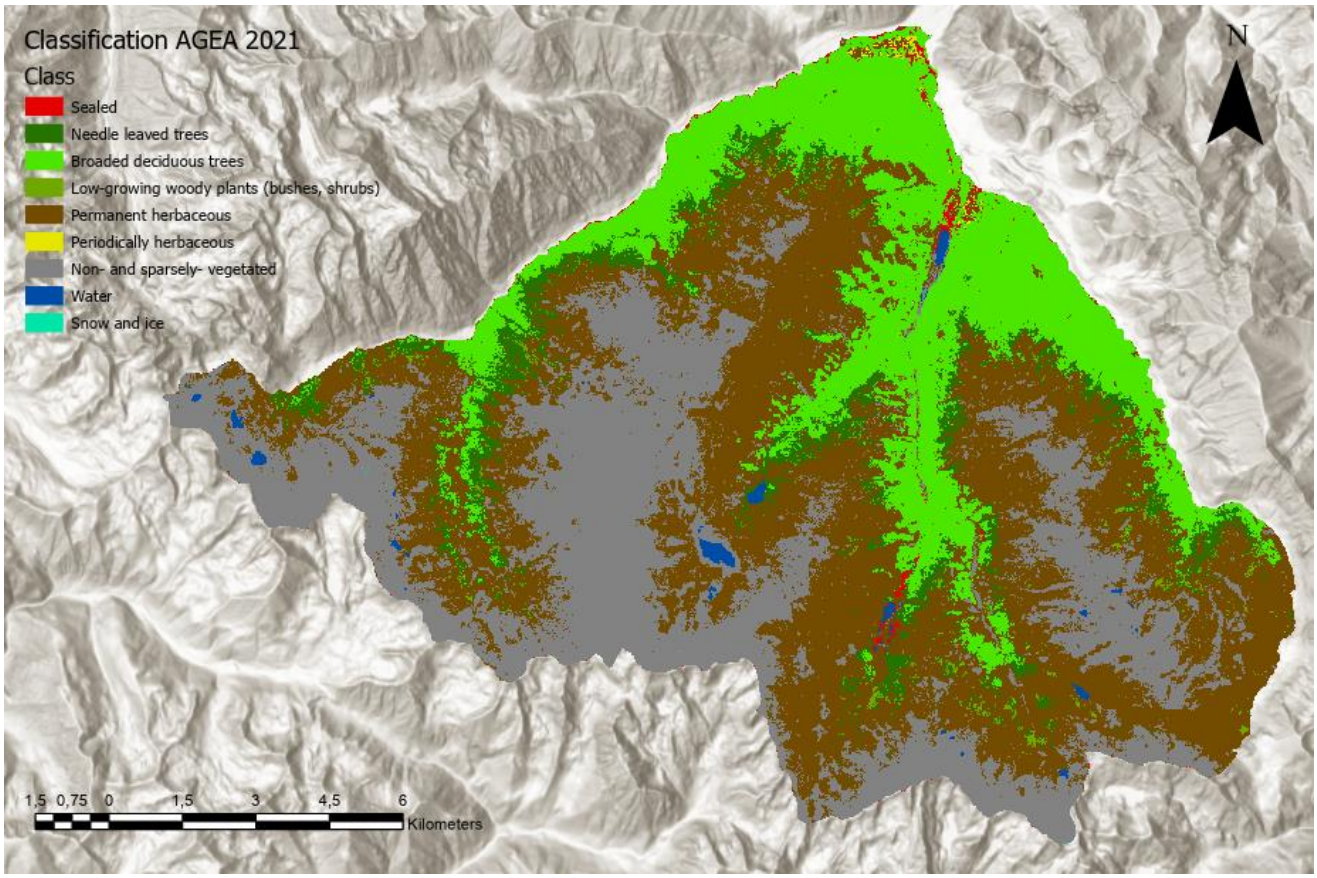

Figure 34 - Classification AGEA 2021

6.1. Change Detection analysis

Always on ArcGIS Pro the Change Detection was carried out: two rasters are compared to detect which classes have changed. Each change is represented by a colour in the output result.

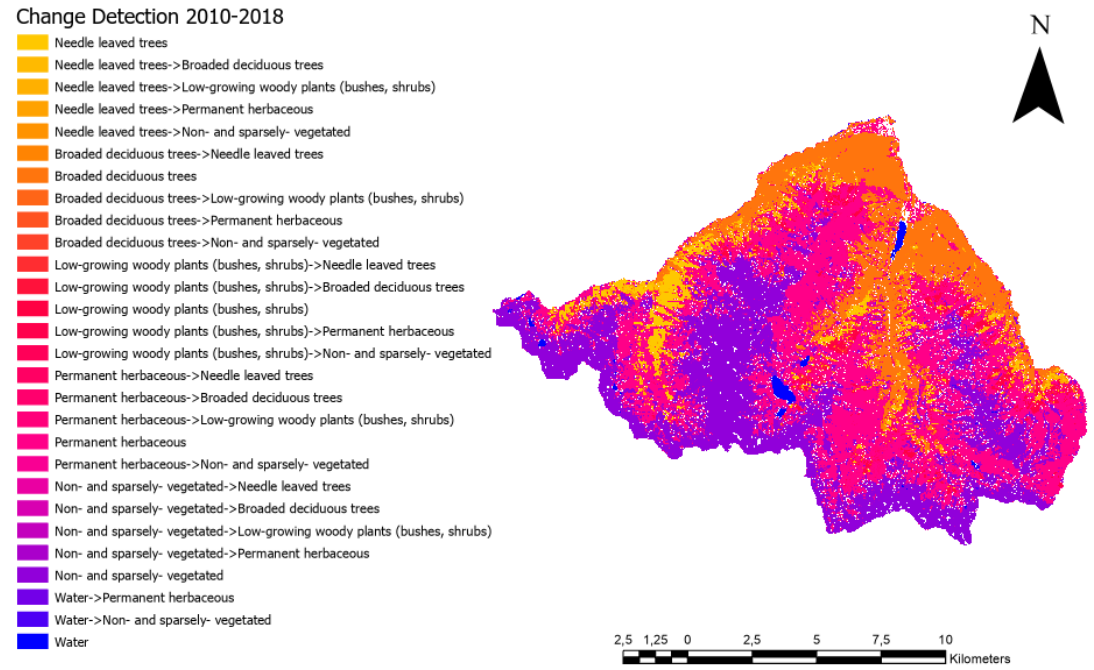

Figure 35 - Change Detection 2010-2018

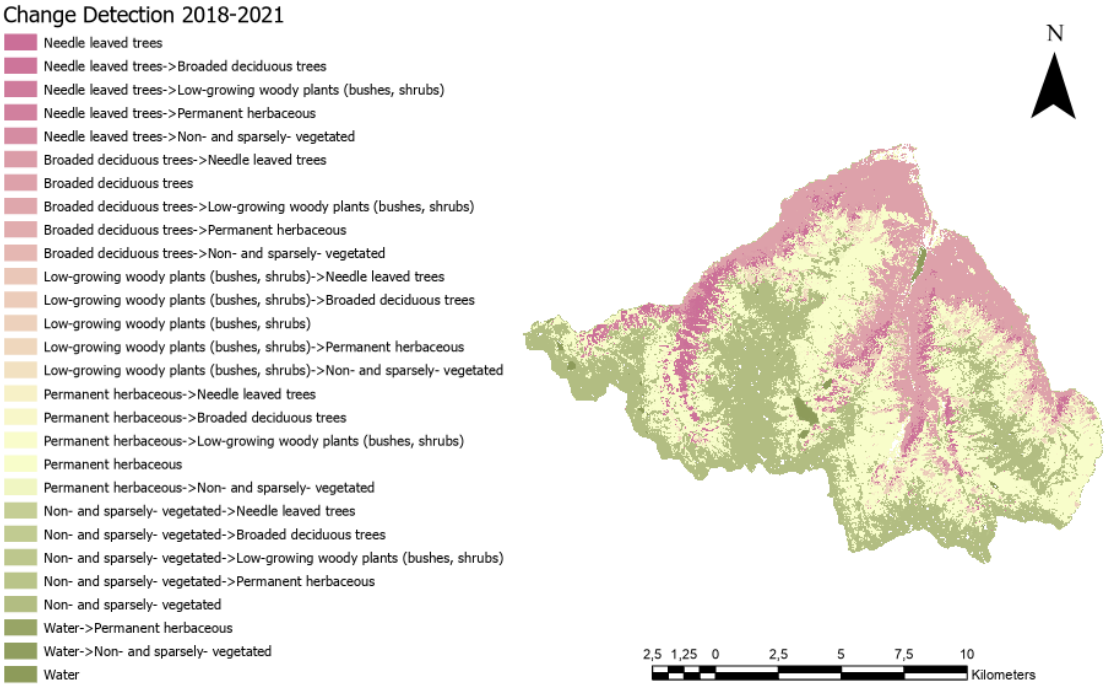

Figure 36 - Change Detection 2018-2021

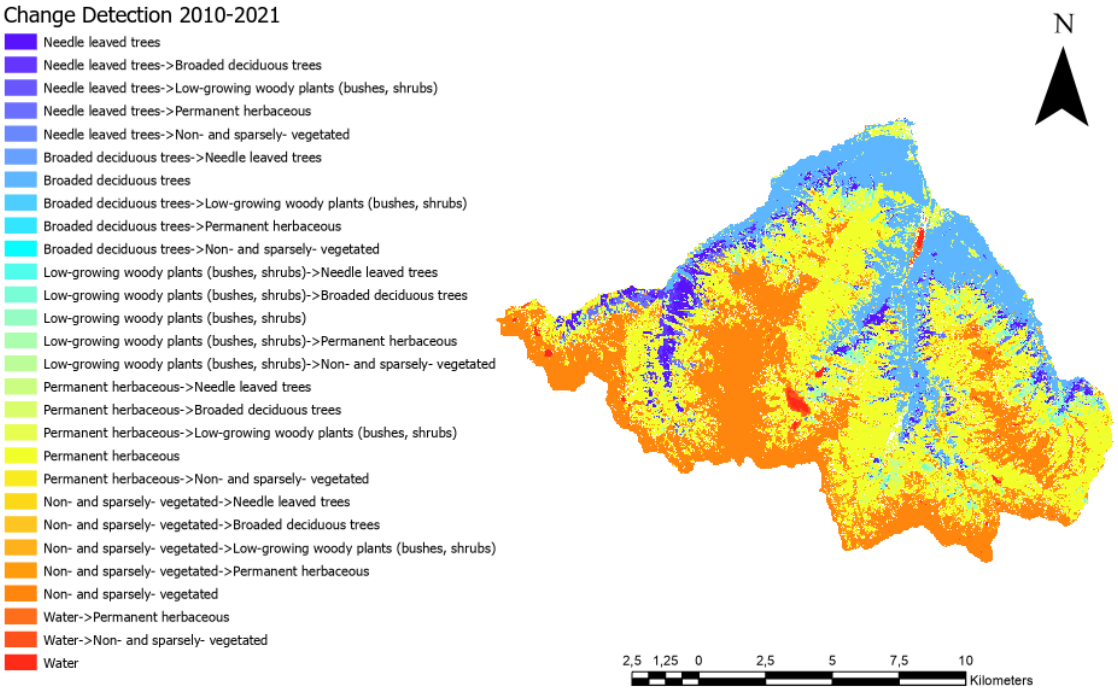

Figure 37 - Change Detection 2010-2021

We only considered changes in vegetation classes, rock class and water.

CLASS CHANGE	Area 2010-2018 (sq.km)	Area 2018-2021 (sq.km)	Area 2010-2021 (sq.km)
Broaded deciduous trees - Low-growing woody plants (bushes, shrubs)	1.04535	0.230433	0.1824488
Broaded deciduous trees - Needle leaved trees	1.80792	4.82971	3.4143292
Broaded deciduous trees - Non- and sparsely- vegetated	1.20335	0.101694	0.06488
Broaded deciduous trees - Permanent herbaceous	0.51912	2.52813	1.4030164
Low-growing woody plants (bushes, shrubs) - Broaded deciduous trees	0.72272	4.4239	1.1453908
Low-growing woody plants (bushes, shrubs) - Needle leaved trees	1.47134	5.6518	2.8357468
Low-growing woody plants (bushes, shrubs) - Non- and sparsely- vegetated	0.0511068	0.741638	0.2957444
Low-growing woody plants (bushes, shrubs) - Permanent herbaceous	2.03525	18.5228	9.8220684
Needle leaved trees - Broaded deciduous trees	5.19207	5.67206	8.0183164
Needle leaved trees - Low-growing woody plants (bushes, shrubs)	5.32921	0.904062	1.0122124
Needle leaved trees - Non- and sparsely- vegetated	0.636945	0.592925	0.3443768
Needle leaved trees - Permanent herbaceous	2.68546	10.08	9.2671032
Non- and sparsely- vegetated - Broaded deciduous trees	0.0710428	1.78697	0.681828
Non- and sparsely- vegetated - Low-growing woody plants (bushes, shrubs)	1.11098	0.0617972	0.1113236
Non- and sparsely- vegetated - Needle leaved trees	0.91764	0.440517	0.546624
Non- and sparsely- vegetated - Permanent herbaceous	18.7223	23.4777	29.0023668
Permanent herbaceous - Broaded deciduous trees	4.80007	5.30988	11.6676964
Permanent herbaceous - Low-growing woody plants (bushes, shrubs)	12.6631	1.23521	1.6560364
Permanent herbaceous - Needle leaved trees	7.70184	6.11616	9.8276192
Permanent herbaceous - Non- and sparsely- vegetated	13.1226	18.4891	17.5438232
Water - Non- and sparsely- vegetated	0.586059	1.2408	1.3857464
Water - Permanent herbaceous	0.160112	0.250748	0.333042
TOTAL	**82.555**	**112.688**	**110.561**

Table 10 - Class area changes in 2018 and 2021

We notice a decrease in the needle leaved trees forest, towards a replacement with broaded deciduous trees forest, which are favoured with warm climate: this trend agrees with rising temperature. In fact, broad-leaved forest has not changed so much.

Firstly, low plants and then permanent herbaceous have increased a lot, occupying wider surfaces than the rock class and other vegetation areas. We suppose that this change is underestimate due to the bad accuracy of 2021 classification.

Lakes contain less water in 2021 than in 2010, we observe this quantity decreases visually through orthophotos. Lake Brocan is a good example of the lowering of the water level and witness of the dry period of 2021. Its area has decreased from 94124.6 m^2 to 30027.6 m^2, while Vej del Bouc area has not changed significantly.

Figure 38 - Brocan Lake in 2010

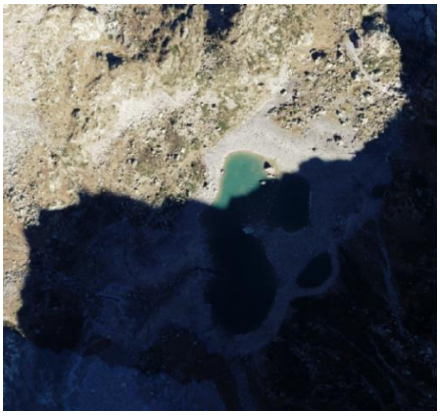

Figure 39 - Brocan Lake in 2021

From the elaboration of change detection data it is possible to obtain other results that confirm what we can immediately visualize from Table 10, like the percentage of change for each class according to the shift.

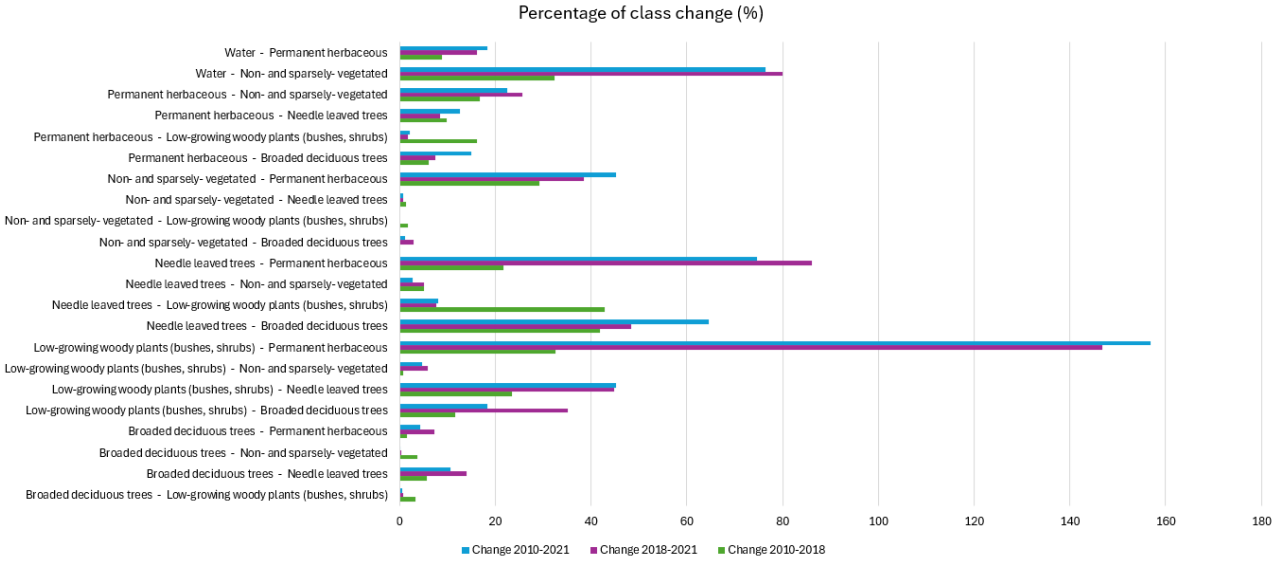

Figure 40 - Percentage of class change with respect to the shift

In fact, from the graph above we observe that major changes occurred from low-growing plants to permanent herbaceous areas, so as needle leaved trees decreased their presence favouring small

plants, while broad-leaved trees have not experienced a significant change in their land cover. As already stated, water quantity in lakes and streams suffered a reduction through years. The most significant changes occurred from 2018 and 2021.

Another parameter that helps to understand how the class area changed is the ratio between the new area of a certain class and the initial area it used to have: if the ratio is higher than 1, the land cover of that class has increased; if lower than 1, the area has decreased; equal to 1, the area of the class has remained unchanged.

	Ratio 2010-2018	Ratio 2018-2021	Ratio 2010-2021
Needle leaved trees	0.9422	0.9933	0.9359
Broaded deciduous trees	1.0721	1.1262	1.2074
Low-growing woody plants	2.0155	0.1489	0.3002
Permanent herbaceous	0.9165	1.1297	1.0355
Non- and sparsely- vegetated	0.9518	0.9788	0.9316
Water	0.8564	0.6794	0.5818

Table 11 - Ratio area for each land cover class

From this ratio another parameter can be calculated, the percentage of variation of each class:

$$V\ (\%) = (Ratio - 1) * 100$$

Figure 41 - Variation of land cover classes in time

From a first wide spread of low growing woody plants from 2010 and 2018, followed by a straight reduction in favour of permanent herbaceous surfaces. Rocky areas and needle-leaved tree forest have decreased in land cover, the water level of basins have diminished, while broad-leaved forest have increased their presence in the territory.

7. Weather data

Another goal of this thesis is to implement weather and climate data with the results of the change detection analysis made with Deep Learning techniques, to find a correlation between the change in land cover and climate variables.

Weather data are provided by ARPA Piemonte for a total of 17 station, representative of our area of interest, Valle Gesso [34]:

STATION	OWNER BODY	ALTITUDE (m)	PERIOD	PARAMETERS
Argentera	ARPA Piemonte	1680	1996-2023	T, T_{max}, T_{min}, P
Boves	ARPA Piemonte	575	1988-2023	T, T_{max}, T_{min}, P
Chiusa Pesio	ARPA Piemonte	935	1997-2023	T, T_{max}, T_{min}, P
Colle Lombarda	ARPA Piemonte	2305	1988-2023	T, T_{max}, T_{min}, P
Cuneo Cascina Vecchia (*)	ARPA Piemonte	575	2003-2023	T, T_{max}, T_{min}, P
Demonte (*)	ARPA Piemonte	765	2002-2023	T, T_{max}, T_{min}, P
Diga Chiotas (*)	ARPA Piemonte	2020	2002-2023	T, T_{max}, T_{min}, P
Diga Piastra (*)	ARPA Piemonte	950	2002-2023	T, T_{max}, T_{min}, P
Monte Malanotte	ARPA Piemonte	1735	1988-2023	P
Neraissa	ARPA Piemonte	1433	1989-2023	T, T_{max}, T_{min}, P
Palanfrè (*)	ARPA Piemonte	1625	2002-2023	T, T_{max}, T_{min}, P
Pradeboni (*)	ARPA Piemonte	985	2002-2023	T, T_{max}, T_{min}, P
Rifugio Mondovì	ARPA Piemonte	1760	1998-2023	T, T_{max}, T_{min}, P
Rocca dell'Abisso (*)	ARPA Piemonte	2753	2003-2023	T, T_{max}, T_{min}
S. Giacomo Demonte	ARPA Piemonte	1297	2000-2023	T, T_{max}, T_{min}, P
Valdieri	ARPA Piemonte	1390	1994-2023	T, T_{max}, T_{min}, P
Vinadio S. Bernolfo	ARPA Piemonte	1695	2000-2023	T, T_{max}, T_{min}, P

Table 12 - Weather stations for the area of interest (T: mean daily temperature [°C], Tmax: maximum daily temperature [°C], Tmin: minimum daily temperature [°C], P: precipitation [mm])

Weather stations record the daily temperature (mean, maximum and minimum) and the daily precipitation. They are automated and record various parameters in real time with standardized measurement criteria, according to the World Meteorological Organization.

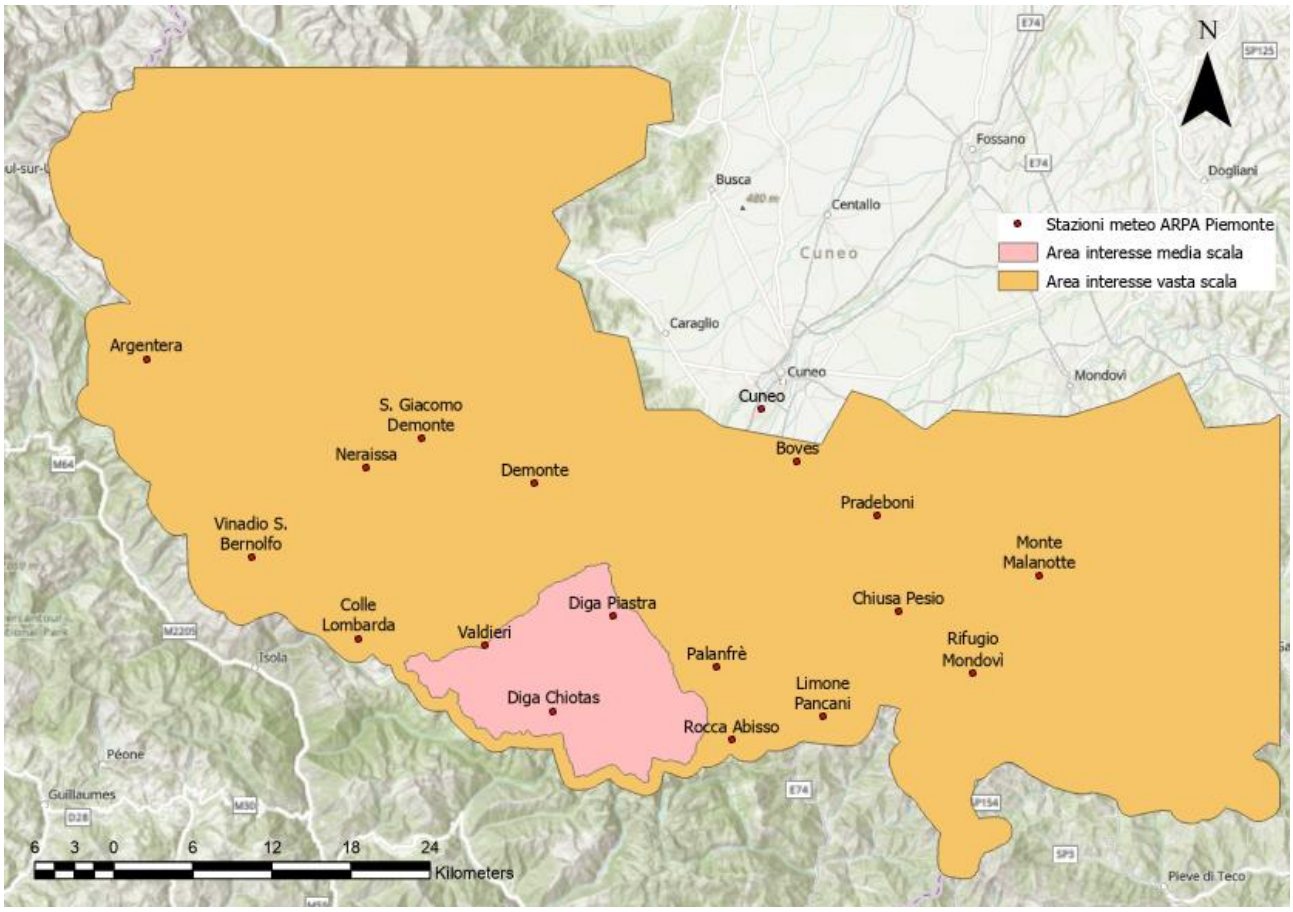

Figure 42 - Weather stations from ARPA Piemonte in our territory of interest

7.1. Temperature

For lack of continuous and homogeneous data series, we cannot make a climate analysis over a period of at least 30 years for the majority of weather stations. According to the number of stations, the period of time for the analysis is 2000-2021. There are 11 stations with this same period in common, with a complete series of data: Argentera, Boves, Chiusa Pesio, Colle Lombarda, Neraissa, Rifugio Mondovì, S. Giacomo Demonte, Valdieri, Vinadio S. Bernolfo. To improve the representativeness of the geography, we also included other 6 stations, as suggested by Luca Mercalli in "Ultimi ghiacci – Clima e ghiacciai nelle Alpi Marittime", with shorter or incompleted periods: Cuneo Cascina Vecchia, Demonte, Diga del Chiotas, Diga La Piastra, Limonte Pancani, Palanfrè, Pradeboni, Rocca dell'Abisso. For Diga del Chiotas and Diga La Piastra it was not possible to find longer series from ENEL Power Plant stations.

STAZIONE	QUOTA	DATI	Gennaio	Febbraio	Marzo	Aprile	Maggio	Giugno	Luglio	Agosto	Settembre	Ottobre	Novembre	Dicembre	ANNO
Argentera	1680	Tmax	2,480276149	3,76578034	6,785191	9,703333	14,016276	19,065909	21,58935	21,445308	16,61242424	11,884961	5,902978056	2,407427445	11,30493407
		Tmin	-6,89459734	-6,73752799	-3,887243	-0,66015	2,916129	6,7716667	8,575083	8,459824	5,055120167	1,7090616	-2,524545455	-5,719462823	0,588613005
		T	-2,61632258	-2,13899463	0,771994	3,857424	8,0741935	12,611818	14,75275	14,345161	10,21954545	6,1283187	1,033939394	-1,960324603	5,423291661
Boves	575	Tmax (°C)	7,473753666	9,118025078	13,24675	16,60818	21,08563	26,096061	28,20544	27,430235	22,93509091	16,942082	11,07971787	8,012346041	17,35277573
		Tmin (°C)	-3,06979472	-1,98881653	1,670943	5,505235	9,4768328	13,785303	15,38182	15,063592	11,22836364	7,1165689	2,099008621	-2,048973607	6,185006755
		T(C°)	1,082844575	2,622469772	6,919871	10,87591	15,157918	19,792403	21,73783	20,997361	16,6480303	11,51217	5,858176594	1,807038123	11,25100175
Chiusa Pesio	935	Tmax	4,76801564	6,197480967	9,971114	12,91697	17,208548	21,8	23,82566	23,25088	18,66969697	13,253079	8,077121212	4,9771261	13,74297434
		Tmin	-3,93900293	-3,26955889	-0,126833	3,315455	7,1806452	11,221515	12,87947	12,71803	9,284545455	5,3324047	0,859848485	-2,641788856	4,401227701
		T	-0,70320137	0,321680475	3,951026	7,607176	11,926833	16,247424	18,08739	17,572581	13,47606061	8,7319648	3,619242424	0,090762463	8,410744989
Colle Lombarda	2305	Tmax	0,257886675	0,559375597	2,70223	4,927931	9,2459929	13,084265	15,66317	15,569648	11,37462382	8,0032994	3,142866097	0,917783499	7,120755987
		Tmin	-6,761892	-7,1232373	-5,26057	-2,73748	1,081334	5,8543723	7,912317	7,8516129	4,251217346	1,3142061	-3,194084372	-5,733019934	-0,212101664
		T	-3,42524886	-3,80971142	-1,971258	0,328136	4,6660836	9,2599849	11,66943	11,459677	7,531818182	4,4275811	-0,214081844	-2,574554563	3,112321228
Cuneo Cascina Vecchia (*)	575	Tmax	8,302037351	9,53896811	13,67997	17,32632	21,658234	26,641754	29,05484	28,281064	23,7577193	17,449236	11,74508772	8,978098472	18,03444334
		Tmin	-1,86757216	-0,68462536	3,075552	7,041579	10,783871	15,377193	17,42649	16,950934	13,35491228	8,4473684	3,205789474	-0,834295416	7,68976594
		T	2,363327674	3,616107078	7,832088	11,82211	15,849406	20,601579	22,88591	22,088455	17,87017544	12,293379	6,797894737	3,139728353	12,26334612
Demonte (*)	765	Tmax	6,866612903	8,700795475	12,49416	15,5665	19,757097	24,785	26,84177	26,210323	21,89433333	16,142742	10,5465	6,670967742	16,37306674
		Tmin	-5,02016129	-3,98102833	-0,35629	3,554333	6,8967742	11,2625	13,16742	12,615645	9,300333333	4,8958065	0,369666667	-3,742096774	4,080241815
		T	-0,32967742	1,292918719	5,530484	9,6175	13,551129	18,267833	20,32919	19,557903	15,32216667	10,013871	4,586	0,288387097	9,83564242
Lago Chiotas (*)	2020	Tmax	2,297580645	2,567986453	4,546452	6,500333	10,197742	15,082393	17,70288	17,401774	13,39961494	9,5706774	4,885833333	2,976084538	8,92744602
		Tmin	-4,98306452	-5,71847906	-3,617097	-0,59283	3,2375806	8,1840833	10,50559	10,319516	6,59145977	3,1206344	-1,157666667	-3,670656285	1,851588933
		T	-1,76983871	-2,26717365	-0,190199	2,446167	6,3982258	11,423917	13,96291	13,538387	9,518247126	6,0118495	1,527166667	-0,721501669	4,989846278
Lago Piastra (*)	950	Tmax	5,899193548	7,203472906	11,03323	14,23533	18,337581	23,0725	25,65306	25,150484	20,78133333	15,290645	9,571166667	6,256188172	15,20701566
		Tmin	-1,72112903	-1,37256773	1,533548	4,732	8,0591935	12,271833	14,40065	14,285974	10,95183333	6,7033871	2,472833333	-0,555612903	5,98016156
		T	1,18016129	1,92669335	5,389032	8,948833	12,811452	17,2535	19,49097	18,997058	14,94766667	10,029032	5,11	1,939408602	9,835317098
Neraissa	1433	Tmax	4,631336406	5,586793338	8,179109	10,51222	14,406911	19,065773	21,45466	21,133284	16,6630303	11,833333	7,023935413	4,832872504	12,11027196
		Tmin	-3,56304985	-3,36997313	-0,772287	2,156364	5,9876253	9,9943528	12,01711	11,773072	8,106956522	4,6298177	0,286818182	-2,682111437	3,713724556
		T	-0,12536657	0,397690671	3,258065	5,975909	9,9799772	14,429138	16,62581	16,219355	11,95848485	7,6563587	3,111060606	0,642517107	7,510749619
Palanfrè (*)	1625	Tmax	3,302080645	4,671169723	8,091785	9,988167	12,622903	17,36992	19,73009	19,249544	15,07193678	11,098871	6,387241379	3,655384946	10,93659126
		Tmin	-4,28374194	-4,44546045	-1,919677	1,298167	5,1153226	9,7188218	11,78563	11,561641	7,923431034	3,9774194	-0,2745	-3,073551613	3,115291734
		T	-0,91228495	-0,88794506	1,952296	4,764464	8,7169355	13,52358	15,72734	15,20425	11,1228046	6,9396774	2,506609195	0,009667742	6,555616454
Pradeboni (*)	985	Tmax	5,96196944	6,466809985	9,89219	13,48567	17,720161	22,648948	24,63181	23,748484	19,08181609	13,214952	8,690666667	6,631446237	14,34791003
		Tmin	-0,90730051	-0,59172932	2,626486	6,055333	9,6458065	14,309833	16,3063	15,849543	12,24617816	7,7710968	3,3865	0,317419355	7,251288538
		T	2,132258065	2,3975888	5,874363	9,492667	13,353871	18,095	20,14214	19,407753	15,31025862	10,228242	5,7475	3,063129032	10,43706406
Rifugio Mondovì	1760	Tmax	1,912170931	3,098648909	5,945596	7,973213	11,110547	15,446061	17,80721	17,461696	13,1665465	9,8190518	5,114968652	2,462649408	9,276530264
		Tmin	-4,85810641	-5,11546595	-2,703812	0,152424	4,0664223	8,545303	10,48019	10,420797	6,658484848	3,2021408	-1,090606061	-3,704873934	2,171074816
		T	-1,52052786	-1,54993036	0,880499	3,448192	7,4618524	12,044091	14,23123	13,893773	9,76030303	6,3073021	1,862178683	-0,614640341	5,517027016
Rocca dell'Abisso (*)	2753	Tmax	-2,2852292	-2,6356862	-1,040068	1,341059	5,2371817	9,7754386	12,35857	12,098812	8,381403509	5,2311404	0,5	-1,363616299	3,966584049
		Tmin	-8,61528014	-9,40042131	-7,702886	-4,9398	-1,060781	3,9770175	6,447029	6,2672326	2,617719298	-0,455539	-4,922631579	-7,387572156	-2,097992794
		T	-5,64872666	-6,29375666	-4,692699	-2,07736	1,8042445	6,6973684	9,297623	9,0460102	5,341754386	2,2887521	-2,260350877	-4,513288059	0,749131219
S. Giacomo Demonte	1297	Tmax	2,98350801	5,811839454	8,894345	11,30652	15,248094	19,748994	22,00205	21,701906	17,25393939	12,478319	6,646212121	2,74251571	12,23485332
		Tmin	-5,59124424	-4,97634908	-1,824856	1,332727	4,8412023	8,5719697	10,19941	10,112317	6,921666667	3,2937427	-1,053484848	-4,424584555	2,283543356
		T	-1,89076427	-0,53741541	2,786044	5,876667	10,004252	14,141742	16,08636	15,66085	11,68545455	7,3340127	2,127727273	-1,287270555	6,832305321
Valdieri	1390	Tmax	3,029497421	4,383269317	8,284506	11,04082	15,04513	19,884242	22,19472	21,962561	17,15287879	11,759971	5,941309524	3,224490187	11,9919496
		Tmin	-5,58951866	-5,41209987	-2,551674	0,568758	4,3533201	8,2006061	10,07991	10,068553	6,66	3,0992669	-1,125941558	-4,415751184	1,994619252
		T	-2,29821519	-1,73992185	1,620432	4,888182	9,2989736	13,745272	15,81349	15,416012	11,04121212	6,394868	1,458771044	-1,535325964	6,17531238
Vinadio S. Bernolfo	1695	Tmax	4,712556181	5,455788177	7,351198	9,280455	13,116422	17,953777	20,64728	20,761538	16,04833333	11,603519	6,781818182	5,076267658	11,56574631
		Tmin	-3,27226548	-3,20724611	-1,177537	1,485303	5,3033724	9,8671753	11,70733	11,841682	8,161818182	4,5516764	0,176363636	-2,370874713	3,588899931
		T	-0,00166695	0,387029781	2,393548	4,856212	8,8596774	13,550184	15,79208	15,663958	11,44651515	7,6143695	2,982659352	0,695755829	7,020027042

Table 13 - Mean annual and monthly temperature for 2000-2021 time period

As reported by Luca Mercalli's book [35] and as we can quickly notice from the table above, the mean annual temperature decreases with the altitude, from 12 °C in the plain of Cuneo to 0.7 °C in Rocca dell'Abisso, with a mean gradient of 0.48 °C every 100 m. This area of Alps does not only receive a mild effect on the Mediterranean Sea from the South, but also the cold impact of Pianura Padana from the North. Of course, the temperature also depends on the solar radiation and on the slope of the mountain.

Analysing the trend of average daily temperatures at different altitudes in the Maritime Alps, we can understand the thermal evolution over the seasons. Usually, the coldest period of the year is between mid-January and mid-February, with temperature varying between 2 °C in the plain area, -2 °C at 1500 m a.s.l. and -4 °C 2500 m a.s.l and beyond. During spring, temperatures rise up to summer, when the temperature reaches its maximum at all altitudes, with 20 °C in the plain, 16 °C at 1500 m a.s.l. and less than 10 °C over 2500 m a.s.l. In the middle of august, but especially in September, the cooling phase starts, initiating the fall season.

As we can notice from the following plot, at the end of December there is a peak, due to the action of subtropical anticyclones.

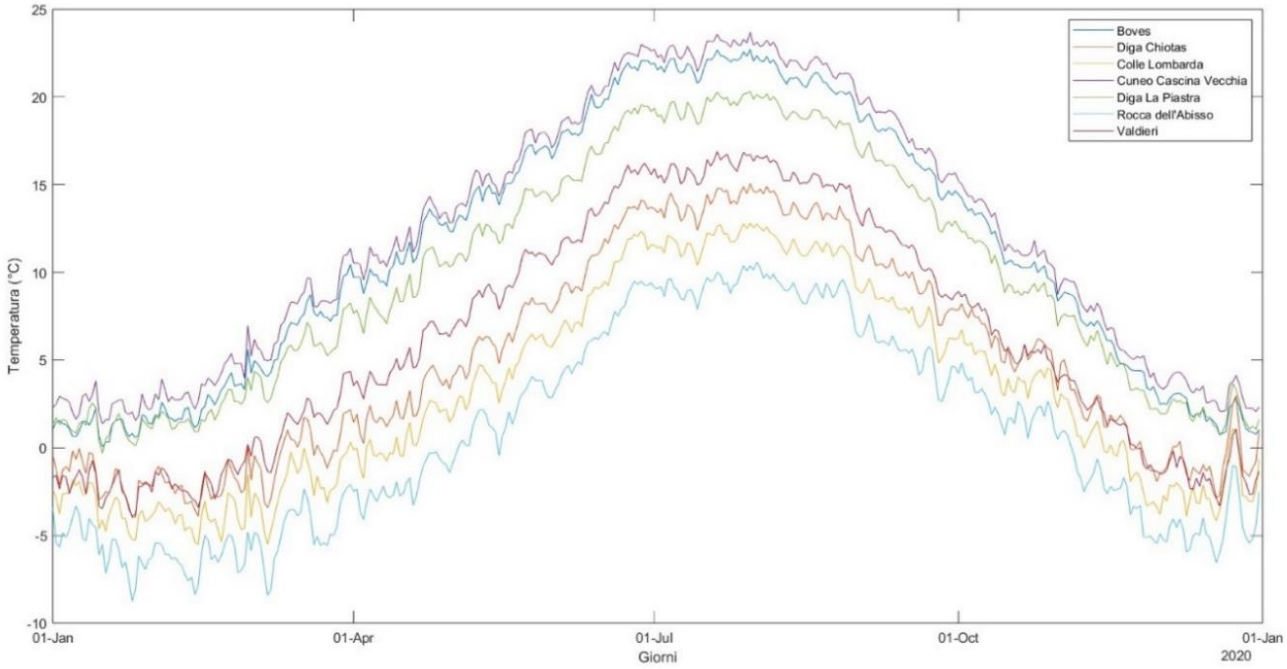

Figure 43 - Mean daily temperatures for 2002-2021 time period

For detecting the trend of temperature in time, an anomaly analysis was carried out. Even if there are no long temperature series, we can detect a positive trend for the annual, maximum and minimum mean temperature.

For this analysis we chose the 1990-2021 time period, for which only 3 ARPA weather stations were active in those years (Boves, Colle Lombarda, Neraissa), compared to the mean temperature of 2000-2021 time period. For the annual scale, there is an increase equal to +0.4 °C/decade, higher than the global and Italian mean temperature increase for the same period (+0.17 °C/decade and +0.39 °C/decade, respectively). Maximum temperature warmed up of +0.5 °C/decade, more than the minimum temperature, +0.3 °C/decade.

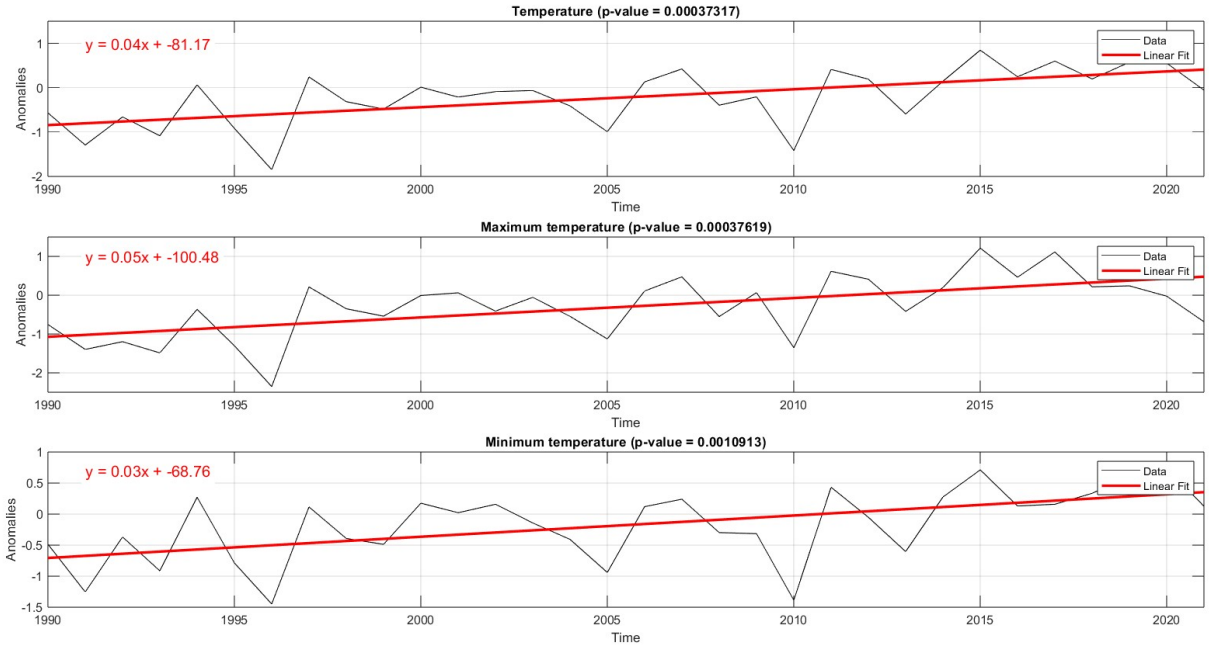

Figure 44 - Mean annual anomaly for temperature, maximum and minimum temperature (1990-2021)

Also, for all seasons we notice an increase in temperature, especially in autumn and summer, with +0.5 °C/decade and +0.6 °C/decade respectively, while increases are less evident for winter (0.2 °C/decade) and spring (+0.3 °C/decade).

From the graphs, it's possible to visualize that the main increments in temperature and hot events have occurred after 2002, in particular in winter 2007 and 2019-2020, spring 2007 and 2017, summer 2003 and 2017, autumn 2006 and 2014.

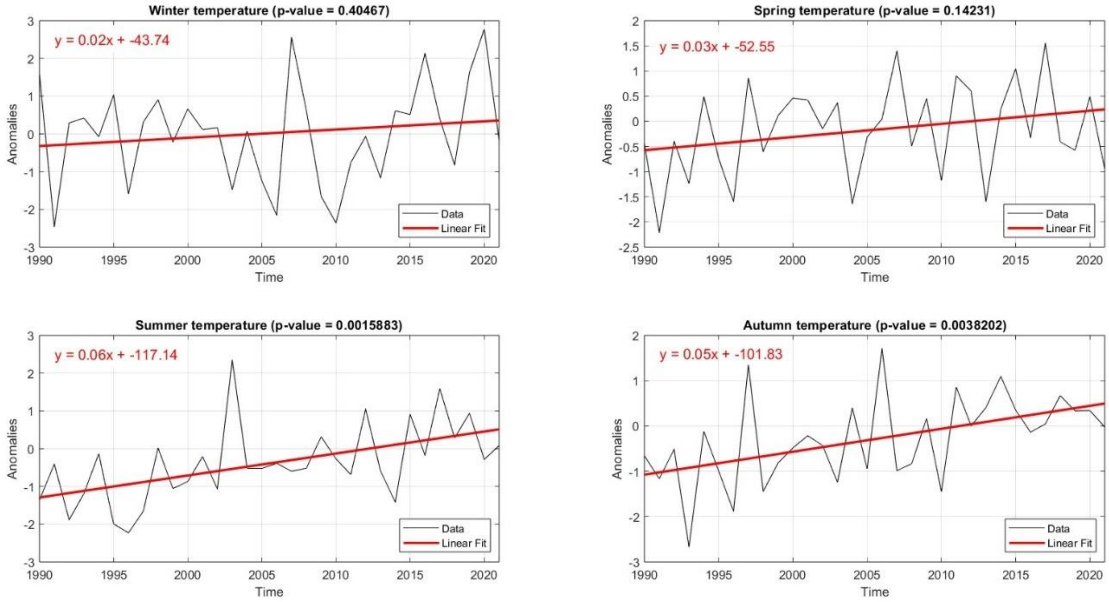

Figure 45 - Mean annual anomaly for seasonal temperature (1990-2021)

The positive trends are statistically significant, except for spring and winter periods. The statistical significance of the trend of thermal anomalies in time was evaluated through the calculation of the p-value of the slope coefficient of the linear regression. If the p-value is lower than α=0.05 (significance level), the trend exists, and it is statistically significant.

The lack of statistical significance for spring and winter could be due to stronger seasonal variations, local or regional effects. We also used short time period data for some weather stations and not close to the area of interest, so this could be another reason for the non-significant result in these two periods.

	T_{min}	T_{max}	T_{mean}
Winter	+0.21	+0.11	+0.23
Spring	+0.17	+0.33	+0.30
Summer	+0.46	+0.69	+0.60
Autumn	+0.42	+0.60	+0.50
Annual	+0.34	+0.50	+0.40

Table 14 - Annual and seasonal trends of temperature in the time period 1990-2021 [°C/decade]

Another methodology to analyse how temperature trend has evolved in time is with the Fourier transform of the daily temperature. The difference between the temperature curve and the sinusoidal curve resulting from the Fourier transform gives the residual temperatures, which are not affected by seasonal variations.

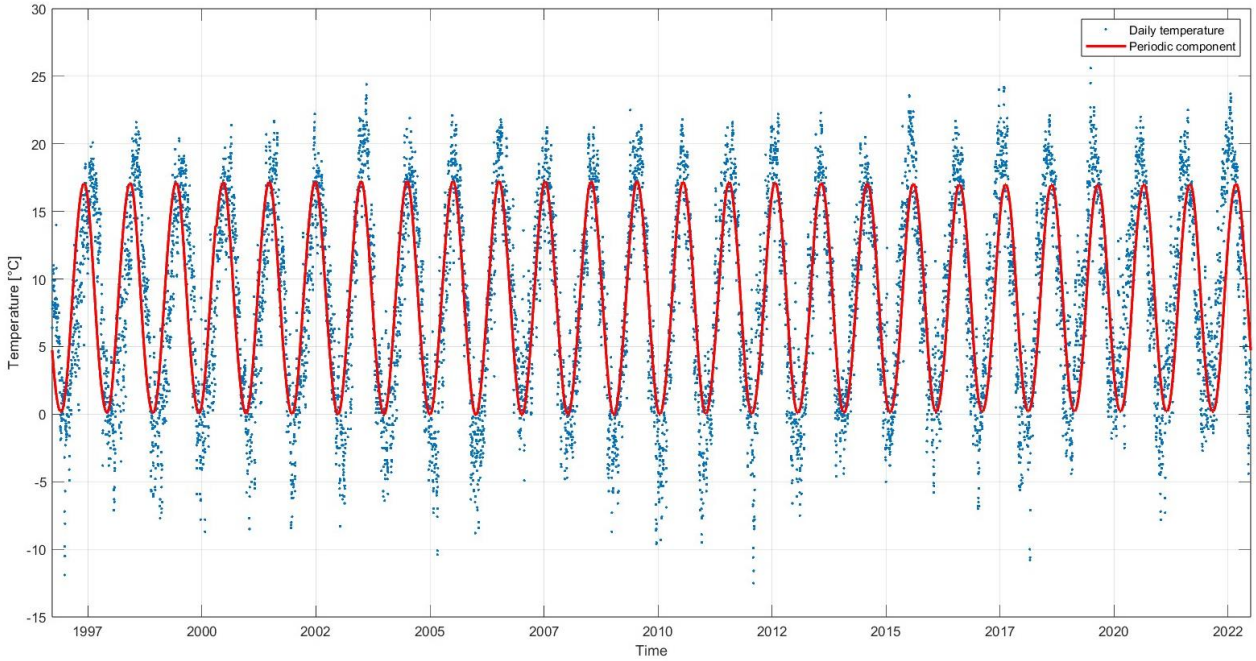

Figure 46 - Daily temperature series vs. periodic component from the Fourier transform

The residual temperatures are then fitted with a linear regression, which represents the daily variation of temperature. Multiplying this quantity for 365.25 days (it considers leap years), we obtain the annual temperature variation.

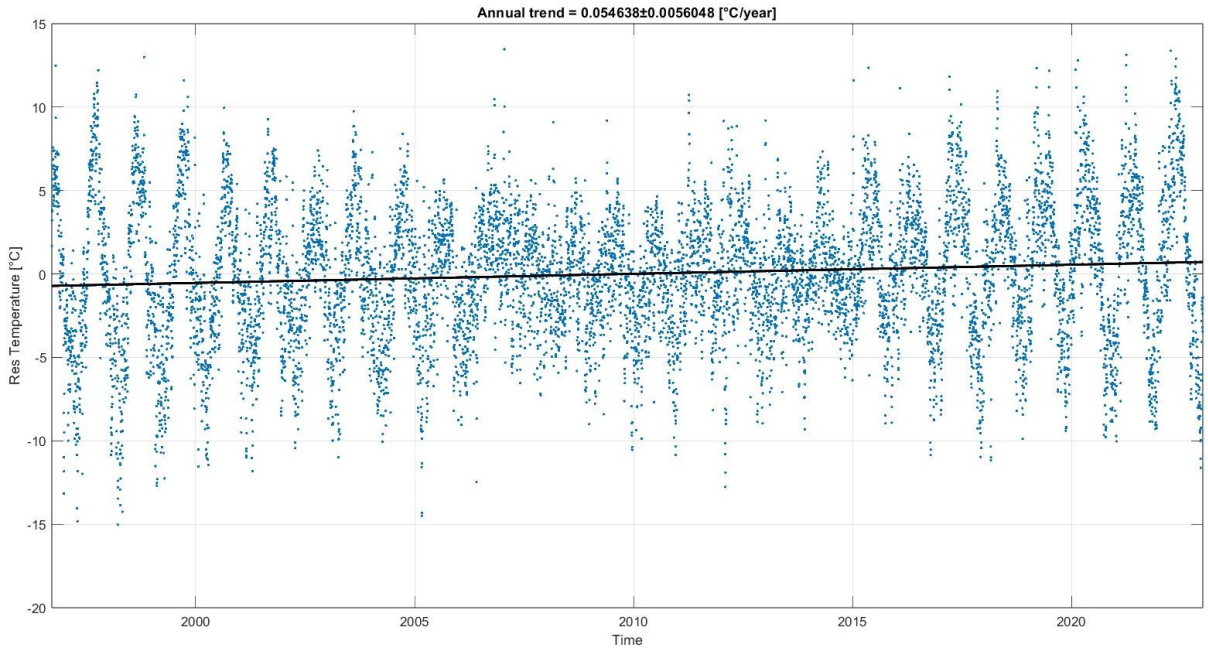

Figure 47 - Annual trend of residual temperature

Multiplying the annual trend for 100 years, we can obtain an estimate of the future temperature in our area. According to the linear regression of residual temperatures, in Chiusa Pesio temperature will rise to +5 °C, a huge increase.

Weather station	**Time period**	**Max trend [°C/year]**	**Min trend [°C/year]**	**ΔT in 100 years [°C]**
Boves	1988-2022	0.5394	-0.6987	+6.8
Colle Lombarda	1987-2022	0.675	-0.5947	+6
Cuneo	2002-2022	1.059	-0.873	+8
Diga Chiotas	2002-2022	1.053	-1.049	+4.17
Rocca dell'Abisso	2003-2022	1.09	-1.17	+6.1
Valdieri	1993-2022	0.6739	-0.5795	+3.8

Table 15 - Maximum, minimum and future trend of temperature for six weather stations

7.2. Precipitation

Also, for precipitation we don't have a continuous and homogeneous 30-years' time series, so we applied calculation for 2000-2021 time period with other short-period weather stations. Other than the precipitation, we also counted the rainy days (ggP ≥ 1 mm). The following table shows the mean annual and monthly rainfall and rainy days in 2000-2021:

STATION	ALTITUDE	PARAMETERS	January	February	March	April	May	June	July	August	September	October	November	December	YEAR
Argentera	1680	Prec (mm)	30,79091	22,25455	62,98182	103,0818	118,3909	96,48182	74,34545	51,218182	78,627273	107,9	97,2909091	37	880,363636
		ggP>1 mm	6,545455	4,636364	8,818182	11,59091	12,18182	10,40909	8,136364	6,7727273	8,3636364	8,59090909	9,72727273	6	101,772727
Boves	575	Prec (mm)	48,70909	69,00909	75,19091	125,5636	125,0455	105,3545	58	56,218182	85,518182	112,781818	151,172727	75,5727273	1088,13636
		ggP> 1 mm	4,045455	5,272727	6,727273	9,772727	9,954545	7,181818	5,818182	5,8181818	6,3636364	7,68181818	8,77272727	5,27272727	82,6818182
Chiusa Pesio	935	Prec (mm)	49,81818	57,27273	106,5091	149,3727	155,1818	126,4636	89,43636	68,972727	111,45455	157,263636	217,945455	82,1181818	1371,80909
		ggP> 1 mm	8,136364	7,818182	10,09091	11,40909	11,68182	8,954545	6,954545	6,2727273	7,7272727	9,04545455	12,2727273	10,7727273	111,136364
Colle Lombarda	2305	Prec (mm)	6,872727	2,4	9,6	42,08182	99,96364	97,80909	77,37273	52,309091	94,5	103,972727	52,4272727	8,18181818	647,490909
		ggP> 1 mm	1	0,590909	2,409091	5,681818	12	9,318182	8,318182	6,0909091	8,1818182	6,22727273	4,63636364	2,04545455	66,5
Cuneo Cascina Vecchia (*)	575	Prec (mm)	50,65263	57,82105	70,10526	114,7579	108,2368	80,935	58,235	45,79	74,86	91,445	151,5	73,475	977,813684
		ggP> 1 mm	4,15	4,8	6,35	8,55	9,25	6,95	5,65	5,45	6,3	7,1	8,9	5,5	78,95
Demonte (*)	765	Prec (mm)	46,93	55,3	65,92	113,14	121,42	79,82	57,195	44,06	72,34	101,51	149,44	71,43	978,505
		ggP> 1 mm	4,2	4,85	6,7	9,85	10,75	7,95	6,2	5,9	6,95	6,8	8,75	5,05	83,95
Diga Chiotas (*)	2020	Prec (mm)	54,59	81,96	122,56	162,57	143,08	104,25	85,07	58,39	101,56	182,655	247,435	93,06	1437,18
		ggP> 1 mm	3,8	5,05	8,05	11,65	11,75	10,6	8,5	6,85	8,45	8	10,4	5,45	98,55
Diga Piastra (*)	950	Prec (mm)	56,93	57,26	75,85	124,94	126,805	94,325	52,41	44,61	76,525	129,64	180,05	87,58	1106,925
		ggP> 1 mm	4,45	4,5	6,4	10,4	10,95	8,75	6,35	6,2	7,35	7,9	9	5,6	87,85
Monte Malanotte	1735	Prec (mm)	25,06471	26,64706	44,35294	90,07647	116,2676	106,9588	67,81765	73,647059	98,844118	98,9441176	114,858824	35,9882353	899,467647
		ggP> 1 mm	3,454545	4,409091	6,454545	9,318182	10,40909	8,545455	6,5	6,3181818	6,5454545	6,86363636	8,36363636	5	82,1818182
Neraissa	1433	Prec (mm)	48,44545	61,32727	68	108,2364	118,4727	89,29091	62,40455	43,836364	73,595455	113,136364	150,545455	79,9409091	1017,23182
		ggP> 1 mm	4,863636	5,636364	7,136364	10,22727	11,54545	9,181818	7,681818	6,4090909	7,6363636	8,09090909	8,95454545	6,31818182	93,6818182
Palanfrè (*)	1625	Prec (mm)	14,67	19,55	73,65	158,16	157,97	125,34	80,69	59,38	113,49	137,46	178,04	34,69	1153,09
		ggP> 1 mm	3,2	3,95	9,15	13,05	12,55	9,8	7,45	7,1	8,75	9,05	10,15	4,4	98,6
Pradeboni (*)	985	Prec (mm)	51,77895	57,13684	86,62105	145	150,11	115,48	90,09	75,8	121,85	135,22	182,37	76,73	1288,18684
		ggP> 1 mm	5,3	5,95	8,35	10,95	10,8	8,7	6,9	6,55	7,25	8,2	9,85	6,85	95,65
Rifugio Mondovì	1760	Prec (mm)	27,20909	13,66364	46,60909	108,5364	153,7091	110,7636	80,81818	78,045455	100,10909	163,272727	200,7	51,4636364	1134,9
		ggP> 1 mm	3,590909	2,363636	5,818182	10,86364	12,59091	9,227273	7,272727	7,3636364	7,8181818	8,09090909	8,68181818	4,77272727	88,4545455
S. Giacomo Demonte	1297	Prec (mm)	53,53636	66,54545	83,28182	122,2545	142,0818	105,9182	76,10909	49,831818	79,104545	111,172727	157,109091	81,2772727	1128,22273
		ggP> 1 mm	5,136364	5,636364	7,727273	11,40909	12,77273	9,954545	7,590909	6,7272727	8,3636364	7,90909091	9,18181818	6,04545455	98,4545455
Valdieri	1390	Prec (mm)	81,81818	78,59091	106,0091	149,4909	156,5818	119,0545	84,43636	53,309091	97,818182	179,081818	229,072727	117,690909	1452,95455
		ggP> 1 mm	5,681818	6,136364	8,090909	11,81818	12,54545	10,5	8,590909	6,6818182	8,5909091	8,36363636	10,0454545	6,81818182	103,863636
Vinadio S. Bernolfo	1695	Prec (mm)	64,75455	64,94545	77,40909	122,2545	141,1273	103,1364	85,65909	54,254545	88,140909	152,090909	203,890909	100,009091	1257,67273
		ggP> 1 mm	5,545455	5,863636	6,909091	10,54545	12,22727	10,31818	8,272727	6,8181818	8,2727273	7,72727273	9,5	6,59090909	98,5909091

Table 16 - Precipitation and rainy days

For this area of the Alps, the distribution of precipitation during the year follows a bimodal trend: there are two peaks in spring and autumn, alternate by two minimum points in summer and winter.

November is the month that shows the maximum precipitation (mean of 167 mm in 2000-2021 time period), because of the recurring mediterranean rainfall. The second peak occurs in spring, with great precipitation amount in spring (120 mm), especially in May. Then the curve lows down in summer, which is the driest period of the year in this area (57 mm in August), typical trend of the Liguria-Mediterranean climate.

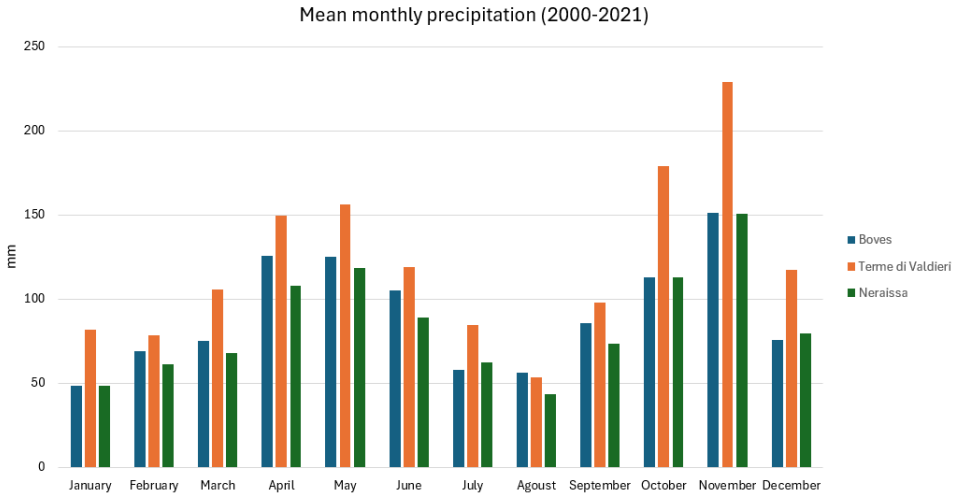

Figure 48 - Mean monthly precipitation for the period 2000-2021

Talking about frequency, precipitation events in autumn are more vigorous but less frequent, while in spring they are less intense but more frequent. This trend is observed in the following figure, which plots the percentage frequency of daily precipitation for the period 1993-2023 in Valdieri. There is a peak in June, with more than 40% of probability to have precipitation.

This same trend is visible both in Valdieri (1390 m a.s.l.) and in Boves (575 m a.s.l.), in the Cuneese-plane.

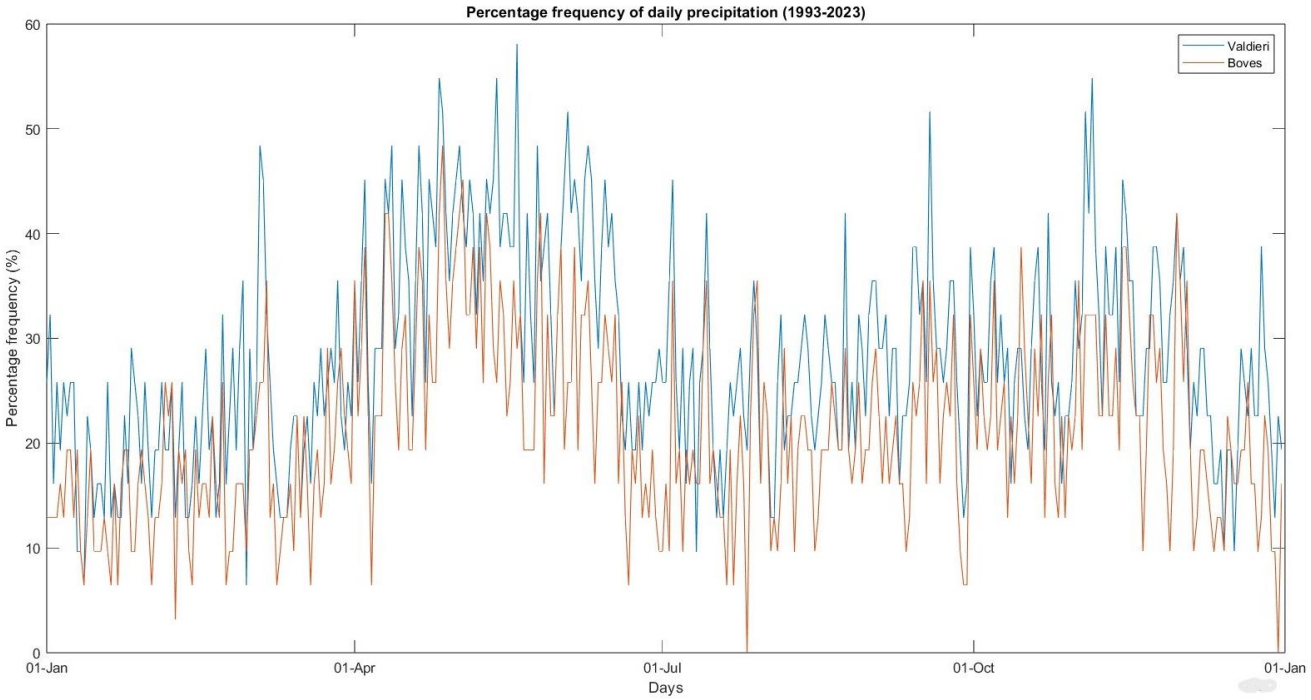

Figure 49 - Percentage frequency of daily precipitation (1993-2023)

Also, for precipitation data we calculated the anomalies for 1990-2021 compared to the 2000-2021 the time period for the weather stations indicated in the table n. The analysis of anomalies doesn't show a clear and statistically significant trend, instead we observe the alternation of consecutive periods with negative contribution of precipitation and other periods with positive supply of rainfall. We don't notice an increase or a decrease of the interannual variability, but just a time period characterized by drier years [36].

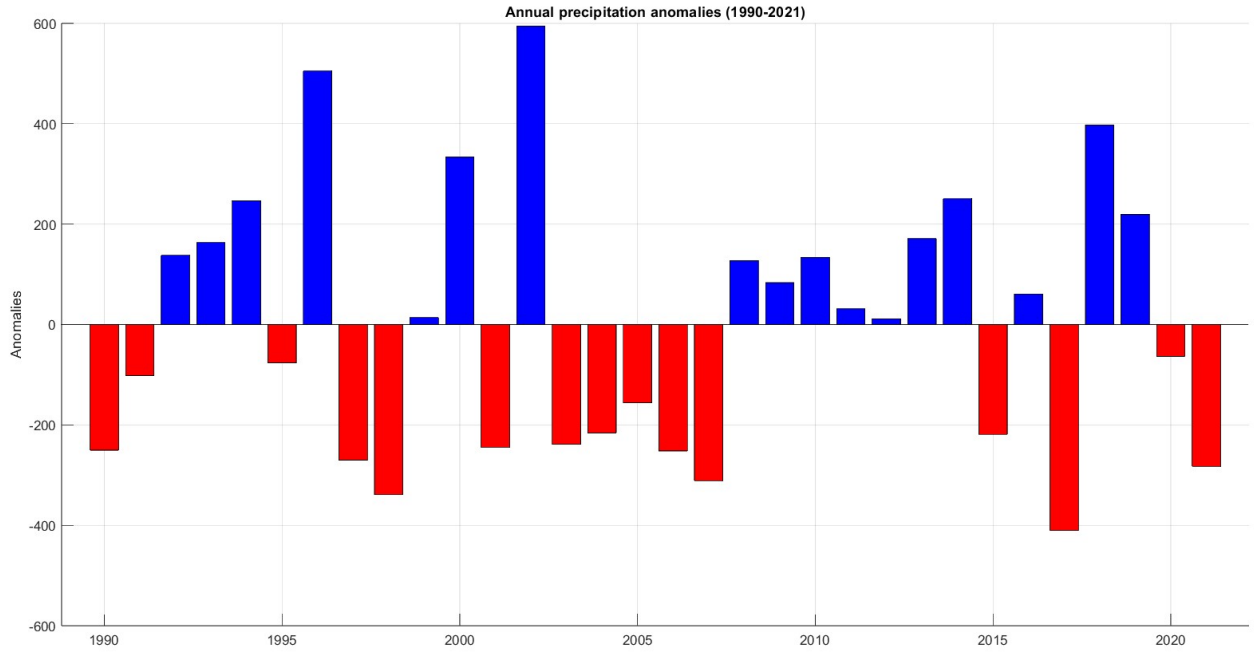

Figure 50 - Annual precipitation anomalies for 1990-2021 compared to 2000-2021 time period

An increase or decrease is not observed neither in the seasonal precipitation. Looking at the following graphs, from 2000 we notice a tendency to drier years, except for autumn where there is a balance in positive and negative precipitation supplies.

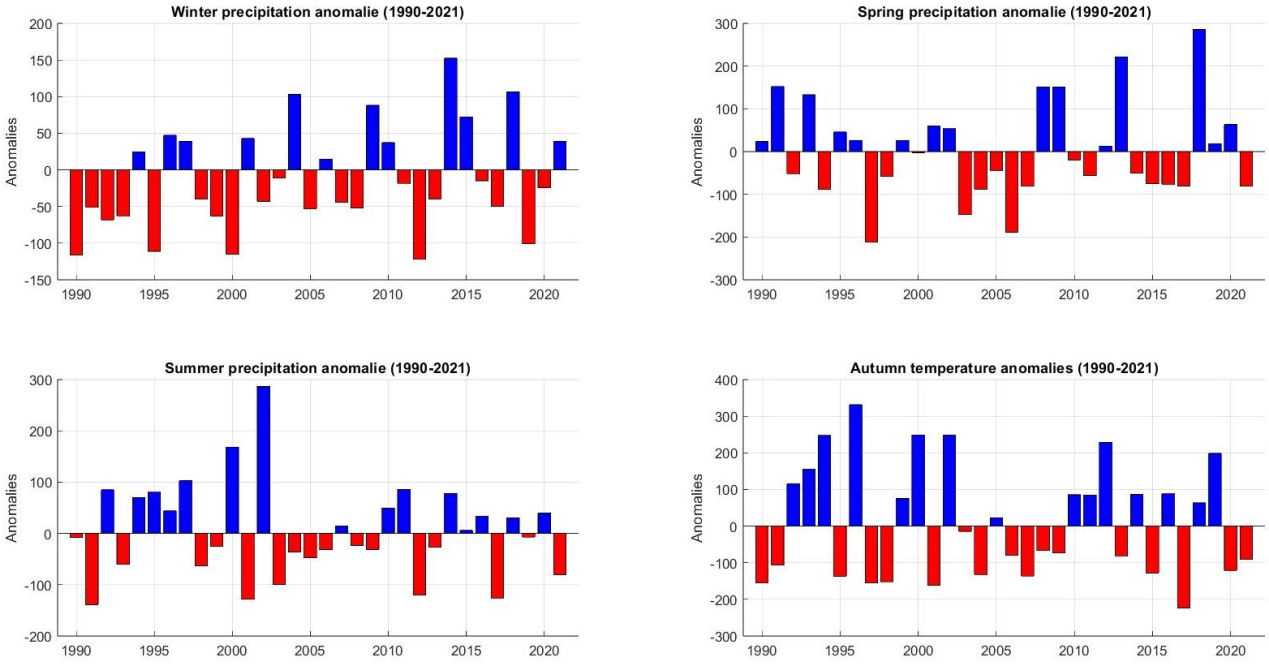

Figure 51 - Seasonal precipitation anomalies for 1990-2021 compared to 2000-2021 time period

Another parameter to be analysed is the rainfall intensity, calculated with the index SDII (Standard Daily Intensity Index), which is the ratio between the annual precipitation and the number of days in the year we have precipitation.

For Valdieri, in 1994-2023 time period, we notice a slight increase in the intensity of rainfall (+0.2 mm/days/decade).

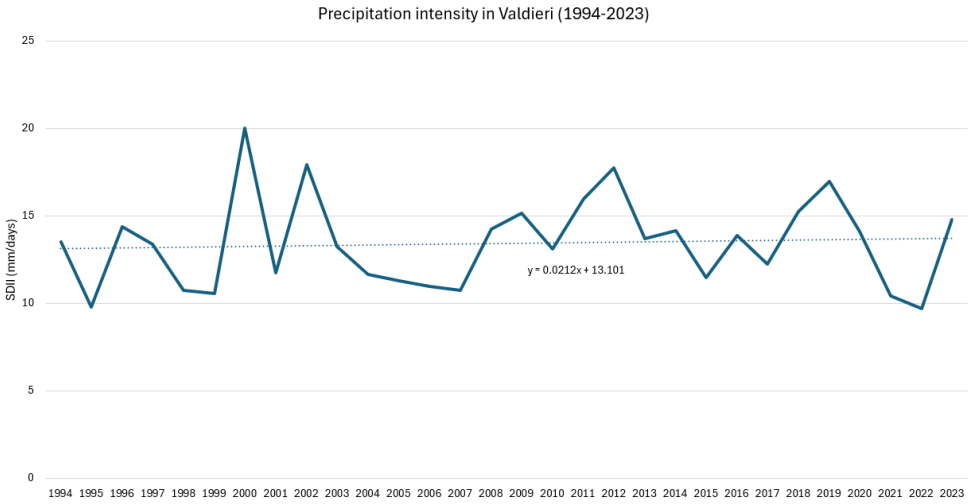

Figure 52 - Precipitation intensity as SDII in Valdieri (1994-2023)

Also, in Colle Lombarda and Neraissa there is a slight increase (+0.086 mm/days/decade and +0.12 mm/days/decade, respectively), while in Boves we notice a decrease (-0.47 mm/days/decade). Seen these soft trends in SDII, we can state that, probably, the intensity has not changed on a daily scale.

On a mean annual scale of all weather stations in the Cuneo area, rainfall intensity shows a decrease from 2000 to 2021:

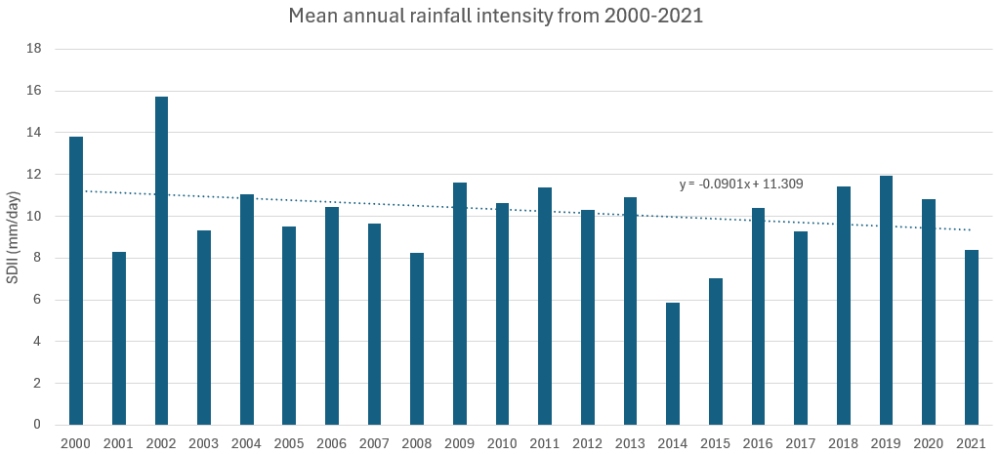

Figure 53 - Mean annual rainfall intensity from 2000 to 2021

8. Discussion

8.1. Change Detection results and climate analysis

As already discussed, from the change detection analysis we noticed a shift from coniferous forest to broad-leaved forest, so as the increase of low plants with respect to high trees, then followed by a straight increase of permanent herbaceous surfaces. For the water class, lakes have experienced the lowering of their water level from 2010 to 2021.

These changes are probably the consequence of the rising of temperatures and of the higher frequency of dry periods. The following maps have been obtained with the IDW interpolation.

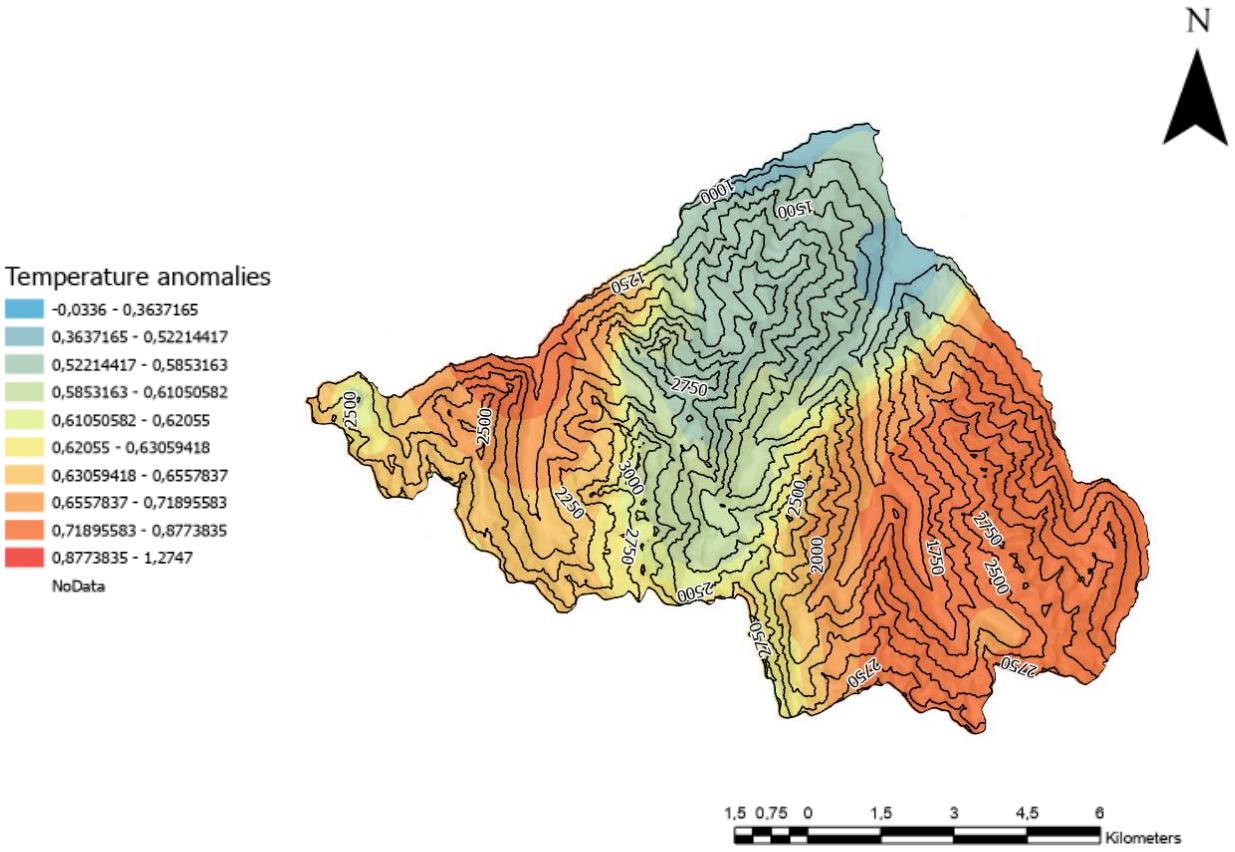

Figure 54 - Temperature anomalies map (2010-2021)

The rise of temperature has been experienced in the whole area, especially at the west and east border of Valle Gesso, at higher altitudes. The correlation between temperature and elevation reaches a value of 0.47. The correlation is inverse, instead, with precipitation; in fact, from the figure below, we notice an increase in valley areas, at lower altitude (Pearson coefficient = -0.11). For sure other parameters linked to the morphology of the territory and to other climate variables, like solar radiation, influence the trend of temperature and precipitation and need to be considered in future and more accurate analysis.

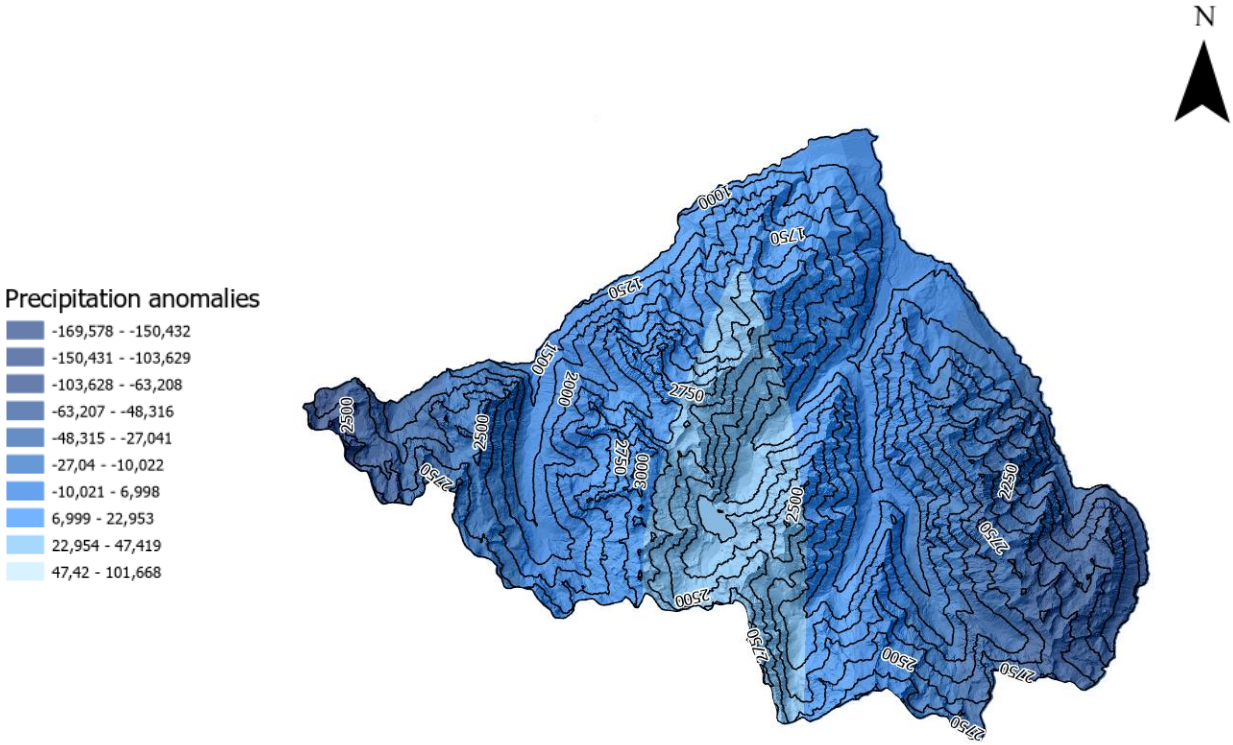

Figure 55 - Precipitation anomalies map (2000-2021)

From the linear correlation analysis, there is no evident correlation between the temperature anomalies and the change in land cover classes (Pearson coefficient ≈ 0), so as for precipitation. This result could be due to the fact that the change in land cover class is a much more difficult event and not linearly influenced by temperature only. We then conducted a simple T-test to the mean temperature anomalies between points with land cover change and points without change, with a level of significance equal to 5%. The p-value obtained is equal to 0.032217 (< 0.05), so there is a statistically significant difference between the two groups of points, that means land cover changes occurred in areas with high temperature anomalies, with a probability of 97%. The same can be said for precipitation anomalies, which show a lower p-value ($3.3*10^{-5}$) and for which the difference of mean precipitation anomaly of the two groups is larger and negative, while for temperature this difference is very small. Still, there is still a level of significance in considering a link between the climate anomalies and the land cover changes, which can be examine more in detail in the future.

From a Kernel density analysis, shown in Figure 55, we notice that the principal land cover changes have occurred at the two south extremities of our area of interest, where higher positive temperature anomalies and negative precipitation anomalies have been registered and at an altitude up to 2000 m a.s.l.

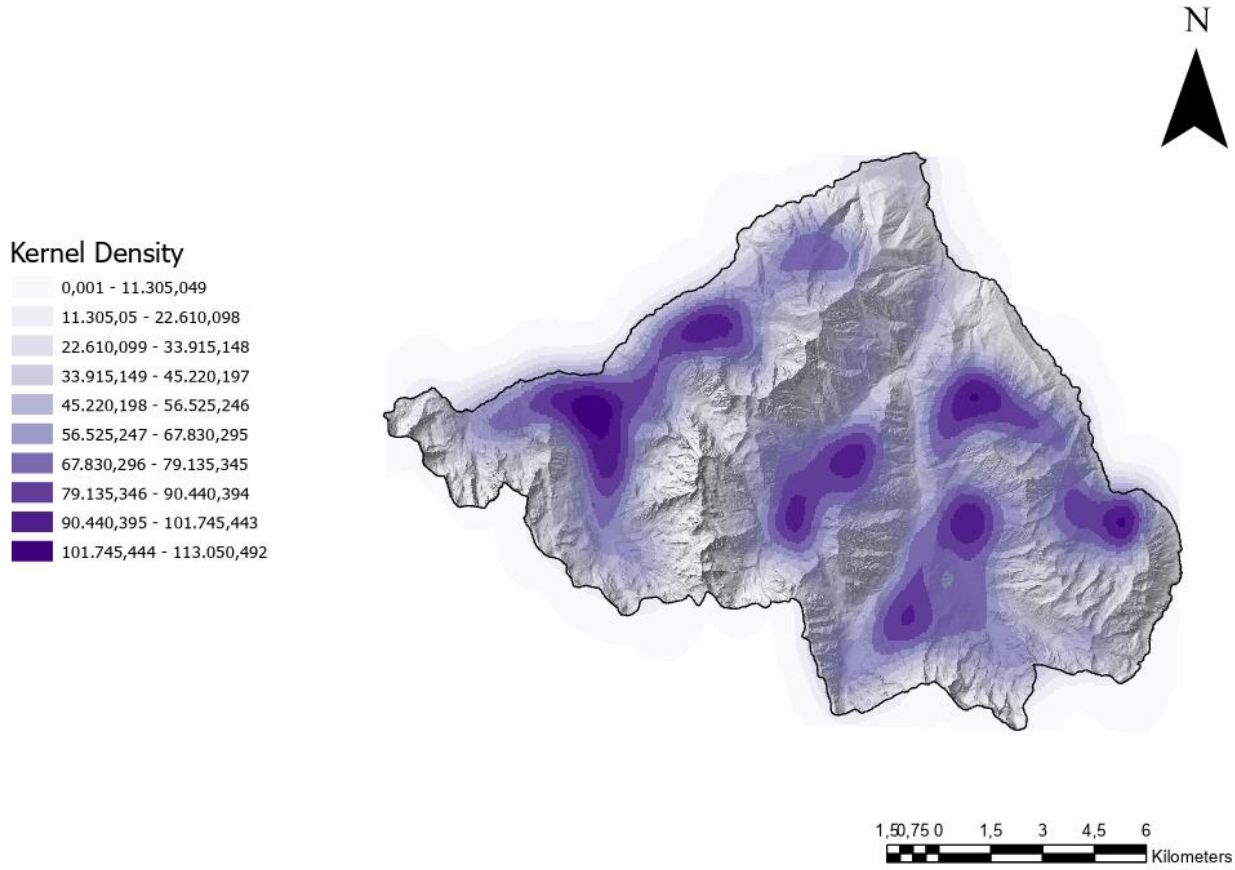

Figure 56 - Kernel density of land cover changes

Regarding each land cover class change, the box plot for each category was generated:

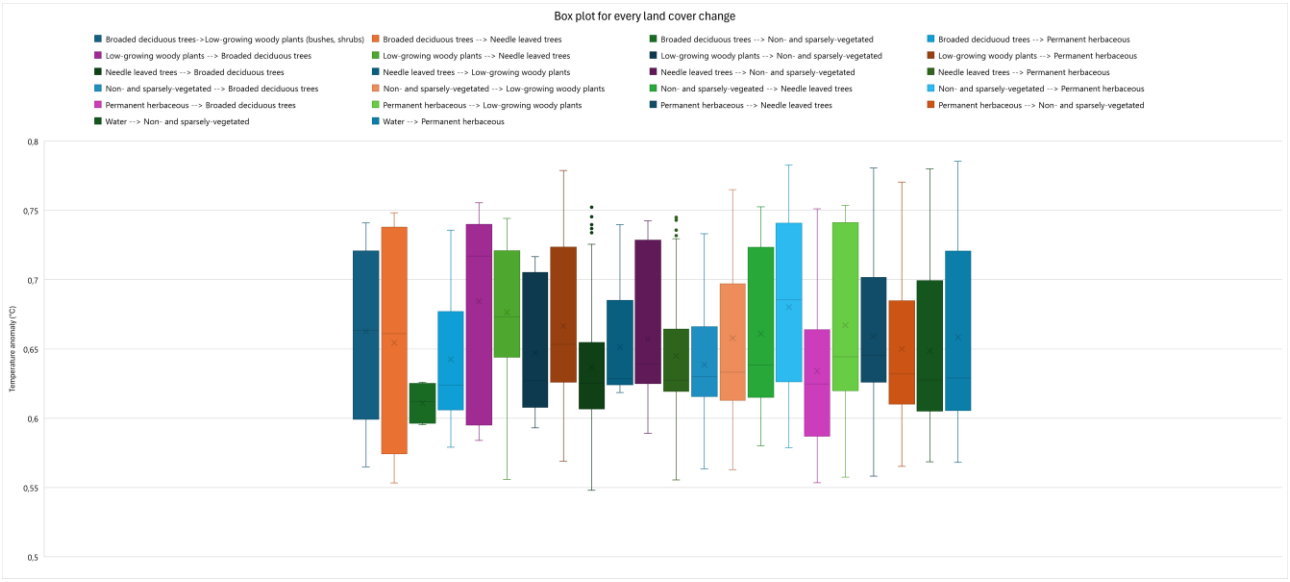

Figure 57 - Box plot for each change category vs Temperature

Almost all categories have a wide temperature anomaly range, meaning that these land cover changes occur in various climatic conditions, except for Broaded trees → Rock, Needle trees → Broaded trees, Needle trees → Permanent herbaceous, Rock → Broaded trees.

The highest median (0.717) is for Low-growing plants → Broaded trees: an elevated rise in temperature causes the transition from shrubs to broad-leaved trees, which favour a mild weather condition.

Also, for precipitation ranges are wide, except for Needle leaved trees → Low-growing woody plants. Almost all changes happen in different climatic conditions,

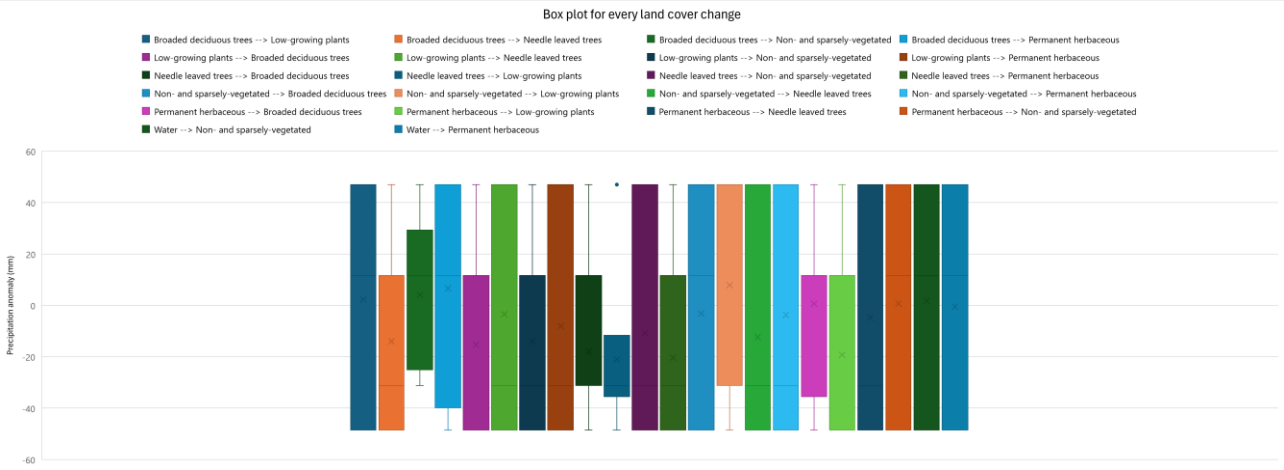

Figure 58 - Box plot for each change category vs Precipitation

For each class change we also calculated the mean, standard deviation, maximum and minimum for temperature and precipitation anomalies. Each of these statistical parameters identify some characteristics of land cover changes related to climate variables change.

The value of the mean indicates the sensitivity of land covers to climate change: high values of the mean temperature anomaly mean that the land cover changes occur with the rise of temperature, like in the case of Permanent herbaceous → Needle leaved trees or Low-growing woody plants → Broaded deciduous trees, while negative anomalies for precipitation indicates that changes occur during dry periods, with a decrease in vegetation cover (ex. Low-growing woody plants → Non- and sparsely-vegetated, Needle leaved trees → Permanent herbaceous).

The standard deviation indicates the variability of changes: high values of Std stand for changes that occur in different conditions, while low values means that the change happens in a certain climate circumstance. For precipitation, the change is very variable, while for temperature we notice that the change always occurs with a significant rise of the temperature.

CHANGE DETECTION CLASS	Mean T	Std T	Mean P	Std P	Max T	Min T	Max P	Min P
Broaded deciduous trees --> Low-growing woody plants (bushes, shrubs)	0,662707	0,064399	2,33211	44,60005	0,740911	0,565025	46,98886	-48,5503
Broaded deciduous trees -->Needle leaved trees	0,654585	0,073075	-14,0009	36,1377	0,748251	0,553344	46,98886	-48,5503
Broaded deciduous trees -->Non- and sparsely- vegetated	0,611025	0,01443	4,047824	30,52955	0,626108	0,595427	46,98886	-31,1785
Broaded deciduous trees -->Permanent herbaceous	0,642543	0,049346	6,619252	38,39773	0,735771	0,579138	46,98886	-48,5503
Low-growing woody plants (bushes, shrubs) -->Broaded deciduous trees	0,684393	0,069817	-15,3225	39,16687	0,755468	0,584032	46,98886	-48,5503
Low-growing woody plants (bushes, shrubs) -->Needle leaved trees	0,676457	0,052162	-3,43235	44,97454	0,744309	0,555942	46,98886	-48,5503
Low-growing woody plants (bushes, shrubs) -->Non- and sparsely- vegetated	0,646926	0,048776	-14,0008	35,12113	0,71663	0,59309	46,98886	-48,5503
Low-growing woody plants (bushes, shrubs) -->Permanent herbaceous	0,666608	0,054708	-8,0506	42,23574	0,778804	0,569079	46,98886	-48,5503
Needle leaved trees -->Broaded deciduous trees	0,636489	0,057487	-17,9504	29,69478	0,752292	0,548029	46,98886	-48,5503
Needle leaved trees -->Low-growing woody plants (bushes, shrubs)	0,651365	0,046488	-21,0459	34,04673	0,739646	0,618612	46,98886	-48,5503
Needle leaved trees -->Non- and sparsely- vegetated	0,65725	0,053045	-10,7025	40,57077	0,742574	0,589246	46,98886	-48,5503
Needle leaved trees -->Permanent herbaceous	0,645043	0,049781	-20,3674	30,5727	0,746729	0,555455	46,98886	-48,5503
Non- and sparsely- vegetated -->Broaded deciduous trees	0,638643	0,047416	-3,21531	40,39708	0,733215	0,563396	46,98886	-48,5503
Non- and sparsely- vegetated -->Low-growing woody plants (bushes, shrubs)	0,657845	0,058943	7,850137	43,01369	0,764967	0,562781	46,98886	-48,5503
Non- and sparsely- vegetated -->Needle leaved trees	0,661017	0,055506	-12,3236	40,04716	0,75258	0,580174	46,98886	-48,5503
Non- and sparsely- vegetated -->Permanent herbaceous	0,680216	0,059996	-3,75981	43,63612	0,782849	0,578724	46,98886	-48,5503
Permanent herbaceous -->Broaded deciduous trees	0,634119	0,055722	0,643643	34,72944	0,751146	0,553446	46,98886	-48,5503
Permanent herbaceous -->Low-growing woody plants (bushes, shrubs)	0,667172	0,062614	-19,2677	38,91596	0,753852	0,557489	46,98886	-48,5503
Permanent herbaceous -->Needle leaved trees	0,65893	0,04969	-4,80494	42,71792	0,780592	0,558274	46,98886	-48,5503
Permanent herbaceous -->Non- and sparsely- vegetated	0,650042	0,051603	0,687065	42,6239	0,770444	0,565285	46,98886	-48,5503
Water -->Non- and sparsely- vegetated	0,648761	0,057439	1,738562	41,72141	0,77999	0,568526	46,98886	-48,5503
Water -->Permanent herbaceous	0,658495	0,063755	-0,52221	42,26555	0,785425	0,568161	46,98886	-48,5503

Table 17 - Statistics of T [°C] and P [mm] anomalies for each land cover change class

The maximum and the minimum define the extreme climate conditions at which there is change. The maximum in temperature, like in the case of Water → Permanent herbaceous, indicates that this change has occurred because of very high temperatures, while the minimum in precipitation, with negative values, suggests that there has been a drought event. As shown in Table 17, classes suffer drought events and heat waves.

We can visualize these results in the following maps:

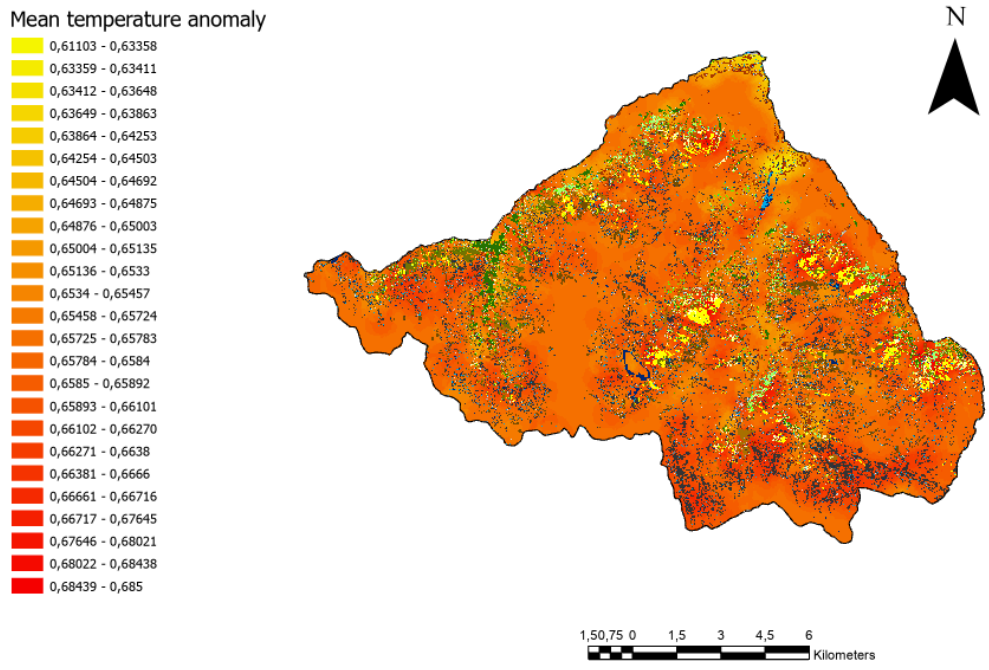

Figure 59 - Mean temperature anomaly with land cover changes (2010-2021)

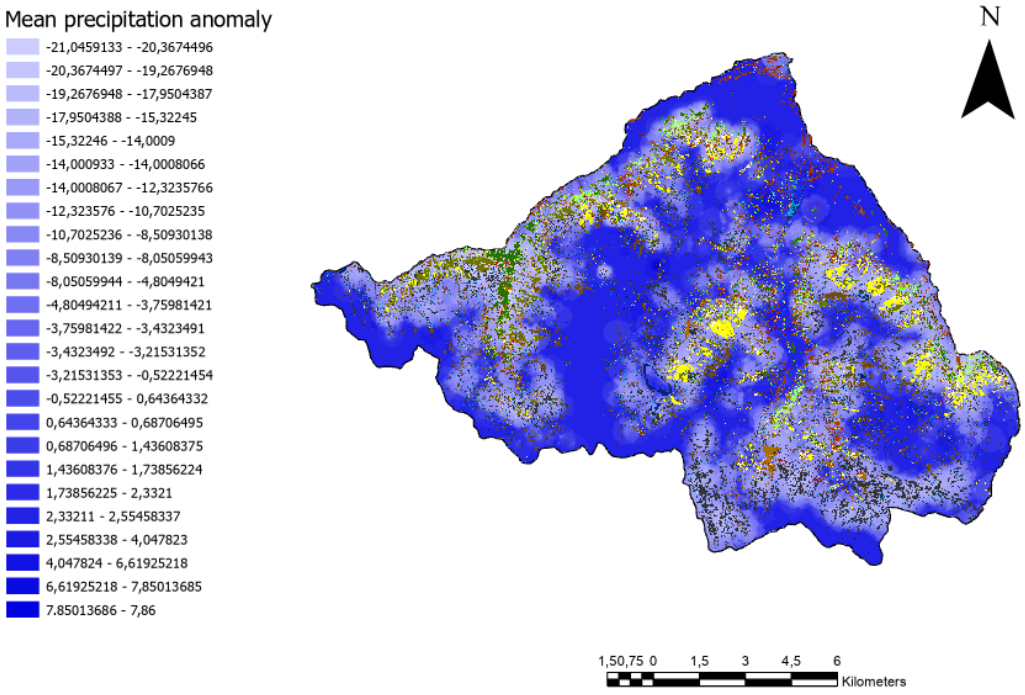

Figure 60 - Mean precipitation anomaly with land cover changes (2010-2021)

As already observed with the Kernel density, land cover changes occur where we have positive temperature anomalies (high mean) and negative precipitation anomalies, and in areas where these conditions are pretty much stable in time, with no large variations, which means low values of standard deviation.

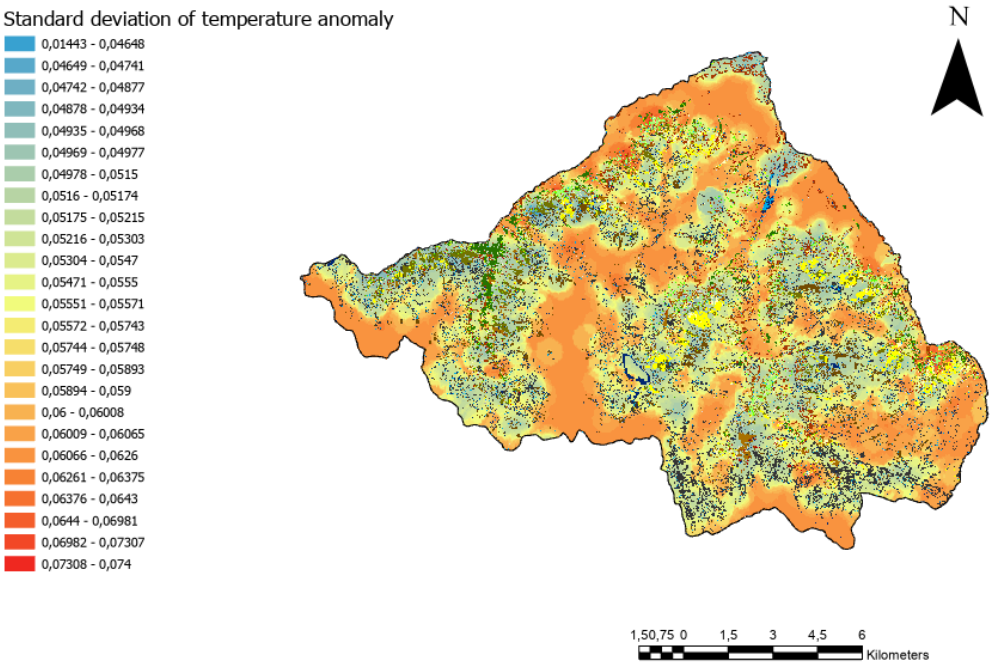

Figure 61 - Standard deviation of temperature anomaly with land cover change (2010-2021)

For precipitation, there is a higher variability of change conditions, which probably depend on morphologic characteristics of the territory.

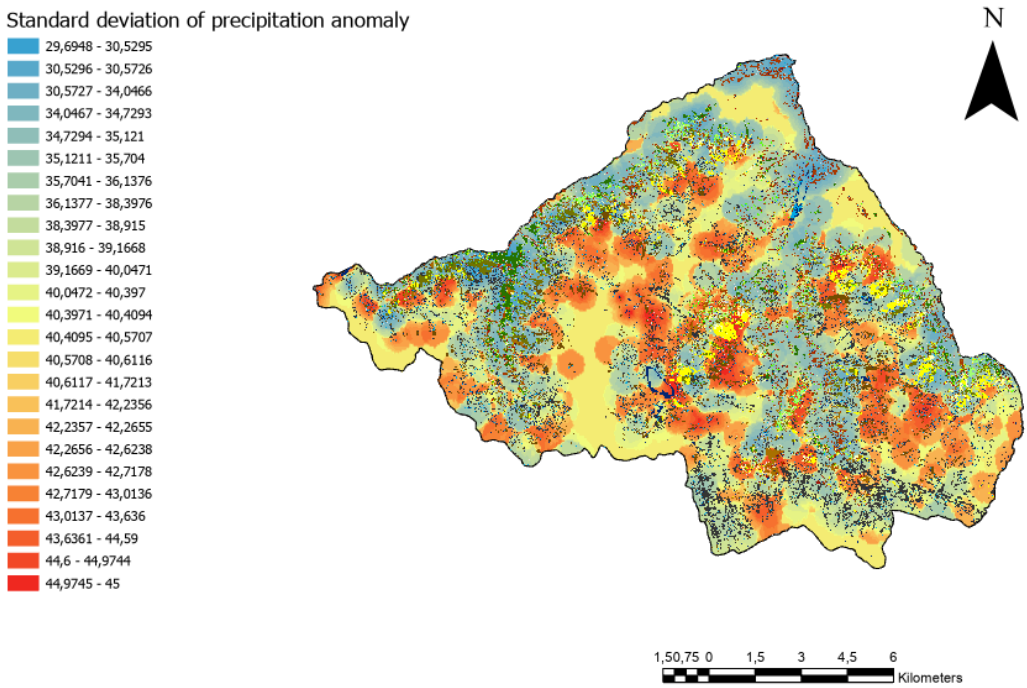

Figure 62 - Standard deviation of precipitation anomaly with land cover change (2010-2021)

8.2. Training of DL models

As mentioned in previous chapters, we met lots of obstacles and limitations during the classification with deep learning CNNs. First of all, many of the tests have been conducted on ICE 2009-2010, exploiting its NIR band, which was probably "corrupted" in the spectral signal. In fact, the best algorithm is the one trained on ICE 2009-2010 with RGB bands only, with an OA of 66%, even if a squaring effect is shown in the classification raster. This effect is not evident in following tests. Starting from the second model, on which we applied not only NIR band but also NDVI and DTM, the accuracy decreased to 55%; the main mistake, immediately evident by just looking at the classification result, is an overestimation of the class "Water bodies" on shadow areas of mountains. This mistake is repeated for all subsequent tests on ICE imagery, again due to the NIR band. Another problem lies on the CLC 2012 dataset: even if all models could recreate the segmentation of the territory based on CLC classes, even with a higher level of detail, the dataset was too coarse with respect to the resolution of our imagery data to discriminate land cover classes accurately, furthermore the definition of some classes was not clear or was too generic to have a good and detailed classification, especially "Transitional woodland-shrub". In the third test (RGB+NIR+DTM) we continue to observe the error in classifying shadows as water bodies. This mistake is lightened in the fourth test, using a different model architecture: MMSegmentation.

We notice a further reduction of the error in the fifth mistake, including an RGB-based vegetation index (ExG). Furthermore, in the fifth test we also applied the class balancing and the focal loss in

the model, and effectively the implementation of these two functions has lowered the classification mistake of the water class.

Even if not recommended by the Copernicus Land Monitoring Service, for the second, the third and the fourth set another land cover class was added to the CLC 2012 dataset: wetland, derived from the shapefile created by Regione Piemonte for the identification and representation of wetlands in Piedmont. This class was included since one of the goals of the medium-scale analysis of ACLIMO Project was to study the evolution of wetlands in time. Unfortunately, DL models were not able to identify and classify wetlands in our territory of interest other than lakes (under the class "Water bodies") and the two Gesso streams.

From the second to the fifth tests, we created the training samples by drawing polygons associated with CLC classes (ROIs). Not including the "Shadow" class in the dataset, this probably caused the classification error for which shadow was classified as water. It is better to import training sample polygons covering the whole area, to associate a class to every portion of the raster.

Test 6 was conducted on AGEA 2018 imagery with CLC+Backbone 2018 dataset, adding three other channels other than RGB: NIR band, DTM and NDVI. As already discussed, this dataset has a higher resolution than CLC 2012 (10 m vs 100 m) and land cover classes are more "generic", so that it is possible to better discriminate surfaces in the territory. The result is in fact accurate for this test, with an OA of 82% for AGEA 2018, of 85% when the model has been fine-tuned and applied to ICE 2009-2011 with four channels, RGB and DTM. The accuracy drops to 77% when the model classifies AGEA 2021 imagery with six channels. The salt-and-pepper effect occurs in the classified raster, which decreased the OA due to the presence of misclassified isolated pixels that erroneously differ from surrounding classes: the most common error is that many pixels classified as forest belong instead to the permanent herbaceous surface. The reason could be that the model could not adapt to the new raster characteristics. For the fine-tuning of two rasters, class balancing and the focal loss were applied.

Finally, for our work we did not normalize the rasters employed as channels (RGB, NIR, DTM, NDVI and ExG). Even if the model was not essentially affected by the non-standardization of channels' intervals, it is better for future classifications to normalize them so that the model can better converge and learn the characteristics of the input image. Without this standardization, a given channel could prevail over the others, with a lack of information for the DL algorithm.

8.3. Critical analysis of the methodology and future perspective

Seen the results of classification, change detection and climate analysis, and the main error of the DL models application, this sub-chapter wants to identify the pros and cons of the methodology adopted in the thesis, and recommend improvements for future investigations.

PROS	CONS
Facility of DL modelling in ArcGIS Pro for pixel-based classification, without the need of coding	Long processing time for the training phase of DL models in ArcGIS Pro, especially for high resolution imagery
Versatility of ArcGIS Pro software for committing other tasks (ex. climate analysis)	Availability of few imagery data, spectral bands, training datasets and climate information for a long time period
Despite the availability of few data, we had enough resources to obtain significant and interesting results	Long wait to obtain necessary data
	Need to improve the knowledge in using AI and DL algorithms

Table 18 - Pros and Cons of the methodology

To improve the classification of aerial images with DL models on ArcGIS Pro and the robustness of our results for ACLIMO Project, it is desirable to have more images for a longer time series in order to better detect and study land cover changes and climate change effects on the territory, and to get these resources in a shorter period of time. These images should have the same number of channels, the same resolution and more spectral bands, to better discriminate other characteristics of the area, despite a greater computational effort already present in our work. It can be suggested to eventually test other softwares for AI segmentation.

Regarding training samples, there should be an equivalence in resolution between the samples and the images to be classified, so that classes fit together with the raster pixels. Also in this case, it is important to create and store different datasets for the training phase, relevant for the European and/or global context.

9. Conclusion

With this thesis we analysed the application of deep learning algorithms for the pixel-based classification of aerial photos on a restricted mountainous area in Valle Gesso. Despite the limited availability of images, spectral bands and dense climate data for a long period of time, we were able to train DL models for the segmentation of three images, adding DTM and a vegetation index, and to detect changes in the land cover classes, then joined with the changes in temperature and precipitation. Thanks to the application of U-Net algorithm for the pixel-based classification of available orthophotos, we observed a change in land cover surfaces due to the rise of temperature and more frequent dry periods registered in the last 20 years in Alpi Marittime from the weather stations distributed in the territory of interest by ARPA Piemonte.

Starting from this short but rich analysis, it is possible to proceed a monitoring activity in Parco Alpi Marittime for studying climate change and its effects in all areas protected by APAM and, eventually, extend this analysis to the entire Alps range with a deeper level of survey capacity. It is important to monitor and study these effects to plan adaptive solutions to face possible damages caused by climate change in a sensitive ecosystem like mountain, and to preserve infrastructures, economic activities, people, flora and fauna that live in the Alps.

Sources

[1] I. Brendt, «Cambiamenti climatici nella Regione Alpina - Conseguenze e sfide (Alpenkonvention),» Lebensministerium, 2006.

[2] D. N. Bravo, M. B. Araújo, T. Lasanta e J. I. L. Moreno, «Climate Change in Mediterranean Mountains during the 21st century,» *Springer Nature,* pp. 280-285, 4 Giugno 2008.

[3] M. Beniston e M. Stoffel, «Assessing the impacts of climate change on mountain water resources,» *Science of the Total Environment,* pp. 1129-1137, 15 Settembre 2014.

[4] European Environment Agency, Regional Climate Change and Adaptation: The Alps Facing the Challenge of Changing Water Resources, 2009.

[5] «Alpi Marittime-Mercantour,» [Online]. Available: https://www.marittimemercantour.eu/territorio/aree-protette-delle-alpi-marittime.

[6] «Interreg - ALCOTRA,» [Online]. Available: https://interreg-alcotra.eu/it.

[7] «Wikipedia - Parco Naturale delle Alpi Marittime,» [Online]. Available: https://it.wikipedia.org/wiki/Parco_naturale_delle_Alpi_Marittime.

[8] E. G. Power, «Centrale idroelettrica Entracque, Italia,» [Online]. Available: https://www.enelgreenpower.com/it/impianti/operativi/centrale-idroelettrica-entracque.

[9] Geoportale Piemonte, «Ppr - Tav. P2.0 Beni Paesaggistici (Quadro d'unione 1:250000),» [Online]. Available: https://www.geoportale.piemonte.it/geonetwork/srv/ita/catalog.search#/metadata/r_piemon:e63d7184-8253-4a0d-9746-e23dd7c86627.

[10] Regione Piemonte, ARPA Piemonte, «Le zone umide del Piemonte,» 2019.

[11] Parco naturale Alpi Marittime, «Boschi,» 18 Novembre 2020. [Online]. Available: https://www.parcoalpimarittime.it/conosci-il-parco/flora/boschi.

[12] Geoportale Piemonte, «BDTRE - Vegetazione,» [Online]. Available: https://www.geoportale.piemonte.it/geonetwork/srv/ita/catalog.search#/metadata/r_piemon:4b40500f-ecc7-47e4-98ea-0b8e78f45ed8. [Consultato il giorno 31 Gennaio 2017].

[13] Parco naturale Alpi Marittime, «Pascoli e praterie,» [Online]. Available: https://www.parcoalpimarittime.it/conosci-il-parco/flora/pascoli-e-praterie. [Consultato il giorno 18 Novembre 2020].

[14] A. Zanchetta, «Remote Sensing Techniques for Change Detection Analysis in Arid and Semi-arid areas,» Bologna, 2017.

[15] M.-D. Yang, H.-H. Tseng, Y.-C. Hsu e H. P. Tsai, «Semantic Segmentation Using Deep Learning with Vegetation Indices for Rice Lodging Identification in Multi-date UAV Visible Images,» *Remote sensing,* vol. 12, n. 633, p. 7, 2020.

[16] ESRI, «Introduction to Deep Learning,» [Online]. Available: https://pro.arcgis.com/en/pro-app/latest/help/analysis/deep-learning/what-is-deep-learning-.htm.

[17] MathWorks, «Che cos'è il Deep Learning?,» [Online]. Available: https://it.mathworks.com/discovery/deep-learning.html.

[18] J. Brand, «Deep Learning for Image Recognition,» Medium, 29 Ottobre 2019. [Online]. Available: https://medium.com/kwadigoai/deep-learning-for-image-recognition-1d612be00bbb.

[19] S. S. Nisha e M. N. Meeral, «Applications of deep learning in biomedical engineering,» *Handbook of Deep Learning in Biomedical Engineering,* n. 9, pp. 247-270, 2021.

[20] K. N. Haque, «What is Convolutional Neural Network — CNN (Deep Learning),» 3 Aprile 2023. [Online]. Available: https://www.linkedin.com/pulse/what-convolutional-neural-network-cnn-deep-learning-nafiz-shahriar/.

[21] P. S, «A Comprehensive Guide to UNET Architecture,» Analytics Vidhya, 10 Settembre 2024. [Online]. Available: https://www.analyticsvidhya.com/blog/2023/08/unet-architecture-mastering-image-segmentation/.

[22] ESRI Developer, «How U-Net works?,» [Online]. Available: https://developers.arcgis.com/python/guide/how-unet-works/.

[23] «Architettura U-Net,» Geeks for geeks, 8 Giugno 2023. [Online]. Available: https://www.geeksforgeeks.org/u-net-architecture-explained/.

[24] MMSegmentation, «Models,» [Online]. Available: https://mmsegmentation.readthedocs.io/en/main/advanced_guides/models.html.

[25] I. Berrios, «DeepLabv3,» Medium, 30 Maggio 2023. [Online]. Available: https://medium.com/@itberrios6/deeplabv3-c0c8c93d25a4 .

[26] «© European Union, Copernicus Land Monitoring Service 2012, European Environment Agency (EEA)».

[27] «© European Union, Copernicus Land Monitoring Service 2018, European Environment Agency (EEA)».

[28] V. Jain, «Handling Class imbalanced data using a loss specifically made for it,» Towards Data Science, 4 Settembre 2019. [Online]. Available: https://towardsdatascience.com/handling-class-imbalanced-data-using-a-loss-specifically-made-for-it-6e58fd65ffab.

[29] T. -Y. Lin, P. Goyal, R. Girshick, K. He e P. Dollár, «Focal Loss for Dense Object Detection,» *IEEE Transactions on Pattern Analysis and Machine Intelligence,* vol. 42, n. 2, pp. 318-327, 2020.

[30] S. Paul, «MixUp augmentation for image classification,» Keras, 6 Marzo 2021. [Online]. Available: https://keras.io/examples/vision/mixup/. [Consultato il giorno 24 Luglio 2023].

[31] A. E. Maxwell, M. P. Strager, T. A. Warner, C. A. Ramezan, A. N. Morgan e C. E. Pauley, «Large-Area, High Spatial Resolution Land Cover Mapping Using RandomForests, GEOBIA, and NAIP Orthophotography: Findings and Recommendations,» *Remote sensing,* vol. 11, n. 12, 2019.

[32] ESRI, «Compute Confusion Matrix (Image Analyst),» [Online]. Available: https://pro.arcgis.com/en/pro-app/latest/tool-reference/image-analyst/compute-confusion-matrix.htm.

[33] G. R. Morgan, C. Wang, Z. Li, S. R. Schill e D. R. Morgan, «Deep Learning of High-Resolution Aerial Imagery for Coastal Marsh Change Detection: A Comparative Study,» *ISPRS: International Journal of Geo-Information,* vol. 11, n. 2, 2022.

[34] A. Piemonte. [Online]. Available: https://www.arpa.piemonte.it/.

[35] L. Mercalli e D. C. Berro, Ultimi Ghiacci - Clima e ghiacciai nelle Alpi Marittime, 2019.

[36] ARPA Piemonte, «Assessment climatico della Provincia di Cuneo,» 2019.

Ringraziamenti

Inizio ringraziando i miei genitori: mi avete dato una grandissima opportunità, quella di andare a vivere in un'altra città per poter studiare, la cosa che più amo fare. Non è stato per niente facile, ma è stato bellissimo. Ho raggiunto obiettivi che all'inizio mi sembravano impossibili, ho conosciuto persone che oggi sono per me fondamentali e ho scoperto una città che è diventata mia e che amo con tutto il mio cuore. Non potrò mai ringraziarvi abbastanza per quello che avete fatto per me, per l'amore e il sostegno che mi avete sempre dato.

Ringrazio poi mia sorella Silvia che, nonostante qualche litigio e qualche scappellotto, mi è sempre stata vicino con la sua dolcezza e la sua saggezza. È più giovane di me, ma spesso sembra lei la più grande tra le due. Stessa cosa posso dirla per le mie due cugine, Ludovica e Vittoria, che si possono definire quasi più come delle sorelle.

Poi certo, ringrazio tutto il resto della mia famiglia, zie e zii, i miei nonni e gli altri cugini, Massimo... mi siete sempre stati accanto dandomi tantissimo affetto durante tutta la mia crescita, arricchendola con momenti preziosi. A volte siete un po' boomer eh, ma va bene lo stesso.

Passiamo ora agli amici. Farò una lista puntata perché sono tanti come i miei parenti (che bello!) e non ho voglia di iniziare ogni frase con "ringrazio" o robe del genere, quindi RINGRAZIO:

- ✓ I miei amici di Torino, i Panchinari: Andrea, Andrè, Cecilia, Davide, Francesca, Ginevra. Voi non avete idea di quanto io vi voglia bene e di quanto io mi senta fortunata ad avervi incontrato. Siete stati una ventata di aria fresca nella mia vita, per la prima volta ho sentito di far parte di un gruppo con cui poter condividere tanto ed è grazie a voi che ho capito il grande valore dell'amicizia. Quando non sono a Torino mi mancate sempre tantissimo e ogni weekend fremo per poter andare a fare festazza insieme a voi, per organizzare qualche altra avventura in giro per il mondo o anche solo per giocare a giochi da tavolo post pizza/aperitivo. Ogni momento con voi è speciale e lo porto sempre nel cuore.
- ✓ Aurora, mia fidata compagna di classe durante la magistrale. È una delle persone che mi fa più scassare dalle risate in assoluto, e anche quella che mi fa aspettare di più quando ci dobbiamo incontrare per un aperitivo o per studiare. Conoscendola, ho scoperto che è una persona con una grande intelligenza emotiva e che sa accoglierti anche nei momenti più difficili. Ti voglio tanto bene, amo, sei una persona stupenda.
- ✓ Deepak, sempre conosciuto tra i banchi di scuola. Deep è una persona d'oro, c'è sempre nel momento del bisogno e credo sia una delle persone più spensierate e chill che io conosca, nonché un grande avventuriero. Zì, ti prometto che da quest'anno scaliamo tutte le vette del Piemonte.
- ✓ I miei amici del Club Alpino Italiano, primo tra tutti Alberto, che conosco da più di 16 anni, compagno di avventure tra le montagne da quando eravamo alle medie, mio collega nelle organizzazioni delle gite e grandissimo amico: ci sentiamo più per affari burocratici e per condividere trash, ma troviamo sempre il momento per darci forza l'un l'altro.
  Il mitico Giovi, una delle persone peggio organizzate e più disordinate che io conosca, ma che porta sempre un botto di allegria ogni volta che lo incontri, ottimi dibattiti di geopolitica e pesantissime dosi di trash.

Ci sono poi Giorgia e Stefania: se avessi messo nell'università lo stesso impegno con cui facevamo i video del CAI di fine anno a quest'ora avrei 5 lauree. Ci sentiamo un po' meno ultimamente, ma ogni volta che ci incontriamo è come se ci fossimo viste il giorno prima. Come non citare poi Filippo, ottimo oratore, economista e persona verso cui ho una stima enorme. Questa società ci vuole imborghesire, ma noi non smetteremo mai di condividere dank meme.

Ci sono tante altre persone che fanno parte di questo gruppo e che ad ogni gita mi regalano sempre bellissimi ricordi che porto nel cuore.

- ✓ Beatrice. Ogni volta che ci vediamo perdo la cognizione del tempo perché c'è sempre troppo di cui parlare. Sei una persona super interessante, meravigliosa e su cui posso sempre contare. Anche lì, possiamo non vederci per mesi, ma sappiamo entrambe che, quando c'è bisogno, ci siamo l'una per l'altra, e questa cosa è bellissima. Poi vabbè, le cit ai film posso solo farle con te, quindi DIESCI!
- ✓ Anna Faaaaaaaaaaaa. Mia adorata vicina di banco per tutto l'anno della seconda liceo, mi ha insegnato a giocare a briscola e a dire una marea di st*onzate (non credo si possono scrivere queste cose su una tesi di laurea magistrale). Anche se mi ha abbandonato dopo la seconda, abbiamo sempre continuato a sentirci e la nostra bellissima amicizia è fortissima, proprio come lo è Anna. Ti voglio tanto bene.
- ✓ Il Mago e la sua crew. Il Mago, per i non amici Jacopo, è il boss della Casbah, degno erede di Joan Sebastian Bach, il re delle fUghe, e che mi ha accolto nella sua banda di scalmanati senza se e senza ma, facendomi sentire parte di un gruppo (tranne quando parlate di calcio ~~quindi sempre ihih~~). Più volte la nostra presenza in locali infastidisce le persone accanto a noi, e alla mia festa di laurea vorrei che ci sbattessero fuori da un locale, per cui prepariamoci a dare il meglio (o peggio) di noi.
- ✓ Enrico, che mi ha aiutato a correggere la tesi e i miei strafalcioni di inglese. Io comunque continuerò a giocare sempre in modo spietato a biliardo e calcetto eh.

Concludo ringraziando i miei due relatori, il professore Andrea Lingua e Francesca Matrone. Siete stati sempre molto disponibili con me e mi sono sentita molto ben accolta all'interno del laboratorio di geomatica, disciplina di cui mi sono innamorata anche grazie alla vostra passione. Vi ringrazio anche per avermi incluso in molte attività, dai rilievi sul campo ad Aisone e in Valle Gesso alla presentazione a Cuneo del mio lavoro svolto in team; sono state per me esperienze estremamente utili e arricchenti.

Se stai leggendo questa tesi e non ti ritrovi nell'elenco, Chiara dice che ti adora.